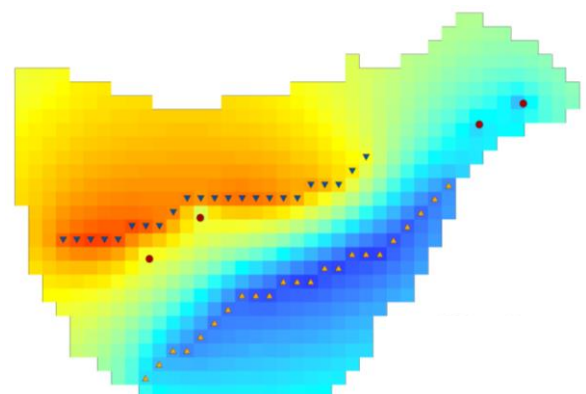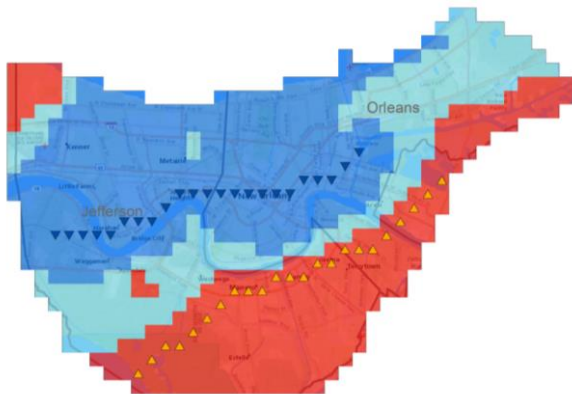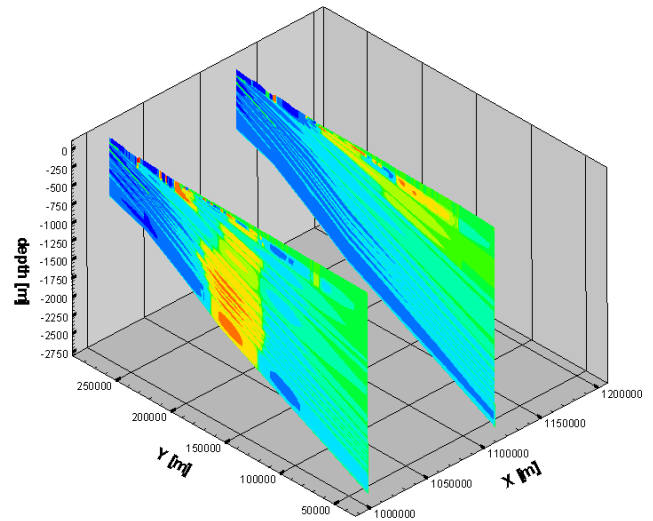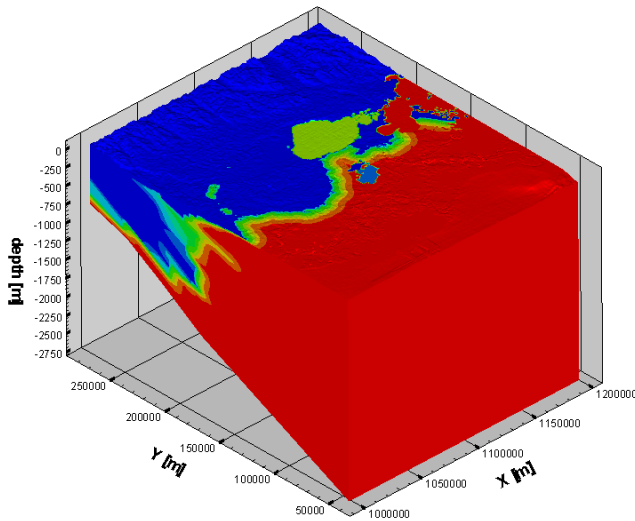# Projecting the Effects of Saltwater Intrusion on the Fresh Groundwater Resources of Southeastern Louisiana and the New Orleans Area, USA, based on 3D Variable-Density Groundwater Modelling

L.P. Brokx

April 2019
Utrecht
Final Version

Supervisors:
Dr. Ir. G.H.P. Oude Essink
Prof. Dr. Ir. M.F.P. Bierkens

Cover Images
Top left: Initial groundwater salinity distribution in Southeastern Louisiana
Top right: Two transects depicting the north-south flow velocity for future scenario FS2
Bottom left: Projected 2119 distribution of fresh and saline groundwater in the Gonzales-New Orleans aquifer of the New Orleans area for mitigation scenario I-E-5
Bottom right: Projected 2119 hydraulic head distribution in the Gonzales-New Orleans aquifer of the New Orleans area for mitigation scenario I-E-5

Abstract

The Southern Hills regional aquifer system in southeastern Louisiana contains large amounts of fresh groundwater, especially in the northern parts. In the New Orleans area, located in the central part of southeastern Louisiana, volumes of freshwater are present in the shallowest aquifers of the groundwater system. Although these fresh groundwater volumes are currently hardly used as a freshwater source, past water quality and water supply problems of the main source of freshwater in the New Orleans area, the Mississippi River and its distributaries, have shown the importance of groundwater as an alternative or back-up freshwater source. However, ongoing groundwater extraction, subsidence, flooding and sea level rise might pose a threat to the available fresh groundwater resources in southeastern Louisiana and the New Orleans area in particular, as they might lead to saltwater intrusion into the fresh groundwater volumes. The effects of these processes on the groundwater resources were studied using a 3D variable-density and coupled solute transport model created in the iMOD-SEAWAT modelling software. Different modelling scenarios were created to project changes of the fresh groundwater availability in the coming century on a regional scale for southeastern Louisiana and on a local scale for the New Orleans area. Additionally, measures such as artificial recharge, using fresh surface water from the Mississippi River, and salt groundwater extraction to sustain or increase the availability of fresh groundwater in the Gonzales-New Orleans aquifer in the New Orleans area were investigated.

The modelling results show that the effects of sea level rise, subsidence and flooding on saltwater intrusion into the fresh groundwater resources of southeastern Louisiana are negligible. Groundwater extraction leads to changing groundwater flow patterns in large parts of the aquifer system. Nevertheless, the consequences of ongoing groundwater extraction at the current rate on the total fresh groundwater volume present in the Southern Hills regional aquifer system are also expected to be small, leading to a decrease of 0.3% of the total available freshwater volume of 3.1 x 10^{12} m^3. However, groundwater extraction can lead to severe saltwater intrusion on a local scale, in areas where large volumes of groundwater are extracted and which are located relatively close to brackish to saline groundwater, such as the Baton Rouge area and the New Orleans area. In the New Orleans area, a continuation of groundwater extraction could lead to a fresh drinking water volume decrease up to 82% in the coming century. The use of solely salt groundwater extraction to counteract saltwater intrusion turned out to have adverse effects on the fresh groundwater resources. Artificial recharge, on the other hand, proved to be an effective solution. Fresh groundwater volumes in the Gonzales-New Orleans aquifer in the New Orleans area could increase up to 45.9% using this method relative to the 5.6 x 10^9 m^3 initially present, resulting from a total infiltration rate of 50 million cubic meters per year equally divided over 23 extraction wells. Saltwater extraction could slightly enhance the volume increase due to artificial recharge. However, due to negative side-effects of large scale groundwater extraction such as subsidence and attraction of highly saline groundwater, the use of solely artificial recharge to increase the future fresh groundwater resources might be the most viable option.

Acknowledgements

Contents

1. Introduction

1.1. Background

New Orleans is a major cultural and economic hub of the United States. Located in southeastern Louisiana along the Mississippi River, close to the Gulf of Mexico, the New Orleans area is part of the largest port of the USA by cargo volume (AAPA, 2016). Apart from its logistic value, the Mississippi River and its distributaries in the Mississippi River Delta are also the main source of freshwater for the New Orleans area. In 2010, 98.6% of the total freshwater use in the two most populous parishes of the New Orleans area, Jefferson Parish and Orleans Parish, was withdrawn from surface water resources and surface water was the only freshwater source used for public supply (Sargent, 2011).

Due to the large availability of surface water in the New Orleans area, it is plausible that it remains the main source of freshwater in the near future. However, past events of water quality deterioration, due to upstream chemical spillages and saltwater encroachment from the Gulf of Mexico during low discharge conditions, have shown that surface water as a freshwater source is too vulnerable to solely rely on (Dial & Sumner, 1989). Furthermore, many water facilities were damaged during Hurricane Katrina in 2005, disrupting freshwater supply in New Orleans for weeks (Copeland, 2005). Groundwater has been proposed as an alternative freshwater source or as an emergency source in case the quantity or quality of the available surface water resources is unsatisfactory (Dial & Sumner, 1989; Dial & Tomaszewski, 1988; Prakken, 2009).

Groundwater is a major source of freshwater in deltaic regions all over the world (Oude Essink et al., 2010; Ranjan et al., 2006). In southeastern Louisiana, large quantities of fresh groundwater are provided by the Southern Hills regional aquifer system, especially north of New Orleans (Griffith, 2003). Currently, the availability and quality of fresh groundwater resources are threatened globally by population increase, economic growth and climate change (Ranjan et al., 2006; Wada et al., 2010). In Southern Louisiana, the severe subsidence rates might pose extra pressures on the groundwater system. If extraction rates from aquifers exceed the recharge rate of fresh groundwater, groundwater depletion occurs. One of the main consequences of groundwater depletion in deltaic areas is saltwater intrusion into fresh groundwater resources (Wada et al., 2010). Saltwater intrusion is a major problem in the New Orleans area, as all major aquifers at least partly contain saltwater within the city limits (Dial & Sumner, 1989; Prakken, 2009). The observed movement of saltwater fronts closely correlates with the presence and location of groundwater extraction wells (Dial & Sumner, 1989). Extensive groundwater withdrawals in the past have led to salinization of the fresh groundwater resources (Prakken, 2009).

Presently, groundwater is hardly used as a freshwater source in the New Orleans area, as only saline groundwater has been produced recently at the four major withdrawal centres within the city limits (Prakken & Lovelace, 2014; Prakken et al., 2014a). However, the examples listed earlier in this section have underlined to need for an alternative source of freshwater to surface water. To establish groundwater as a sustainable source of freshwater, research regarding the current fresh groundwater resources and the expected future changes are needed. Only then, groundwater can be considered as a trustworthy freshwater reserve for long-term use.

1.2. Objectives & Research Questions

In this report, the current state of saltwater intrusion and future possibilities regarding fresh groundwater resources in southeastern Louisiana and specifically the New Orleans area will be studied. This will be done by creating a 3D variable-density groundwater model including a solute transport module to simulate the effects of saltwater intrusion. The model will be created using iMOD-SEAWAT (Verkaik & Janssen, 2015) based on the data available for the study area acquired from several data sources. This model will cover the full depth and nearly the full extent of the Southern Hills regional aquifer system, which dominates the hydrogeology underlying southeastern Louisiana (Griffith, 2003). As of now, no groundwater model has been developed that covers aquifer system on a regional rather than local scale (Ecology and Environment, 2011). Therefore, the first subject of interest is studying the groundwater flow model in a regional setting. Then, the focus will be shifted to the New Orleans area on a more local scale. In particular, the Gonzales-New Orleans aquifer will be subject of interest, as it has been the major source of fresh groundwater in the New Orleans area throughout the past decades (Dial & Sumner, 1989; Eddards et al., 1956; Prakken, 2009; Rollo, 1966). In summary, the model will be used to fulfil the following research objectives:

- Use available data to create an accurate representation of the current distribution of fresh and saline groundwater in southeastern Louisiana.
- Investigate the effects of groundwater extraction, sea level rise, subsidence and a short-term flooding on the fresh groundwater resources of the Southern Hills regional aquifer system on a regional scale.
- Project the changes of fresh groundwater availability in the Gonzales-New Orleans aquifer of the New Orleans area for the coming century using different extraction scenarios.
- Examine the possibilities of infiltrating freshwater from the Mississippi River into or extracting saline groundwater from the Gonzales-New Orleans aquifer to increase the available fresh groundwater volume in the New Orleans area.

By accomplishing these objectives, the following research questions can be addressed:

- What are the effect of sea level rise, subsidence and flooding on the fresh groundwater resources of southeastern Louisiana?
- To what extent does groundwater extraction lead to saltwater intrusion and the accompanied loss of fresh groundwater volumes on both regional and local scale?
- How will the fresh groundwater volumes present in the Gonzales-New Orleans aquifer change during the coming century and what are the effects of different extraction scenarios?
- Are artificial recharge and/or saline groundwater extraction effective measures to sustain or enlarge the fresh groundwater volumes in the Gonzales-New Orleans aquifer of the New Orleans area?

1.3. Thesis Outline

This report will elaborate on the steps taken to fulfil the aforementioned research objectives and to answer the research questions. Chapter 2 will expand on the relevant literature regarding saltwater intrusion. Furthermore, the main governing equations used in the iMOD-SEAWAT modelling software and the theory behind some relevant model variables will be discussed. Additionally, the study area will be presented and the relevant background information relating to the study area will be discussed, including the stratigraphic evolution, the hydrogeology and the current groundwater use. Chapter 3 will be used to elaborate on the acquirement and modification of available data needed as model input, and on the choices made during the model set-up. Moreover, the simple model calibration and different research scenarios used for completing the research objectives will be discussed in this chapter. The results of these scenarios will be summarized in Chapter 4 and discussed in Chapter 5. Finally, Chapter 6 will be used to answer the research questions and to summarize the findings of this research, as well as posing some recommendations for future research.

2. Literature Review

2.1. Saltwater intrusion

2.1.1. Fresh and Saline Groundwater

Saltwater intrusion is defined as mass transport of saline groundwater into areas that previously contained freshwater (Stewart, 1999). Fresh and saline groundwater are distinguished by their salinity, which is defined as the concentration of dissolved salt, mainly consisting of dissolved sodium chloride (Faneca Sanchez et al., 2015). Groundwater salinity can be given as either chloride concentration or Total Dissolved Solids (TDS) concentration, both expressed in mass per unit volume (Faneca Sanchez et al., 2015). Groundwater can be categorized based on its salinity. An example of such a classification was given by Rhoades et al. (1992), as shown in Table 2.1. Note that seawater has as a TDS concentration of approximately 35.0 kg/m^3. Drinking water standards are based on the taste of the water rather than health concerns. In the United States, a maximum TDS concentration of 0.5 kg/m^3 is used as a drinking water standard for aesthetic (taste) and technical reasons (USEPA, 2017), although water with TDS concentrations up to 1.0 kg/m^3 is commonly used for drinking purposes in other parts of the world (e.g. NHMRC & NRMMC, 2011).

Table 2.1. Groundwater classification based on its total dissolved solids concentration (modified from Rhoades et al., 1992)

Water Class	TDS Concentration	Water Use
Non-Saline (Fresh)	< 0.5	Drinking and Irrigation
Slightly Saline	0.5 - 1.5	Irrigation
Moderately Saline	1.5 - 7.0	Drainage
Highly Saline	7.0 - 15.0	Drainage
Very Highly Saline	15.0 - 35.0	-
Brine	> 35.0	-

Groundwater salinity is directly related to its electrical conductivity (or specific conductance), as the conduction of an electrical current through water is primarily determined by the concentration of ionic species, or salt, present (Hayashi, 2004). Since measuring the electrical conductivity is more straightforward than directly determining the salt content by ionic analysis (Pickwell, 2012), it is widely used to gather salinity data for groundwater modelling (e.g. Antonellini et al., 2008; Faneca Sanchez et al., 2015). Electrical conductivity, normalized for a temperature of 25 °C, can be converted to salinity (in terms of TDS concentration) using the equation described by Schemel (2001):

$$S = \sum_{n=1}^{6} K_n \left(\frac{\frac{EC}{1000}}{53.087} \right)^{\frac{n-1}{2}} \tag{2.1}$$

Where:
- S = salinity (‰)
- EC = electrical conductivity (µScm^{-1})
- K_n is a constant that has the following value for a given n:
    - K_1 = 0.012

- K_2 = -0.2174
- K_3 = 25.3283
- K_4 = 13.7714
- K_5 = -6.4788
- K_6 = 2.5842

Since the density of water is approximately 1000 kg/m^3, the resulting salinity (S) in ‰ can be assumed to be equal to the groundwater TDS concentration (C) in kg/m^3.

2.1.2. Basic Principles

Groundwater flow in coastal aquifers is complex as the salinity difference between fresh and saline water leads to groundwater density differences, causing it to be subject to density-driven flow (Bear & Cheng, 1999). Moreover, mixing occurs between fresh and saline groundwater due to hydrodynamic dispersion, creating a transition zone between the fresh- and saltwater bodies (Bear et al., 2001). Groundwater density and TDS concentration are therefore important variables for coastal groundwater modelling. These two variables are related following (Guo & Langevin, 2002):

$$\rho = \rho_f + E \cdot C \tag{2.2}$$

Where ρ is the groundwater density (kg/m^3), ρ_f is the density of freshwater, assumed to be 1000 kg/m^3, C is the TDS concentration (kg/m^3) and E is a dimensionless constant equal to 0.7143.

Research on variable-density groundwater flow has been carried out since the late 1800s (Guo & Langevin, 2002), when the hydrostatic equilibrium between saline and fresh groundwater for an unconfined aquifer connected to the sea was described independently by Badon Ghijben (1888) and Herzberg (1901) as:

$$h = \frac{\rho_s - \rho_f}{\rho_f} H \tag{2.3}$$

Where h is the hydraulic (piezometer) head (m), H is the depth of the interface between fresh and saline water (m), and ρ_f and ρ_s are the density of respectively fresh and saline water (kg/m^3). This equation, known as the Badon Ghijben-Herzberg relationship, is also applicable to confined and semi-confined aquifers (Naik, 2018). This approach is only valid if a sharp interface between fresh and saline groundwater exists or the width of the mixing zone is in the order of meters at most (Oude Essink, 2001a).

The first solution to a saltwater intrusion problem including both density-driven groundwater flow and the effects of dispersion resulting from salinity differences was created by Henry (1964). This case, known as the Henry problem, dealt with a homogeneous confined aquifer with a steady seaward flow of fresh groundwater towards a stationary boundary of seawater. Since then, several analytical and numerical solutions were proposed for this problem (Guo & Langevin, 2002) and it has become the benchmark problem for many density-dependent groundwater flow models (Simpson & Clement, 2004).

2.1.3. Current State

Saltwater intrusion has been a major problem in coastal regions all across the globe for decades (Post, 2005). The amount saltwater intruding into the fresh groundwater resources is mainly determined by hydraulic head differences in the relevant aquifers. Processes influencing the hydraulic head, and therefore saltwater intrusion, in an aquifer are groundwater extraction, land-use changes, sea level changes and other climatic fluctuations (Werner et al., 2013). Climate change and increased water use due to population and economic growth are expected to amplify the problem of saltwater intrusion in the future (Oude Essink, 2001a; Wada et al., 2010).

As saltwater intrusion is a problem of ever-growing concern, much research has been conducted since the first steps described in Section 2.1.2. The main focus areas of these studies are the processes determining groundwater flow in coastal aquifers, conservation of the fresh groundwater resources and numerical modelling of saltwater intrusion processes (Khublaryan et al., 2008). Analytical solutions to saltwater intrusion problems are limited to cases where fresh and saline groundwater are considered to be two immiscible fluids, i.e., mixing at the interface between fresh and saline groundwater is disregarded. The Henry problem (Section 2.1.2) is the only problem for which an analytical solution exists incorporating variable-density flow. Nevertheless, even this solution only accounts for diffusion and not for dispersion (Werner et al., 2013). As a result, numerical modelling is for now the single most important method to study saltwater intrusion processes and to project changes in the future fresh groundwater resources. These models are mostly able to incorporate both variable-density groundwater flow and solute transport and are therefore able to produce results that can be directly related to real world problems (Werner et al., 2013).

2.1.4. Large Scale Modelling

Three-dimensional numerical models have become an irreplaceable tool to gain insight in saltwater intrusion problems and possible solutions (Oude Essink, 2001a; Werner et al., 2013). Because saltwater intrusion is a large-scale problem, extensive models are often required, covering areas with a width and length up to several hundreds of kilometres, such as the one presented in this study. Multiple problems arise due to the scale of these models.

One of the main issues of working with large scale models is the large spatial variability of the input variables required in the model. Generally, detailed information for the entire study area on these variables is not available. Application of small-scale experimenting results to real world problem is hampered by this knowledge gap (Werner et al., 2013). Moreover, coarse grid sizes are used to cut the computational power required (Diersch & Kolditz, 2002). Therefore, model simplifications, assumptions and approximations are often inevitable (Mantoglou, 2003). Scale-dependent properties that often lead to model inaccuracies include layer heterogeneities and dispersion in the mixing zone (Post, 2005; Simmons, 2005; Werner et al., 2013).

Despite the uncertainties accompanied with large-scale three-dimensional models, they have been widely used to study the processes and effects of saltwater intrusion. The models have provided useful output for a wide range of case studies, including paleo-reconstructions of saltwater intrusion (Gossel et al., 2010), groundwater pumping and depletion scenarios (Hussain, Javadi, & Sherif, 2015;

Paniconi et al., 2001), the effects of climate change and sea level rise on the inland movement of saline groundwater (e.g. Oude Essink et al., 2010; Van Baaren et al., 2016) and strategies for groundwater resource management and saltwater intrusion prevention (e.g. Faneca Sanchez et al., 2015; Kopsiaftis, Mantoglou, & Giannoulopoulos, 2009).

2.1.5. Mitigation of Saltwater Intrusion

Sustainable groundwater management is of great importance to prevent saltwater intrusion. If the freshwater demand exceeds the natural recharge of the aquifer, fresh groundwater depletion results in the intrusion of saline water into the volumes of fresh groundwater. Once seawater has intruded into the fresh groundwater resources, removing the intruded saltwater is often an expensive and time-consuming process (Abd-Elhamid & Javadi, 2011; Bear & Cheng, 1999). However, as groundwater is an indispensable source of freshwater in many regions across the globe, additional measures to ensure or enlarge the fresh groundwater reservoirs might be needed.

The most common method to mitigate saltwater intrusion is artificial recharge, which can be applied both through infiltrating freshwater directly into an aquifer (Fig. 2.1b) using infiltration wells or by creating artificial infiltration ponds (Lu et al., 2017). Sources of freshwater utilized for artificial recharge include excess rainfall, surface water bodies such as rivers and lakes, desalinated brackish or saline water, and treated wastewater (Hussain, Javadi, Ahangar-Asr, et al., 2015; Hussain, Javadi, & Sherif, 2015; Javadi et al., 2015; Shi & Jiao, 2014). The aim of artificial recharge is to increase the hydraulic head of the areas containing fresh groundwater relative to the parts containing brackish to saline groundwater, thereby decreasing or reversing saltwater intrusion (Luyun Jr. et al., 2011). Injection wells can be applied for both confined and unconfined aquifers (Lu et al., 2017) and regularly a set of wells is installed parallel to the coast, and therefore parallel to the saltwater front, to fully control the effects of saltwater intrusion (Luyun Jr. et al., 2011). The use of infiltration ponds is limited to unconfined aquifers, for which they were found to be as effective as direct infiltration through wells (Lu et al., 2017). Artificial recharge has been successfully applied in multiple coastal aquifers, for example in Oman (Abdalla & Al-Rawahi, 2013), China (Shi & Jiao, 2014) and Australia (Werner, 2010).
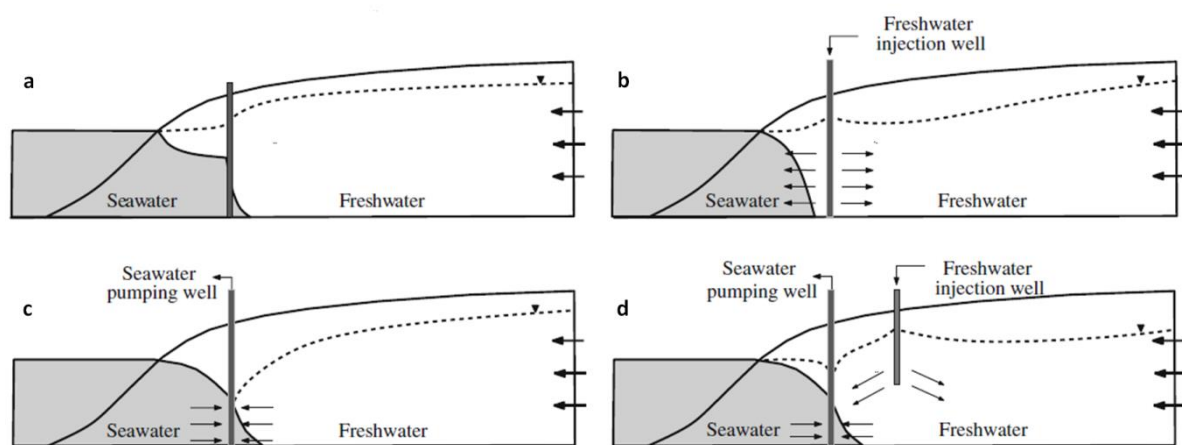
Fig. 2.1. Techniques used to mitigate saltwater intrusion: (a) physical flow barrier (b) artificial research through well infiltration (c) saltwater extraction (d) both artificial recharge and saltwater extraction (modified from Pool & Carrera, 2010).

Another measure to counteract saltwater intrusion is the extraction of brackish or saline groundwater (Fig. 2.1c). This method, also known as saltwater extraction, is especially suitable if artificial recharge cannot be applied due to a lacking availability of fresh surface water, e.g. in arid and semi-arid regions (Sherif & Hamza, 2001). According to several modelling studies (e.g. Kacimov et al., 2009; Sherif & Hamza, 2001), extracting saline or brackish water from an aquifer successfully terminates the landward migration of seawater. Extraction of brackish water is preferred to seawater if the withdrawn groundwater is used for other purposes such as desalinisation or crop irrigation (Sherif & Hamza, 2001). However, extracting closer to the freshwater zone enlarges the risk of extracting fresh instead of saline water in the long run (Pool & Carrera, 2010).

Other techniques used to prevent or reverse saltwater intrusion include low permeability physical barriers (Fig. 2.1a) and land reclamation (Oude Essink, 2001a; Pool & Carrera, 2010). Combining the aforementioned methods, along with groundwater management decisions such as withdrawal reductions and groundwater extraction well relocation, can be to fully prevent saltwater intrusion (Oude Essink, 2001a; van Dam, 2013). According to several studies (Lu et al., 2017, 2013; Siarkos et al., 2017), freshwater use can be optimized by collecting part of the extracted fresh groundwater and using it for artificial recharge in the area between the extraction wells and the saltwater front. Moreover, desalinizing abstracted brackish water and using it for artificial recharge, a technique known as ADR (Abstraction, Desalinisation and Recharge), has been proven to be more cost efficient than using only saltwater extraction or artificial recharge (Abd-Elhamid & Javadi, 2011). Fulfilling local water demands with the desalinized water and using treated waste water for freshwater infiltration instead could further lower the costs of counteracting saltwater intrusion (Hussain, Javadi, Ahangar-Asr, et al., 2015; Javadi et al., 2015).

2.1.6. Effects of Sea Level Rise, Subsidence and Flooding on Saltwater Intrusion

Due to climate change, global mean sea level is expected to have risen 26 cm to 82 cm by 2100 relative to the 1986-2005 average (IPCC, 2013). As the hydraulic head at the interface between an aquifer and the sea increases, sea level rise generally enhances saltwater intrusion into coastal aquifers (Werner & Simmons, 2009). Furthermore, land surface inundation resulting from sea level rise might cause a considerable landward shift of the transition zone between fresh and saline groundwater (Ataie-Ashtiani et al., 2013; Ketabchi et al., 2016), as depicted in Fig. 2.2 for an unconfined aquifer. Increased salinity in rivers and estuaries following sea level rise might also pose a threat to adjacent freshwater containing aquifers (Oude Essink, 2001a). Groundwater depletion is estimated to contribute approximately 25% to the current rate of sea level rise (Wada et al., 2010), causing groundwater extraction to harm the fresh groundwater resources of coastal aquifers in two ways. A simple estimation of the change of fresh groundwater depth due to sea level rise can be made based on the Badon Ghijben-Herzberg relation (Eq. (2.3)). Using densities of 1000 kg/m^3 and 1025 kg/m^3 for respectively fresh- and saltwater, each centimetre of sea level rise would lead to a 4 cm decrease of the fresh groundwater depth.

Although the adverse effects of sea level rise on fresh groundwater resources seem straightforward, the magnitude of these effects varies largely for different studies and locations. Sherif & Singh (1999) estimated that a 50 cm rise of the mean sea level would lead to 9.0 km of additional horizontal

saltwater intrusion in the unconfined Nile Delta aquifer in Egypt, but only to a 0.4 km increase in the confined Madras aquifer in India for the same amount of sea level rise. On the other hand, a conceptual study by Chang et al. (2011) showed that the long-term steady-state location of the interface between fresh and saline groundwater in confined aquifers is not altered due to sea level rise. Mazi et al. (2013) described certain tipping points beyond which sea level rise causes a significant amount of saltwater intrusion. These points are reached if a certain aquifer depth or sea level elevation is surpassed or if the freshwater outflow rate of an aquifer is below a certain threshold.

Whether an aquifer is susceptible to enhanced saltwater intrusion due to sea level rise also depends on the aquifer properties. According to Werner & Simmons (2009), the sensitivity of an aquifer to saltwater intrusion resulting from sea level rise is determined by the fact whether the hydraulic heads in the aquifers rise along with the sea level rise, causing unchanged seaward fluxes in the aquifer. In that case, saltwater intrusion for a sea level rise of 1.5 m is in the order of 50 meters at most. In the case that the hydraulic heads in the aquifer remain constant, sea level rise can cause inland intrusion of saltwater for several kilometres. In the constant flux scenario, enhanced intrusion into confined aquifer due to sea level rise is even non-existent (Werner et al., 2012). If an inland general head boundary is applied, the effect of sea level rise was found to be in between constant head and constant flux conditions, with larger boundary heads leading to less saltwater intrusion (Lu et al., 2015).

Along with decreasing inland hydraulic heads and sea level rise, subsidence is a third consequence of groundwater extraction that can lead to increased saltwater intrusion. Subsidence leads to lowering of the hydraulic heads on land, inducing the risk of rapid saltwater intrusion as observed at some locations in the Netherlands (Oude Essink, 2001a). Saline water was found to move further inland in areas with higher subsidence rates following modelling studies by Giambastiani et al. (2007) for Ravenna, Italy and Oude Essink et al. (2010) for the Netherlands. Effects of long term subsidence of the Po Plain in Italy were found to be limited to a zone within 20 km from the coast (Antonellini et al., 2008). Apart from direct effects on the hydraulic head in the aquifers, subsidence can lead to enhanced saltwater intrusion as coastal regions become more prone to flooding and inundation, and it causes further salinization of rivers and estuaries (Liu & Huang, 2013; Rahmawati et al., 2013).
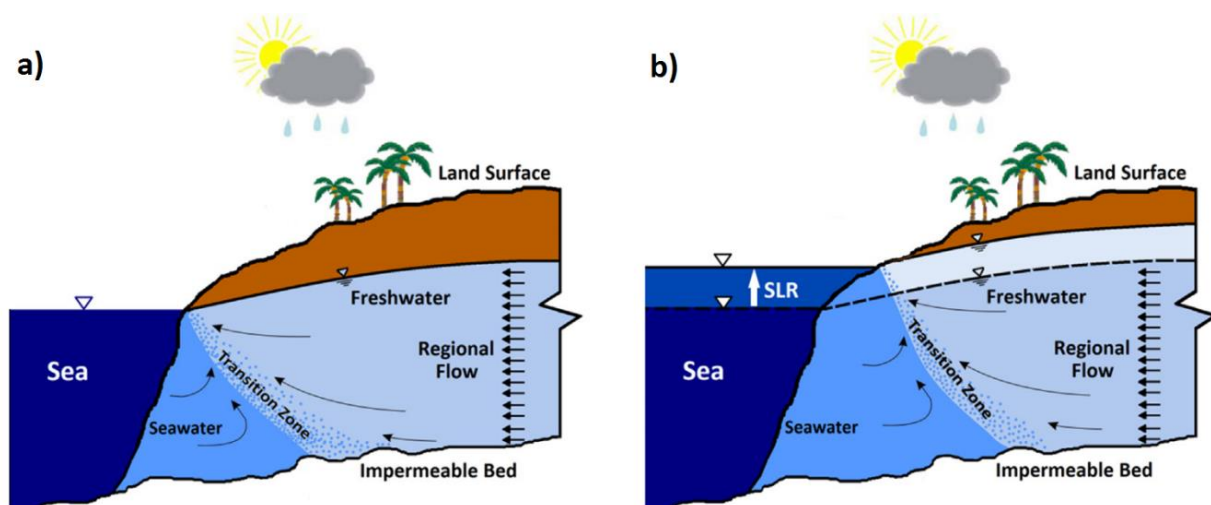
Fig. 2.2. Schematic representation of the effect of sea level rise on saltwater intrusion (b), compared to the situation without sea level rise (a), for an unconfined aquifer (modified from Ketabchi et al., 2016).

As discussed previously, coastal areas become more prone to flooding due to both sea level rise and subsidence. Seawater flooding of coastal areas is able to generate salinization of the coastal aquifers. In the aftermath of the 2004 tsunami, many coastal fresh groundwater lenses in Sri Lanka showed increased salinity levels, as the seawater infiltrated into the fresh groundwater resources either directly through open wells or by percolation through the unsaturated zone (Illangasekare et al., 2006). On a smaller scale, a flooding event on one of the Marshall Islands deteriorated the drinking water present in shallow fresh groundwater lenses for nearly two years (Gingerich et al., 2017).

2.2. Variable-Density Groundwater Modelling

2.2.1. iMOD-SEAWAT

The 3D variable-density groundwater flow and coupled solute transport model of southeastern Louisiana presented in this study was created using the iMOD-SEAWAT modelling software (Verkaik & Janssen, 2015), which is a version of SEAWAT Version 4.0 (Langevin et al., 2008) modified for iMOD (Vermeulen et al., 2017). iMOD is a Deltares-made Graphical User Interface for and an accelerated version of MODFLOW. The required data for iMOD-SEAWAT model runs is assembled in run-files, the input data being listed either as a constant or as one of the specific files used in iMOD. These files, being iMOD Point Files (IPF) for point data (e.g. wells) and iMOD Data Files (IDF) for raster layers, can be created and modified using iMOD or converted to other file types (e.g. the ASCII file format) to use and modify externally.

SEAWAT Version 4.0 (Langevin et al., 2008) was developed by the USGS as a tool for the simulation of three-dimensional, variable-density, multi-species, saturated groundwater flow. It combines MODFLOW-2000 (Harbaugh et al., 2000) to solve the variable-density groundwater flow equation with MT3DMS (Zheng, 2010; Zheng & Wang, 1999) to solve the solute transport equation. SEAWAT was originally created to model saltwater intrusion (Werner et al., 2013), although it can be used for all kinds of heat and solute transport groundwater problems (Langevin et al., 2008).

2.2.2. Governing Equations & Equation of State

The SEAWAT code makes use of two governing equations to calculate variable-density groundwater flow and solute transport in the model based on the input variables. The first one, the variable-density groundwater flow equation, is given by Langevin et al. (2008):

$$\nabla \cdot \left[\rho \frac{\mu_0}{\mu} K_0 \left(\nabla h_0 + \frac{\rho - \rho_0}{\rho_0} \nabla z \right) \right] = \rho S_s \frac{\partial h_0}{\partial t} + \theta \frac{\partial \rho}{\partial C} \frac{\partial C}{\partial t} - \rho_s q'_s \tag{2.4}$$

Where:
- ρ = fluid density [ML^{-3}]
- ρ_0 = fluid density at reference concentration and temperature [ML^{-3}]
- μ = dynamic viscosity [ML^{-1}T^{-1}]
- μ_0 = dynamic viscosity at reference concentration and temperature [ML^{-1}T^{-1}]
- K_0 = saturated hydraulic conductivity tensor [LT^{-1}]

- h_0 = hydraulic head at reference concentration and temperature [L]
- S_s = specific storage [L^{-1}]
- θ = porosity [-]
- C = solute concentration [ML^{-3}]
- q'_s = source/sink of a fluid [T^{-1}] with density ρ_s [ML^{-3-}]

The specific storage (S_s) is defined as the volume of water released from storage per unit volume per unit decline of the hydraulic head (h_0) (Langevin et al., 2008). Since temperature is assumed to be constant and salt to be the only solute present during the modelling process, the most obvious choice for the reference density in this case is the density of freshwater (ρ_f), approximately equal to 1000 kg/m³. The reference hydraulic head will then become the freshwater head (h_f), which will be discussed in Section 2.2.4.

The second governing equation solves for solute transport and is given by Langevin et al. (2008):

$$\left(1 + \frac{\rho_b K_d^k}{\theta}\right)\frac{\partial(\theta C^k)}{\partial t} = \nabla \cdot \left(\theta D \cdot \nabla C^k\right) - \nabla \cdot \left(q C^k\right) - q'_s C_s^k \tag{2.5}$$

Where:
- ρ_b = solid matrix bulk density [ML^{-3}]
- K_d^k = distribution coefficient of species k [L³M^{-1}]
- C^k = concentration of species k [ML^{-3}]
- C_s^k = source/sink concentration of species k [ML^{-3}]
- q = specific discharge [LT^{-1}]

The main constituents of salt are conservative, i.e., it does not adsorb or decay in groundwater. Therefore, the distribution coefficient of salt can be assumed to be zero. The equation of state, assuming a constant temperature, relates groundwater density to pressure (P [ML^{-1}T^{-2}]) and solute concentration following (Langevin et al., 2008):

$$\rho = \rho_0 \exp\left[\beta_C\left(C - C_0\right) + \beta_p(P - P_0)\right] \tag{2.6}$$

Where β_C and β_P are the volumetric expansion coefficients of respectively solute concentration and pressure.

2.2.3. Cauchy Boundaries
In most cases, the boundary conditions of an iMOD-SEAWAT model are determined by a set of head-dependent or Cauchy boundaries, which are represented by the so-called GHB-package (Section 3.2.4). For this boundary type, a user-specified hydraulic head value should be assigned to each boundary cell. However, this value is not by default assigned to that cell during model calculations, but rather calculated by the model itself. Groundwater flow Q_b [L³T^{-1}] into or from a Cauchy boundary model cell is calculated according to (Guo & Langevin, 2002):

$$Q_b = COND(h_c - h) \tag{2.7}$$

Where:
- o h = calculated head at the boundary cell [L]
- o h_c = assigned boundary head [L]
- o $COND$ = boundary conductance [L^2T^{-1}]

The conductance term determines the extent to which the head in the boundary cell is influenced by the boundary condition. If the conductance term is small, the head in the boundary cell is largely determined by other model variables. If, on the other hand, the conductance term is large, it approaches a constant head or Dirichlet boundary. In solute transport modelling, a concentration also has to be specified as a boundary condition, which is also returned to the model boundary cell depending on the boundary conductance. Apart from the general head boundary conditions of the model system, river systems (Section 3.2.5) and drains (Section 3.2.6) are also implemented in iMOD-SEAWAT as a Cauchy boundary.

2.2.4. Freshwater Heads

Groundwater flow in SEAWAT is determined by the concept of freshwater heads rather than point water heads as measured in piezometers (Guo & Langevin, 2002). If the groundwater density is constant throughout the modelled area, point water heads are sufficient to determine pressure differences in the system and therefore groundwater flow. However, as the pressure head component of the hydraulic head is dependent on both pressure and groundwater density, point water heads cannot be directly used in variable-density groundwater modelling. For this reason, the concept of freshwater head has been introduced, which is defined as the hydraulic head of a groundwater column at a given pressure and for the density of freshwater, regardless of the real groundwater density, or in equation form (Post et al., 2007):

$$h_f = z + \frac{P}{\rho_f g} \tag{2.8}$$

Where:
- o h_f = freshwater head [L]
- o z = elevation head above reference level [L]
- o P = pressure at the well screen [$ML^{-1}T^{-2}$]
- o ρ_f = density of freshwater [ML^{-3}]
- o g = gravitational acceleration [LT^{-2}]

Freshwater head can be calculated from measured point water heads using (Post et al., 2007):

$$h_f = \frac{\rho}{\rho_f} h - \frac{\rho - \rho_f}{\rho_f} z \tag{2.9}$$

Where ρ and h represent respectively the density [ML^{-3}] and the point water head [L] in the observation well. SEAWAT uses the calculated freshwater head values as an input for the variable-density flow equation (Guo & Langevin, 2002). Conversely, piezometric point water head values are often the desired output heads, which can be derived from the calculated freshwater heads by rearranging Eq. (2.9):

12

$$h = \frac{\rho_f}{\rho} h_f - \frac{\rho_f - \rho}{\rho} z \qquad (2.10)$$

2.2.5. Hydrostatic Conditions using Freshwater Heads

In some cases, hydrostatic conditions are assumed at certain locations, for example at the general head boundaries, to increase the model stability. In SEAWAT, the required input hydraulic head values are given in the form of point water heads, which are converted by SEAWAT itself to freshwater heads used for calculation following Eq. (2.9). Thus, if hydrostatic conditions are required, input point water heads should be modified in such a way that vertical flow components in a groundwater column are eliminated after conversion to freshwater heads. Vertical flow in terms of freshwater head is defined, assuming that the dynamic viscosity is independent of salinity, as (Post et al., 2007):

$$q_z = K \left(\frac{dh_f}{dz} + \frac{\rho - \rho_f}{\rho_f} \right) \qquad (2.11)$$

Where q_z [LT^{-1}] is the vertical specific discharge and K [LT^{-1}] is the hydraulic conductivity. Hydrostatic conditions are acquired if q_z is equal to 0 (no vertical flow). In that case, the vertical flow equation can be simplified to:

$$\frac{dh_f}{dz} = -\frac{\rho - \rho_f}{\rho_f} \qquad (2.12)$$

And the freshwater head can be determined by integration:

$$h_f = -\int \frac{\rho - \rho_f}{\rho_f} \, dz \qquad (2.13)$$

In groundwater modelling, hydrostatic conditions are achieved when there is no vertical flow between adjacent model layers, using a single value for the hydraulic head in a groundwater column for each layer. The corresponding freshwater head value can be calculated by discretizing Eq. (2.13). By adding a correction term ($\Delta h_{f,i}$) for each model layer to the water table in the top layer (h_0), the new hydrostatic freshwater head ($h_{f,i}$) for each model layer i from the top can be determined. The correction term is given by:

$$\Delta h_{f,i} = \sum_{0}^{n=i} \frac{\rho_n - \rho_f}{\rho_f} \Delta z_n \qquad (2.14)$$

Where Δz_n [L] is the layer thickness of model layer n. Then, the required input point water head for each model layer can be achieved by implementing the calculated freshwater head ($h_{f,i}$) in Eq. (2.10).

2.3. Study Area

2.3.1. Southeastern Louisiana

Although no formal definition of southeastern Louisiana exists, it will be defined in this report as the part of Louisiana that is located directly south of the 31st parallel north state border with Mississippi. The model extent (Fig. 2.3) covers most of this area, with the exception of the westernmost part and the outer tip of the Mississippi River Delta. The study area includes parts of the Gulf of Mexico in the south and east. Furthermore, the northeastern part of the modelling area includes a part of the State of Mississippi.

The study area includes the lower stretches of the Mississippi River, travelling from the northwest to the southeast, as it passes through the two largest urban areas of Louisiana: New Orleans and Baton Rouge. The southern part of the study area, to the south and west of Lake Pontchartrain, is dominated by the Holocene Mississippi Delta Plain (Blum & Roberts, 2009), consisting of a network of swamps, fresh to saline marshes and some elevated parts on which most of the urbanized areas are located (Coleman et al., 1998). Several brackish estuarine lakes can be found in this area, most notably Lake Pontchartrain, Lake Maurepas slightly to the west of Lake Pontchartrain and Lake Salvador/Lake Cataouatche to the south of New Orleans (Fig. 2.3). The area north of Lake Pontchartrain is more hilly and is generally covered by pine forests and agricultural areas (D'Arconte, 2002; Griffith, 2003). Other major river systems in the study area are the Pearl River on the easternmost Louisiana-Mississippi state border and several distributaries of the Mississippi River, including the Atchafalaya River in the southwest (Fig. 2.3).

Fig. 2.3. Study area location and extent.

According to the Köppen-Geiger classification (Kottek et al., 2006), the climate in southeastern Louisiana is warm and humid year-round, with warm to hot summers. In New Orleans, the average high temperature varies between 17 °C in January to 33 °C in July and August. The average daily rainfall peaks in June at 200 mm/d and drops to 90 mm/d in October (US Climate Data, 2019). Southeastern Louisiana is subject to the North Atlantic hurricane season which generally lasts from early June to late November. The most notable hurricane that struck the study area was Hurricane Katrina in late August 2005, leading to an estimated death toll of 1833 (Zimmermann, 2015), most of them in New Orleans (Kates et al., 2006), and an estimated damage of 125 billion dollars (NOAA, 2018).

Fig. 2.4. Parishes in the study area categorized based on the hydrogeological nomenclature as summarized by Griffith (2003) and the definitions used in the present study.

Other
Eastern Florida Parishes
Baton Rouge Area + Florida Parishes
Baton Rouge Area
New Orleans Area

The highest order subdivisions of Louisiana are the 64 parishes, 24 of which are (partly) included in the study area (Fig. 2.4). The three most populous parishes are East Baton Rouge Parish, in which the city of Baton Rouge is located, followed by Jefferson Parish and Orleans Parish, forming the major urban centre of New Orleans. The parishes north of Lake Pontchartrain and east of the Mississippi River, including East Baton Rouge Parish, are collectively known as the Florida Parishes. The hydrogeological nomenclature (Section 2.3.3) alters between different parts of the study area. These areas are the Baton Rouge area, the New Orleans area and the Eastern Florida Parishes. The classification of these areas, as derived from Griffith (2003), is depicted in Fig. 2.4. Note that some of the Florida Parishes are incorporated in the Baton Rouge Area with respect to the hydrogeological research. The definitions as introduced here will be used throughout the remainder of this report.

2.3.2. Stratigraphic Evolution

The subsurface of southeastern Louisiana is part of the Coastal Lowlands aquifer system, which consists of alternating aquifers and confining layers from Miocene to Holocene age and stretches along the Gulf Coast from northwestern Florida to the border with Mexico (Grubb, 1984). The subsystem underlying southeastern Louisiana is referred to as the Southern Hills regional aquifer system, comprising a complex, southward thickening and dipping alternation of sandy and clayey layers (Buono, 1983). These strata were formed by depositional cycles related to sea level transgressions during interglacial periods. During early stages of sea level rise, increased meltwater fluxes from the retreating glaciers led to large sedimentation rates of sands, silts and clay and thereby generating the formation of the aquifers (McFarlan & LeRoy, 1988), which are therefore fluvial in origin (Chamberlain et al., 2013). Further sea level rise and a decrease of the available meltwater followed by inundation led to the deposition of increasingly finer sediments, resulting in the formation of the confining units (McFarlan & LeRoy, 1988).

Sea level change is therefore the main factor determining the past depositional environment and its influence was found to have reached more than 600 km inland from the present shoreline (Shen et al., 2012), stretching far beyond the borders of southeastern Louisiana. Since northern parts were river-dominated for a longer timespan than southern parts, which were predominantly located in a marine environment, the deposits become progressively finer towards the south (Martin Jr. & Whiteman Jr., 1999). As most sediment was deposited during the early stages of sea level transgression (McFarlan & LeRoy, 1988), when the delta coastline was further seaward, the aquifers thicken in a southward direction. The increased sediment loading caused subsidence in the southern parts of the region and uplift more inland, which amplified the southward dip of the aquifer system (McFarlan & LeRoy, 1988; Nunn, 1985). Furthermore, glacial isostatic adjustment, in the form of forebulge collapse and ocean loading due to sea level rise, was also found to be a contributing factor to the southward orientation of the aquifer system (Wolstencroft et al., 2014).

A southward-thickening, Holocene confining top layer is present in the southern parts of the study area (Fig. 2.5) approximately from the northern shore of Lake Pontchartrain southwards (Shen et al., 2012). This layer has been formed as a result of sea level rise during the last 20,000 years (Ayrer, 2013; Ayrer & Wicks, 2013). The last 5000 years, during which the current Mississippi Delta Plain was formed, have been characterized by several course changes of the Mississippi River throughout
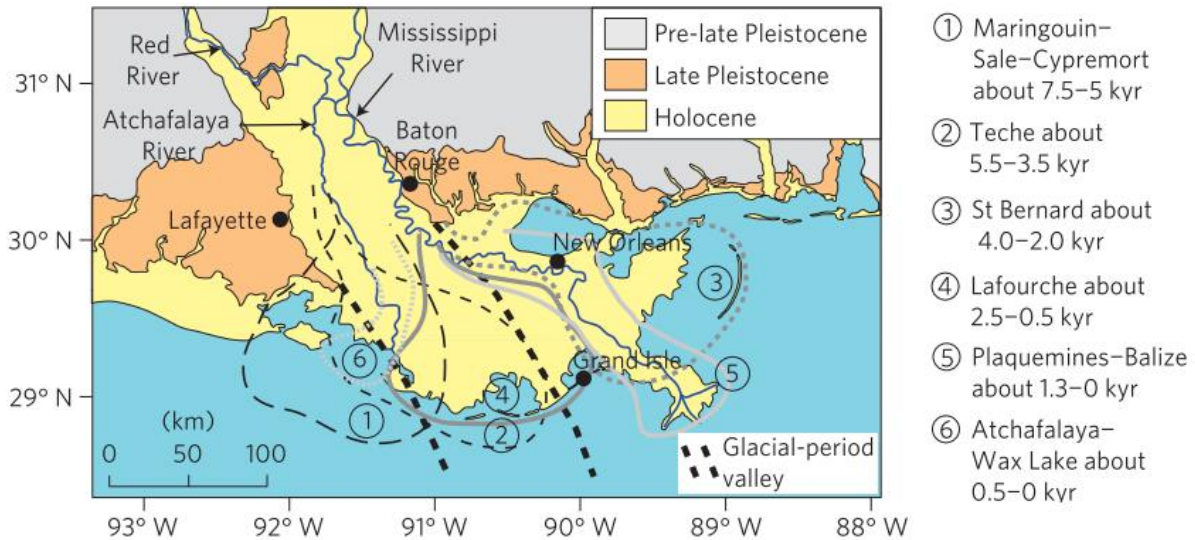
Fig. 2.5. Extent of the Holocene Mississippi Delta Plain and the current and former locations of the Mississippi River Delta (modified from Blum & Roberts, 2009).

southeastern Louisiana (Fig. 2.5), which has led to a complex environment of fluvial and marine deposits (Kolb & Van Lopik, 1966).

2.3.3. Hydrogeology and Groundwater Resources

2.3.3.1. Southern Hills Regional Aquifer System

As discussed in Section 2.3.2, the hydrogeology of southeastern Louisiana is dominated by the Southern Hills regional aquifer system, which extends from central Mississippi to beyond the shoreline of the Gulf of Mexico (Griffith, 2003). Aquifer recharge is primarily controlled by percolation of water in areas where one of the aquifers intersects the land surface, with deeper layers cropping progressively further north. The recharge area extends from Lake Pontchartrain up to the latitude of Jackson and Vicksburg in the State of Mississippi (Buono, 1983). Natural groundwater flow is generally directed southwards analogues to the dip of the aquifers (Griffith, 2003). In general, the presence of saline groundwater increases with depth and towards the coast (Griffith, 2003; Sargent, 2011). In the western part of the study area, groundwater flow is hampered by the presence of the Baton Rouge fault system, which stretches from West Baton Rouge Parish to the northern shore of Lake Pontchartrain (Griffith, 2003). Therefore, large fresh groundwater volumes at more than 300 m depth are restricted to the areas north of the fault system in the Baton Rouge area (Griffith, 2003). On the other hand, the effect of the fault system on groundwater movement is negligible in the Lake Pontchartrain area to the north of New Orleans (Dial & Sumner, 1989).

The Southern Hills regional aquifer system can be subdivided into three smaller aquifer systems. From top to bottom, these aquifer systems are: the Chicot equivalent aquifer system, the Evangeline equivalent aquifer system and the Jasper equivalent aquifer system (Stuart et al., 1994; White, 2017). Each of the subsystems consists of a set of alternating aquifers and aquitards (Fig. 2.7). The nomenclature of the aquifers (Table 3.1) is based on their depth below the land surface in the Baton Rouge region, while they are named after settlements in the Eastern Florida Parishes and the New

Orleans area (Griffith, 2003). The Southern Hills aquifer system is the primary source of freshwater in southeastern Louisiana in the parishes north and northwest of Lake Pontchartrain (White, 2017). In the most northern parts of the study area, fresh groundwater is also present in the Catahoula equivalent aquifer system, which underlies the Southern Hills regional aquifer system (Griffith, 2003). A schematic representation of aquifers present and the distribution of fresh and saline water in the Southern Hills (and Cathahoula equivalent) aquifer system is shown in Fig. 2.7.

Another fresh groundwater containing aquifer in the western part of the study area is the Mississippi River alluvial aquifer (White, 2017), a shallow Holocene and Pleistocene layer located along the west bank of the Mississippi River (Fig. 2.6a), on top of the Southern Hills regional aquifer system. This aquifer is not present east of the Mississippi River and therefore only covers a small part of the study area.

2.3.3.2. New Orleans Area

Groundwater resources are limited to relatively shallow aquifers in the New Orleans area. The Holocene confining layer is present throughout the area and contains a number of point-bar deposits and fluvial shallow aquifers (Tomaszewski, 2003). The Holocene layer is underlain by four Pleistocene aquifers belonging to the Chicot equivalent aquifer system (Stuart et al., 1994). These aquifers are: the Gramercy aquifer, the Norco aquifer, the Gonzales-New Orleans aquifer and the "1200-foot" sand (Fig. 2.7 and Fig. 2.8). The Gramercy aquifer does not contain any fresh groundwater in the New Orleans area and is highly discontinuous. The Norco aquifer is also absent in large parts of the New Orleans area, but does contain fresh groundwater along the shoreline of Lake Pontchartrain in parts of Jefferson Parish (Prakken, 2009). The Gonzales-New Orleans aquifer is the main source of fresh groundwater in the area and continuous throughout the largest part of the New Orleans area. It contains fresh groundwater in the northern parts of New Orleans (Fig. 2.9). The "1200-foot" aquifer is almost fully saline and is not used as a source of freshwater in the New Orleans area (Prakken, 2009). These aquifers can be considered as the upper aquifers of the Southern Hills regional aquifer system. The aquifers crop in the area directly north of Lake Pontchartrain, which is therefore the main recharge area of these aquifers (Jones et al., 2014).
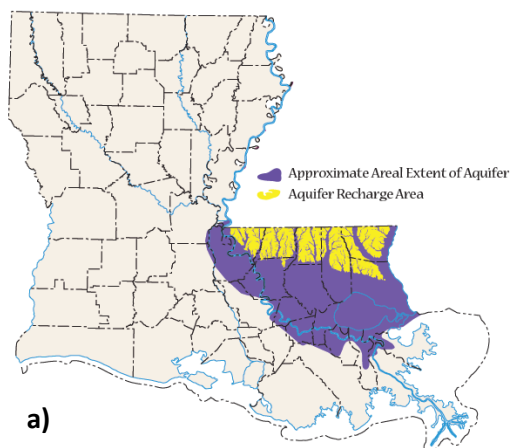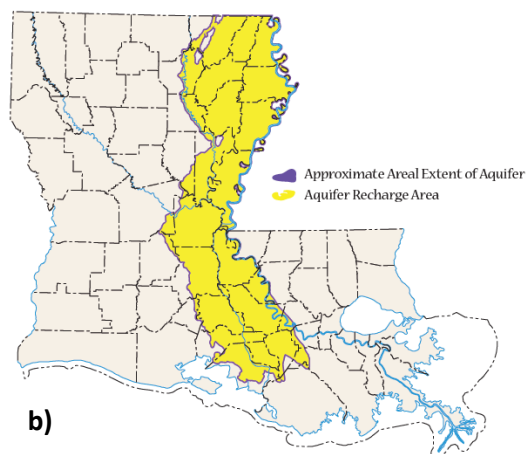
Fig. 2.6. Approximate fresh groundwater extent and recharge area of (a) the Southern Hills regional aquifer system and (b) the Mississippi River alluvial aquifer (modified from Van Biersel, Carlson & Miller, 2010).
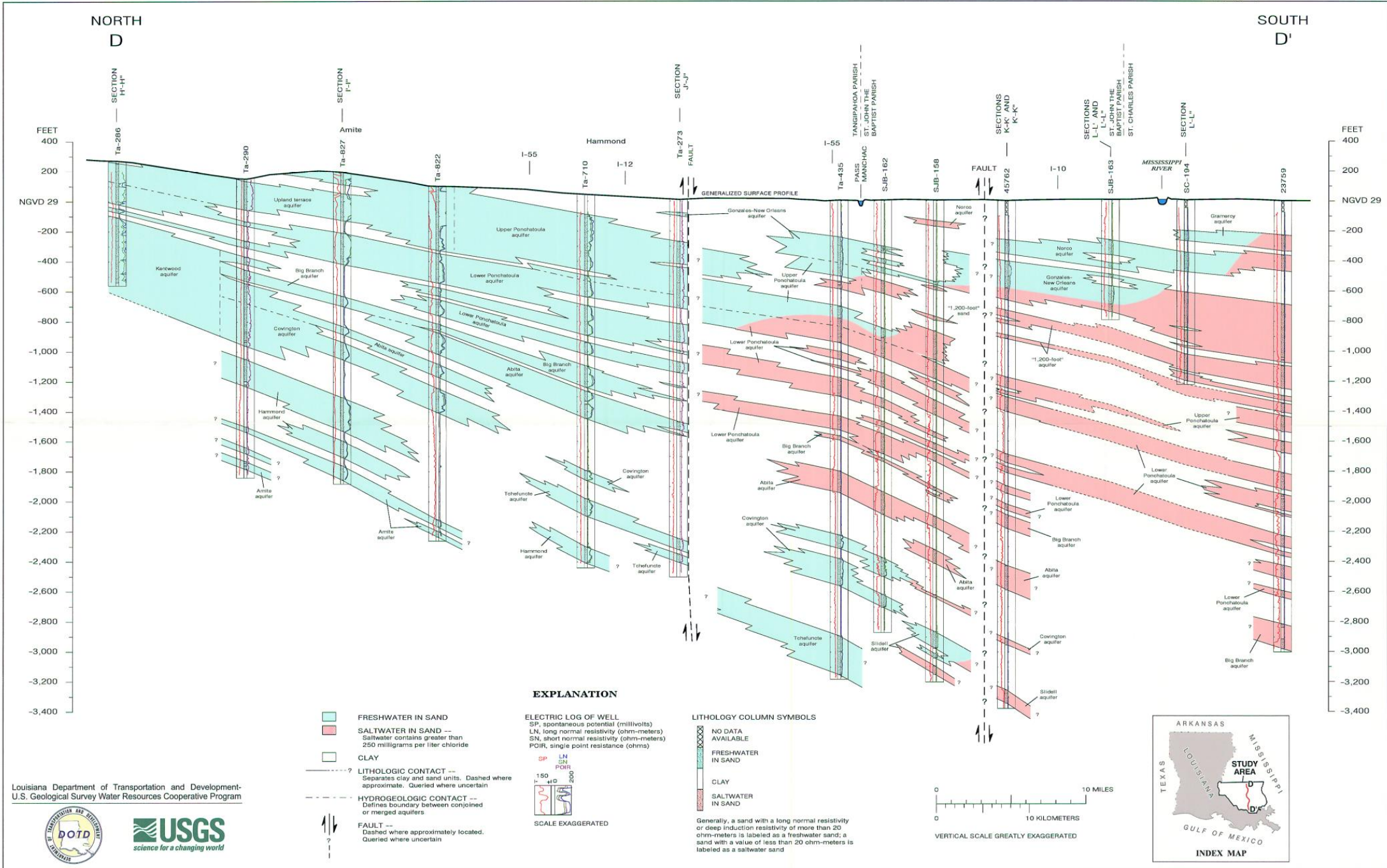
Fig. 2.7. General hydrogeology of southeastern Louisiana and the distribution of fresh groundwater (blue) and saline groundwater (red) (Griffith, 2003).
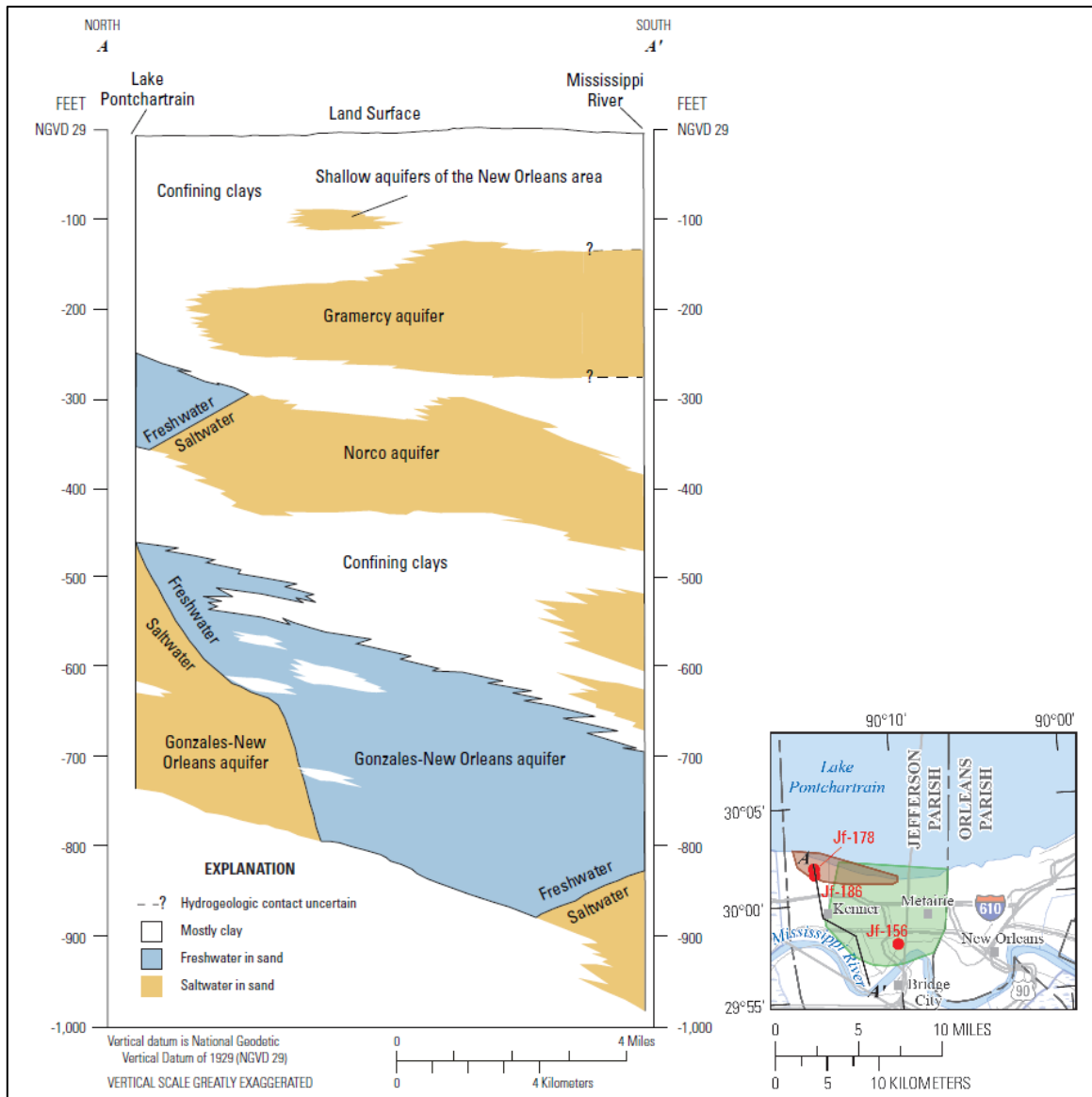
Fig. 2.8. Generalized north-south cross section through northern Jefferson Parish showing the hydrogeology and the distribution of fresh and saline groundwater (modified from Prakken & Lovelace, 2014).

2.3.4. Groundwater Use

The Southern Hills regional aquifer system is an important source of freshwater in southeastern Louisiana. In 2014, on average approximately 1.11×10^6 m³/d (USGS, 2018) were extracted from the three subsystems combined in the 23 parishes relevant for this study. About 80% of the groundwater withdrawals in the area was used for either public supply or domestic use, while smaller amounts were extracted for power generation, irrigation, personal use in rural areas, livestock and aquaculture (White, 2017). The total groundwater withdrawals from the Southern Hills regional aquifer system have been doubled between 1960 and 2014. More than half of the 2014 daily groundwater extractions in the study area, about 0.56×10^6 m³/d, occurred in East Baton Rouge parish (USGS, 2018). This area contains the city of Baton Rouge, which is largely dependent on groundwater for public supply and industrial purposes (White & Prakken, 2015a).

20

On the contrary, only 0.069 x 10^6 m^3/d was extracted in the two most populous parishes of the New Orleans metropolitan area, Jefferson Parish and Orleans Parish, combined (USGS, 2018), as both parishes obtain more than 95% of their freshwater from surface water resources (Prakken & Lovelace, 2014; Prakken et al., 2014a). The Gonzales-New Orleans aquifer is the main fresh groundwater source in these parishes, while small amounts are withdrawn from the Norco and Gramercy aquifers (Prakken & Lovelace, 2014; Prakken et al., 2014a). Groundwater usage in this area has been steadily decreasing since the seventies, when it peaked at a rate of approximately 0.20 x 10^6 m^3/day (Prakken, 2009; Prakken & Lovelace, 2014; Prakken et al., 2014a). In 2007, four major withdrawal centers were located in Jefferson Parish and Orleans Parish, two in both. None of these four wells was extracting fresh groundwater in 2008 according to Prakken (2009), who used a chloride concentration of 250 mg/l as the upper limit of freshwater, which is equal to a TDS concentration of 0.45 kg/m^3, following a 0.55 ratio of chloride concentration over TDS concentration as proposed by Faneca Sanchez et al. (2015). The majority of the total extracted groundwater volume was withdrawn at the Michoud Gas Power Plant (Prakken, 2009), which closed in 2016 (AAE, 2016). Plans have been made to open another electric generation facility on the same spot using the extraction wells of the former power plant, but only using a fraction (<10%) of the groundwater the former facility used (CK Associates Environmental Consultants, 2016).

In the western part of southeastern Louisiana, the Mississippi River alluvial aquifer is also used as a source of fresh groundwater (USGS, 2018). Extractions from this aquifer are relatively minor compared to extractions from the Southern Hills aquifer system in the study area and the Mississippi River alluvial aquifer is not present in large parts of the study area. Therefore, this aquifer will be ignored in the remainder of this research.

2.3.5. Saltwater Intrusion Issues

The two major areas of concern regarding saltwater intrusion in southeastern Louisiana are the Baton Rouge and New Orleans areas, as both are located near the transition zone between fresh and saline groundwater and both contain or contained some major withdrawal centers (Section 2.3.4). In the Baton Rouge area, the Baton Rouge fault, located just south of Baton Rouge, acts as a leaky flow barrier. Therefore, the fault used to separate the fresh groundwater to the north of the fault from the brackish and saline groundwater to the south (Anderson, 2012). Extensive groundwater extraction has led to encroachment of saline groundwater into the Baton Rouge area. Recent studies (e.g. Anderson, 2012; Wendeborn & Hanor, 2013) have shown that the saline groundwater that intruded into the Baton Rouge area moved across the fault rather than up the fault from the deeper layers, as was proposed in early work by Rollo (1969).

Extensive groundwater extraction has also led to saltwater intrusion in the New Orleans area, especially in the Gonzales-New Orleans aquifer (Ayrer, 2013; Prakken, 2009). Dial & Sumner (1989) have shown that extensive use of groundwater in Orleans Parish from the Gonzales-New Orleans aquifer could lead to northward movement of saline groundwater into the fresh groundwater resources at a rate of over 100 m/yr. In Jefferson Parish, the Gonzales-New Orleans aquifer contains brackish groundwater to the west of the fresh groundwater resources, leading to northwest-southeast saltwater encroachment following the general groundwater flow direction (Prakken, 2009). As of now, no groundwater treatment projects are in practice. A small-scale field test on the storage

Fig. 2.9. Distribution of fresh (blue) and saline (red) groundwater in the Gonzales-New Orleans aquifer in Jefferson Parish and Orleans Parish (modified from Prakken, 2009).
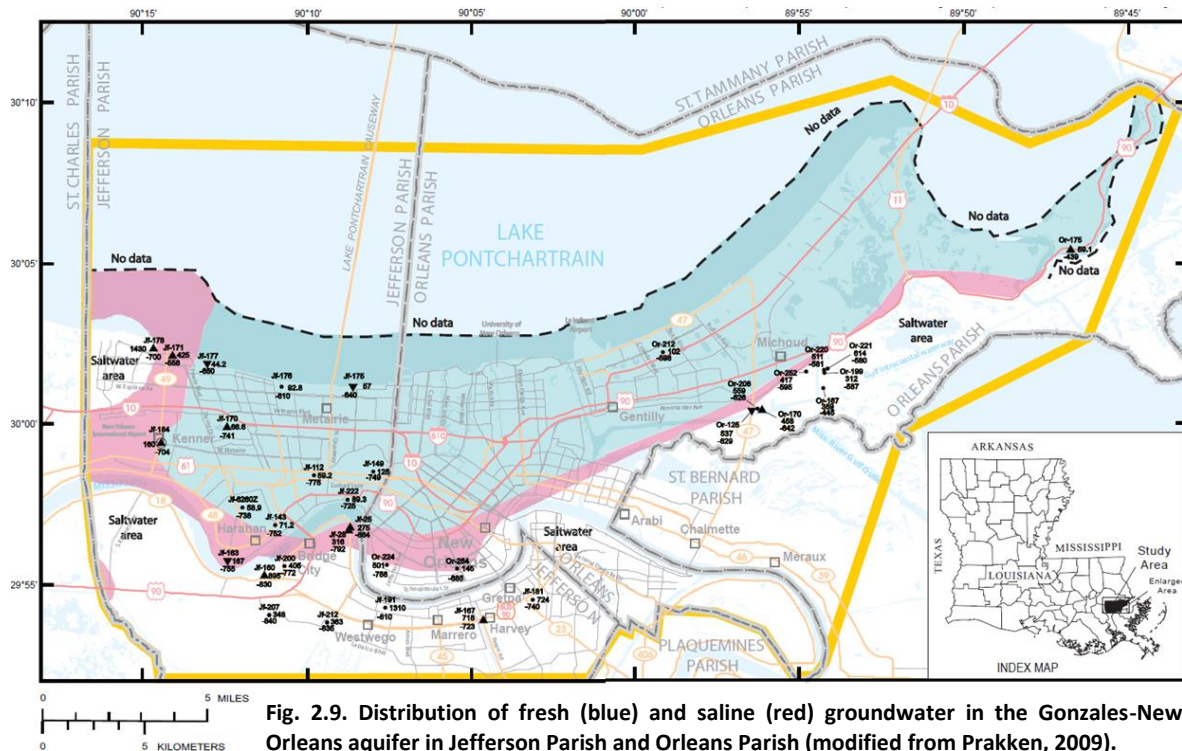
of treated wastewater in the Norco aquifer in Jefferson Parish (Smith & Hanor, 1975) turned out to be unsuccessful, as only a quarter of the initially injected amount of freshwater (757 m^3) could be recovered after 6 days. The remainder could not be recovered as it was flushed by the background groundwater flow.

2.3.6. Subsidence and Sea Level Rise

Subsidence is a major problem in the low-lying parts of Southeastern Louisiana and has already led to significant wetland loss in coastal areas (Meckel et al., 2006). Declining ground surface levels have been omnipresent in Southeastern Louisiana (Shinkle & Dokka, 2004). The current subsidence rates cannot be attributed to a single mechanism, but are related to several natural and anthropogenic processes which can be subdivided into six main categories as summarized by Yuill et al. (2009):

1) Tectonic subsidence due to salt migration and movement along fault systems (e.g. the Baton Rouge fault system)
2) Compaction of Holocene depositional sediments and the deficiency of sediment supply due to anthropogenic measures
3) Sediment loading (section 2.3.2)
4) Glacial isostatic adjustment (section 2.3.2)
5) Gas and oil production and groundwater withdrawals
6) Surface water drainage and changes in surface water storage

These categories are not fully independent, as one process might enhance subsidence related to another process (Yuill et al., 2009). For example, extensive drainage leads to faster compaction of Holocene sediment. The presence and influence of the different mechanisms varies largely across southeastern Louisiana, which is therefore also the case for the total subsidence rate. Subsidence

22

rates vary from less than 1 mm/y up to 30 mm/y (Blum & Roberts, 2009; Nienhuis et al., 2017; Shinkle & Dokka, 2004). In heavily industrialized areas in Southeastern Louisiana, including the Michoud area at the eastern edge of New Orleans, subsidence was found to be mainly determined by groundwater extraction (Dokka, 2011; Jones et al., 2014).

Contributing to the adverse effects of subsidence is eustatic sea level rise. As much of Southeastern Louisiana, including New Orleans, is located at a low elevation, the combination of subsidence and eustatic sea level rise, or relative sea level rise, will cause the occurrence and risk of flooding to increase (Burkett et al., 2003). Different generalized subsidence and sea level rise scenarios for the Mississippi delta plain, which includes large parts of the study area, were summarized by Blum & Roberts (2009). The minimum relative sea level rise by 2100, relative to 2000, was expected to be 0.5 m. In the worst-case scenario, the relative sea level rise was equal to 1.4 m, resulting from a 60 cm eustatic sea level rise and 80 cm of land subsidence (Fig. 2.10).
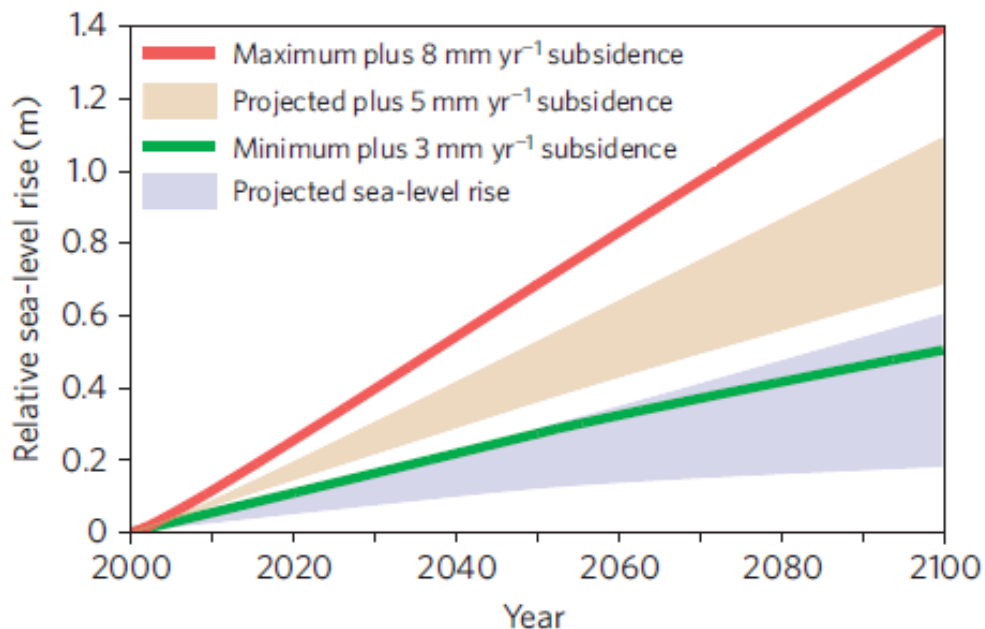
Fig. 2.10. Generalized predictions of relative sea level rise for the Mississippi delta plain (Blum & Roberts, 2009).

23

3. Methods

3.1. Data Acquisition and Modification

3.1.1. Model Setup and Tools

The modelling area was formed by a grid of 237 by 203 cells with a cell size of 1 km^2, thereby covering an area of 48,111 km^2. The location of the modelling area was discussed in Section 2.3.1 and depicted in Fig. 2.3. The used coordinate system is the NAD 1983 StatePlane Louisiana South FIPS 1702 with unit meters (Stem, 1990). Conversion of external data into this coordinate system was done using ArcMap 10.5.1. The variable units used in the model were meters for length, kilograms for mass and days for time.

The coming sections will be used to expand on the collection and modification of the required model input data. Much of the acquired data needed to be converted or modified to contain the correct file format, to fit to the model boundaries and resolution or to estimate the values at locations where no direct data was available. Data was modified using Python 3.6 tools in the Scientific Python Development Environment (SPYDER), iMOD 4.3 and ArcMap 10.5.1. These programs, together with Tecplot 10, were also used for model input and output visualisation and analysis.

3.1.2. Digital Elevation Model

The elevation of the upper boundary of the top model layer was determined using a digital elevation model (DEM), representing the elevation of the earth surface. As a substantial part of the modelling area is covered with estuarine lakes and the Gulf of Mexico, a DEM containing both land topography and bathymetry was needed. Therefore, the General Bathymetric Chart of the Oceans (GEBCO) was used, which combines regional bathymetric compilations and publicly available digital elevation models, mainly derived from the NASA SRTM30 DEM (NASA, 2019). The latest GEBCO_2014 DEM with a grid spacing of 30 arc sec was used in the model (Weatherall et al., 2015). This version is available on: https://www.gebco.net/data_and_products/gridded_bathymetry_data/. Fig. 3.1 shows the resulting DEM, converted to the cell size and coordinate system used in this study (Section 3.1.1). Note that the hilly northern parts of the study area and the flat Mississippi Delta Plain can be easily distinguished in Fig. 3.1.

3.1.3. Geology

As the geology throughout southeastern Louisiana is extremely complex and accurate information is limited to specific regions such as the New Orleans area (Ayrer, 2013; Ayrer & Wicks, 2013) and the Baton Rouge area (Pham & Tsai, 2017), a simplified geology was used in this research, based on the transects attached to the work of Griffith (2003). The Mississippi River Alluvial aquifer and the fault systems were not incorporated in the model, as both are of little importance in the New Orleans area. Although information on the hydrogeology of the State of Mississippi is even scarcer, the general hydrogeological framework is similar to the one in southeastern Louisiana, with generally southward dipping aquifers (Lang, 1972). The geology was therefore assumed to be continuous across the Louisiana-Mississippi State border. The shallow aquifers of the New Orleans area and point-bar deposits were also ignored, as these are absent in large parts of the New Orleans area and
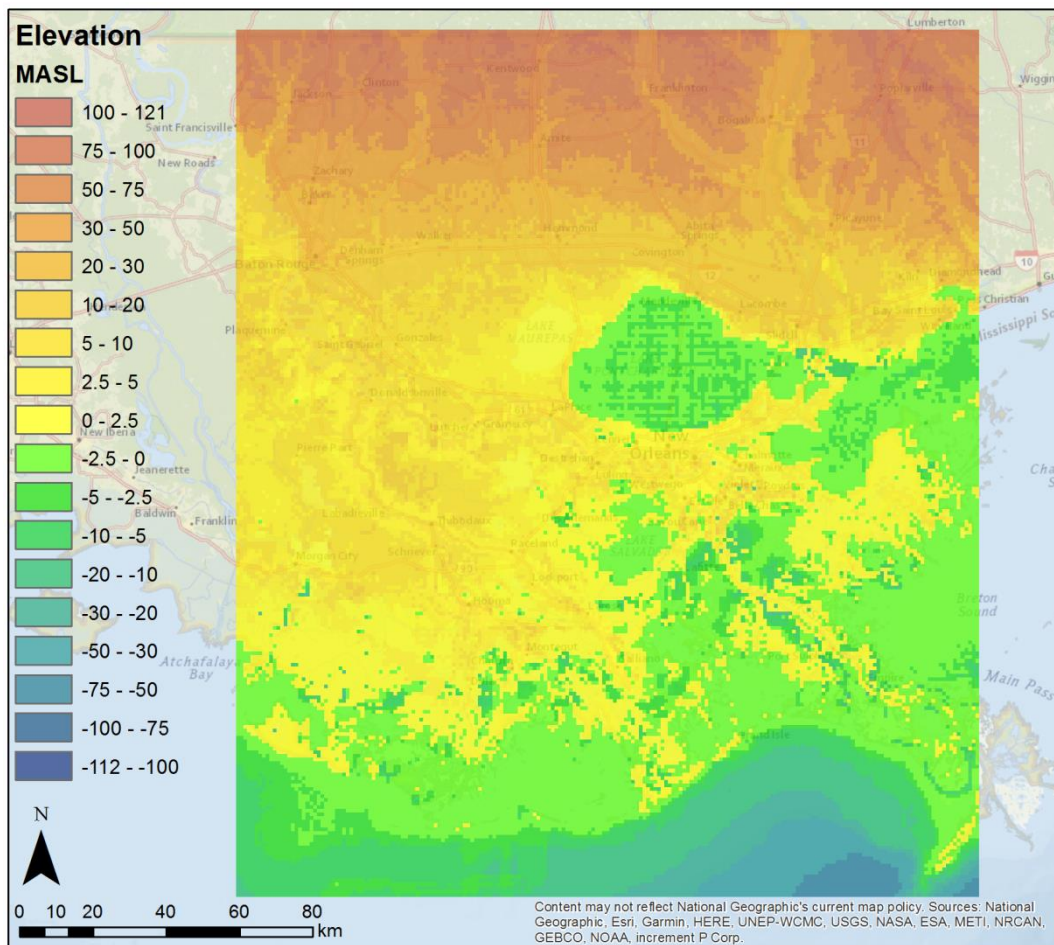
Fig. 3.1. GEBCO_2014 Digital Elevation Model (Weatherall et al., 2015) of the study area, used as the top of the groundwater model presented in this study.

do not contain significant amounts of fresh groundwater (Prakken, 2009). Consequently, only the Southern Hills regional aquifer system and the Catahoula equivalent aquifer system were taken into account in the model. The bottom depth of each aquifer and confining layer of these aquifers was estimated at 5 different locations in the Eastern Florida Parishes and the New Orleans area using respectively transect *H'H''*, *I'I''*, *J'J''*, *K'K''* and *L'L''* and the southern part of *DD'* (Fig. 2.7) of Griffith (2003). The main assumption made for creating the simplified geology was that layer thickness only varies in the north-south direction, i.e. that the thickness and depth of each layer is constant in the east-west direction, or the x-direction in the model.

A total number of 15 aquifers were distinguished in the study area, 14 of which comprised the entire Southern Hills regional aquifer system. All these aquifers were assumed to be separated by confining layers. Corresponding aquifers with different nomenclature for the New Orleans area and Eastern Florida Parishes, and the Baton Rouge area were linked based on Figure 3 in Griffith (2003), which can be found in Appendix A. The aquifers and confining units corresponding to the different model layers were summarized in Table 3.1.

The model layers were then created by connecting the bottom depth points for each layer linearly, i.e., creating straight lines between subsequent data points for each layer and continuing the slopes

25

Table 3.1. Used model geology and the corresponding aquifers in southeastern Louisiana, including the (ranges of) hydraulic conductivity corresponding to each layer. Colours on the left hand side represent aquifer systems as displayed in Fig. 3.2: Red = Chicot equivalent aquifer system, blue = Evangeline equivalent aquifer system, green = Jasper equivalent aquifer system & orange = Catahoula equivalent aquifer system. Layer types: (H)C = (Holocene) confining layer & A = aquifer.

Layer number	Layer type	Aquifer unit Eastern Florida Parishes	Aquifer unit Baton Rouge area	Horizontal Hydraulic Conductivity (m/day)
1	HC	-	-	0.005
2	HC	-	-	0.005
3	HC	-	-	0.005
4	HC	-	-	0.005
5	A	Gramercy	*Not present*	53.3
6	C	-	-	2E-4 - 3E-5
7	A	Norco	*Not present*	51.8
8	C	-	-	2E-4 - 2E-5
9	A	Gonzales-New Orleans	*Not present*	38.1
10	C	-	-	2E-4 - 2E-5
11	A	"1200-foot"	"400-foot"	30.5
12	C	-	-	1E-4 - 2E-5
13	A	Upland Terrace/Upper Ponchatoula	"600-foot"	54.9
14	C	-	-	1E-4 - 2E-5
15	A	Lower Ponchatoula	"800-foot" & "1000-foot"	15.2
16	C	-	-	1E-5 - 1E-5
17	A	Big Branch	"1200-foot"	22.4
18	C	-	-	9E-5 - 9E-6
19	A	Abita	"1500-foot"	36.6
20	C	-	-	8E-5 - 8E-6
21	A	Covington	"1700-foot"	67.1
22	C	-	-	7E-5 - 7E-6
23	A	Slidell	"1700-foot"	57.9
24	C	-	-	6E-5 - 7E-6
25	A	Tchefuncte	"2000-foot"	30.5
26	C	-	-	5E-5 - 7E-6
27	A	Hammond	"2000-foot" & "2400-foot"	43.4
28	C	-	-	4E-5 - 6E-6
29	A	Amite	"2400-foot" & "2800-foot"	45.7
30	C	-	-	3E-5 - 6E-6
31	A	Ramsay	"2800-foot"	65.2
32	C	-	-	2E-5 - 6E-6
33	A	Franklington	Catahoula	88.4
34	C	-	-	7.0E-7

at the outer data points towards the northern and southern model area boundaries. The used linear relationship was expressed in equation form as:

$$z_{x,y,i} = z_{x,y_1,i} + \frac{z_{x,y_2,i} - z_{x,y_1,i}}{y_2 - y_1} * (y - y_1) \qquad (3.1)$$

Where $z_{x,y,i}$ (m) is the elevation of the bottom of layer i in the model cell x, y and $z_{x,y_1,i}$ and $z_{x,y_2,i}$ (m) are the bottom elevations at the used observation points x, y_1 and x, y_2 as derived from the transects provided by Griffith (2003).

To maintain the stratigraphic order of the Southern Hills aquifer system, a minimum thickness was assumed for each model layer. This minimum value was set to 5 meter, as very small model layer thicknesses could harm the model performance and lead to prolonged simulation times resulting from very small solute transport calculation time steps. The assignment of this minimum value was done using the following equation:

$$z_{x,y,i} = z_{x,y,i-1} - 5 \qquad \left(if\ z_{x,y,i-1} - z_{x,y,i} < 5\right) \tag{3.2}$$

Where $z_{x,y,i-1}$ is the bottom elevation of the layer on top of layer i. The bottom clay layer was a model boundary layer and was therefore given a constant thickness of 30 meters. The top Holocene confining layer was divided into four model layers each containing a quadrant of the distance between the DEM and the top of the Gramercy aquifer or model layer 5. Following the previous discussion, a southward dipping geology containing 34 model layers representing the Southern Hills regional aquifer system and the top aquifer of the Catahoula equivalent aquifer system was created. A schematic representation of the three-dimensional model geology is depicted in Fig. 3.2. The total model extent now consisted of a grid of 203x237x34 and elevation values of the model, including DEM, ranged from 121 m above to 2788 m below mean sea level.
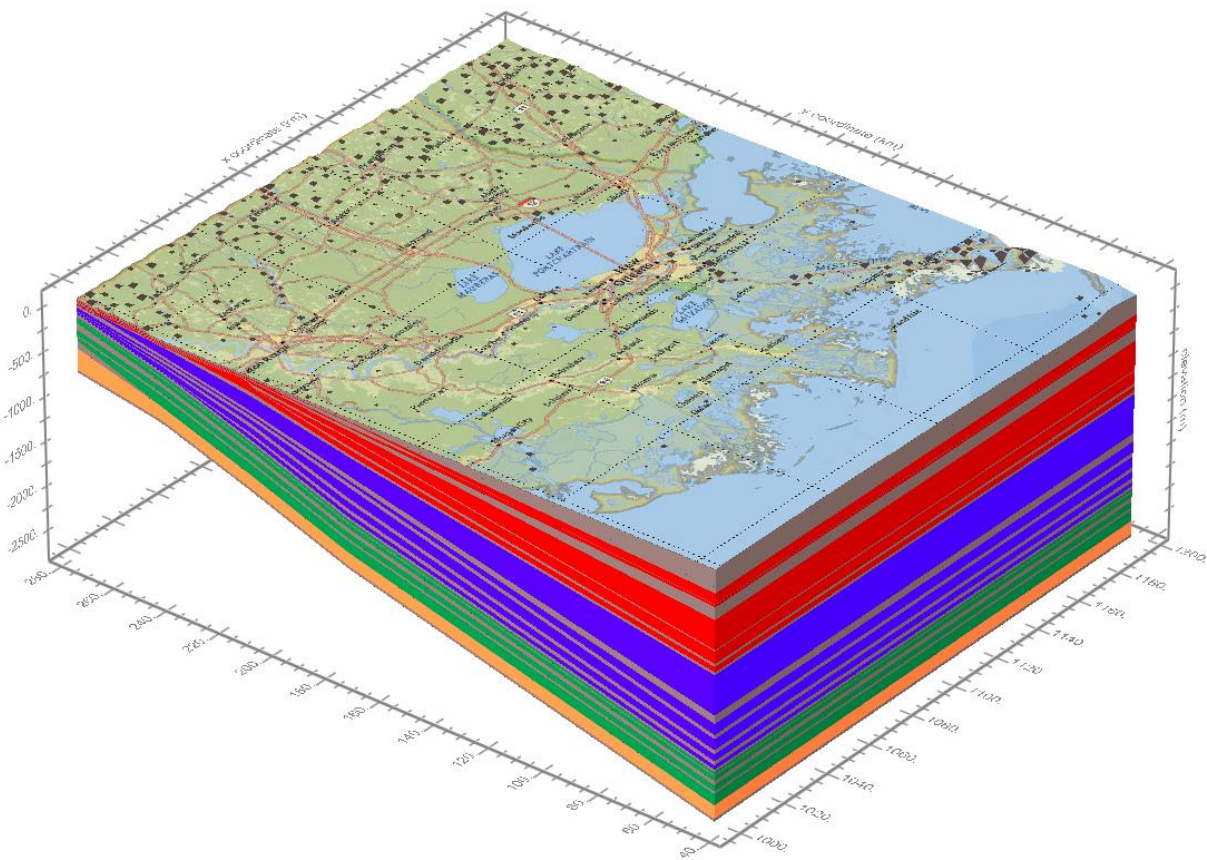
Fig. 3.2. Schematic representation of the model geology. Confining layers are depicted in greyish brown. Other colours correspond to the aquifers of the aquifer systems as summarized in Table 3.1. (Red = Chicot equivalent aquifer system, blue = Evangeline equivalent aquifer system, green = Jasper equivalent aquifer system & orange = Catahoula equivalent aquifer system.

3.1.4. Hydraulic conductivity

Similar to the geology, the hydraulic conductivity values of the aquifers for the entire study area were estimated based on the available information for the New Orleans area and the Eastern Florida Parishes. In this section, hydraulic conductivity refers to the horizontal hydraulic conductivity, from which the vertical conductivity values were derived (Section 3.2.3).

Estimates of hydraulic conductivity values of the aquifers of southeastern Louisiana were summarized from previous studies by Griffith (2003). The hydraulic conductivities of the 4 upper aquifers were retrieved from measurements and estimates in the Gramercy Area (Dial & Kilburn, 1980) and around New Orleans (Dial & Sumner, 1989), while the conductivities for the 11 remaining aquifers were derived from measurements in Tangipahoa Parish and Saint Tammany Parish (Nyman & Fayard, 1978).

Compaction of aquifers was assumed to be negligible and therefore their hydraulic conductivity was considered to be constant with depth. Confining clay layers, however, are subject to compaction (Muskat, 1937, p.17). As the depth of the clay layers in the modelled aquifer system increased going south, the hydraulic conductivity of the clay layers could not be assumed to be constant. In this study, the hydraulic conductivity of the clay layers was estimated similar to the approach used for estimation of the hydraulic conductivity of the confining layers in the New Orleans area by Dial & Sumner (1989), who combined the relationship between hydraulic conductivity and porosity with the relationship between burial depth and clay porosity to link the clay burial depth to horizontal hydraulic conductivity.

The relation between porosity and burial depth for shales in coastal Louisiana was plotted by Dickinson (1953). The adapted version of this graph, Figure 17 in Dial & Sumner (1989), was used to find the equation relating these two parameters, as no equation was given in both studies. The used equation was equal to the third order polynomial trend line through the data points deduced from that figure for burial depths of 0, 500, 1000, 1500 and 2000 feet. These data points and the corresponding trend line are depicted in Fig. 3.3a. The corresponding equation, with n (-) as the porosity and z as the burial depth in feet, was given by:
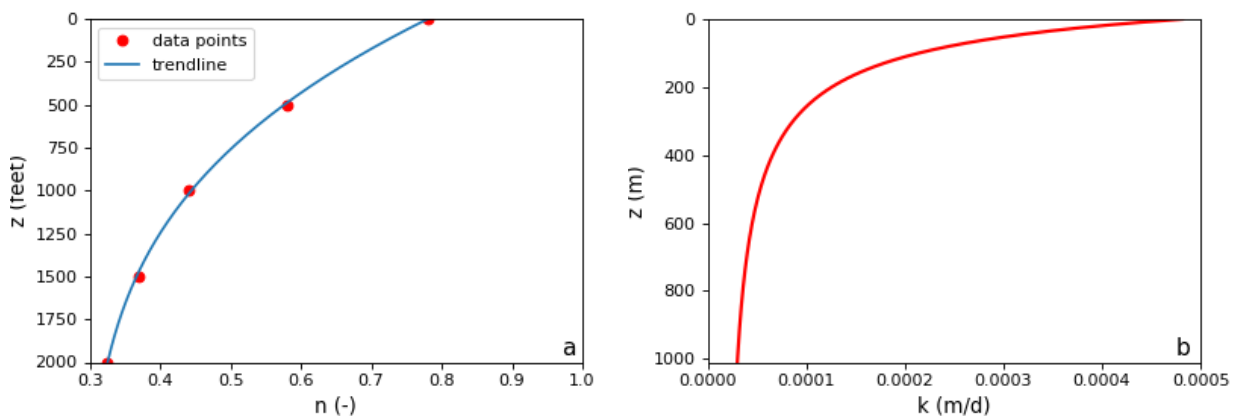
Fig. 3.3. (a) Recreated relation of depth in feet versus porosity for clay layers based on Figure 17 of Dial and Sumner (1989). The equation corresponding to the resulting trendline was used to calculate the hydraulic conductivity of clay at a certain depth. (b) Depth (m) versus hydraulic conductivity (m/d) as used in the model.

28

$$n = -2.33 * 10^{-11} * z^{-3} + 1.79 * 10^{-7} * z^2 - 0.00049 * z + 0.78 \tag{3.3}$$

After calculating the porosity for every model cell of the confining layers, the hydraulic conductivity values were calculated using the following equation as defined by Dial & Sumner (1989):

$$K = K_{ref} e^{C(v - v_{ref})} \tag{3.4}$$

Where:
o K = hydraulic conductivity (ft/d)
o K_{ref} = reference hydraulic conductivity at burial depth of 1000 feet (ft/d)
o C = slope of log-transformed hydraulic conductivity against void ratio (-)
o v_{ref} = reference void ratio at burial depth of 1000 feet (-)
o v = void ratio (-), a function of porosity (n) defined as:

$$v = \frac{n}{1 - n} \tag{3.5}$$

Using calibration of the model based on hydraulic head observations, Dial & Sumner (1989) found the best simulation for C = 1 and K_{ref} = 1.0 x 10^{-4} ft/d (or 3.0 x 10^{-5} m/d). As their study was conducted in a part of the study area of this research, these parameter values were also used here for the calculation of the hydraulic conductivities. Since v_{ref} is equal to the void ratio at a burial depth of 1000 feet, its value, equal to 0.80, was determined by solving Eq. (3.3) and Eq. (3.4.) for z = 1000 feet. This method was used to determine the hydraulic conductivity of the confining layers in the model, using the midpoint elevation of each confining layer model cell as input depth. The resulting relation between hydraulic conductivity and depth, after conversion to m/d, is given in Fig. 3.3b and the ranges for each confining layer of the model in Table 3.1.

The hydraulic conductivities of the top and bottom confining layers were not determined using the method described above. The hydraulic conductivity of the top confining layer was assumed to be 0.005 m/d, which was based on the order of magnitude found by Hanor (1993) at clay beds in the western part of the study area. The bottom aquitard was assumed to be impenetrable bottom of the modelled aquifer system and was therefore given a very small constant hydraulic conductivity value of 7.0 x 10^{-7} m/d.

Due to the southward dip of the modelled aquifer system, some of the aquifers and confining layers crop inside the study area and are therefore not present in the northernmost parts of the study area (Dial & Sumner, 1989; Griffith, 2003; Tomaszewski, 2003). However, iMOD-SEAWAT required each model layer to be present throughout the entire modelling area. Therefore, the cropped layers were still present in the northern parts of the study area as layers with a thickness of 5 meters following the discussion in Section 3.1.3, creating a set of thin, alternating aquifers and clay layers near the surface in the northern parts of the modelling area (Fig. 3.2). To cancel the effect of these 'non-existent' layers, the hydraulic conductivity value of a model cell with a thickness of 5 m was converted to the hydraulic conductivity value of the first model cell directly below with a cell thickness larger than 5 m.
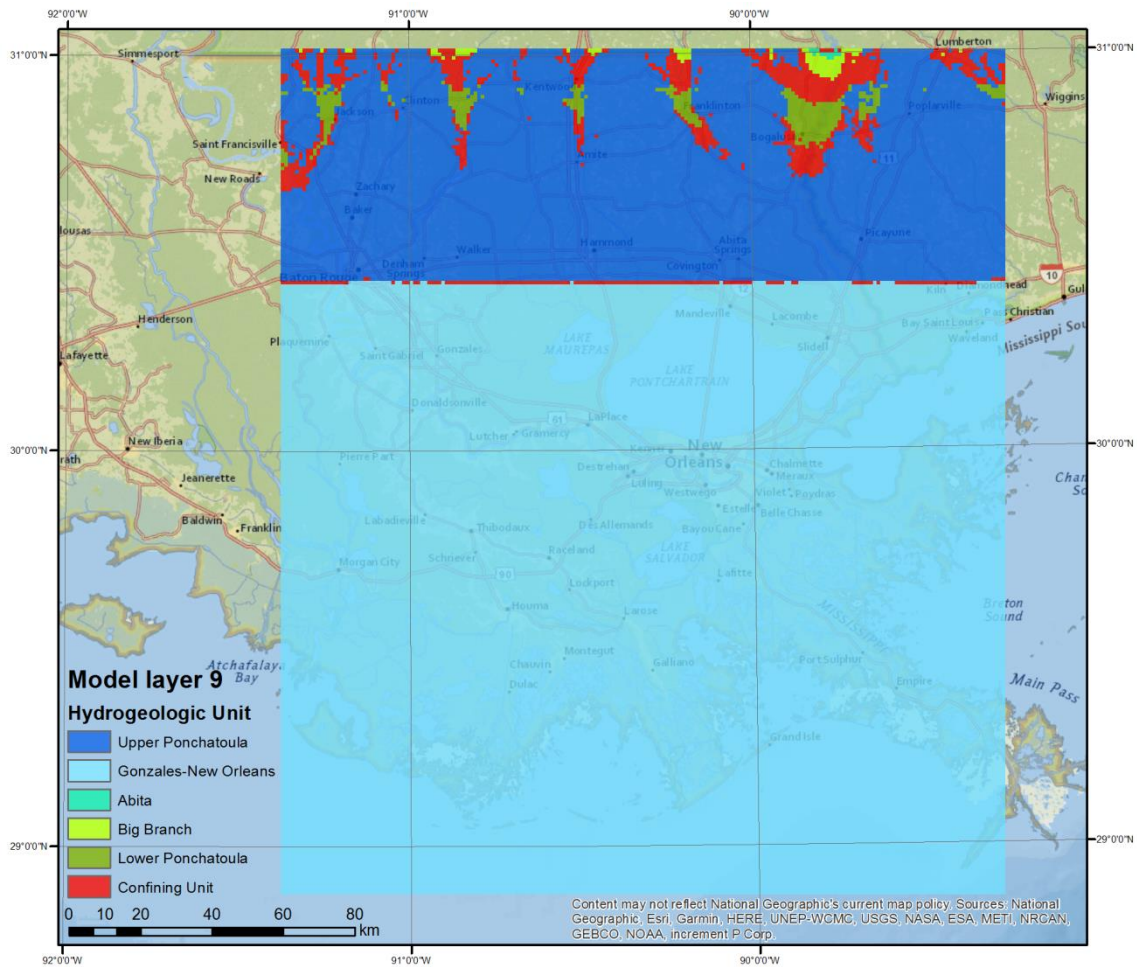
Fig. 3.4. Hydrogeological units corresponding to the hydraulic conductivity values used for model layer 9. The corresponding conductivity values can be found in Table 3.1.

As a result of this hydraulic conductivity correction, a single model layer could now contain multiple hydraulic conductivities representing different hydrogeological units. An example is given in Fig. 3.4, showing the geologic units corresponding to the hydraulic conductivity value at a certain location in model layer 9. In the original geologic setup, this model layer resembled the Gonzales-New Orleans aquifer only and the model layer still represented this aquifer in the southern part of the study area after the correction. In the northern part of the study area, however, the Gonzales-New Orleans aquifer did not determine the hydraulic conductivity anymore, as the outcrop area of this aquifer is in the area directly to the north of Lake Pontchartrain (Section 2.3.3.2), which is in agreement with the available literature (Dial & Sumner, 1989; Griffith, 2003). In the northern parts of the study area, where the thickness of model layer 9 was equal to 5.0 m, the hydraulic conductivity was now mainly determined by the Upland Terrace or Upper Ponchatoula aquifer, the first aquifer from the top of the system present throughout the entire study area (Griffith, 2003). In the river valleys (compare Fig. 3.1 to Fig. 3.4), even deeper aquifers and confining layers surface.

3.1.5. Initial Distribution of Fresh and Saline Groundwater

To properly project the future changes of the fresh groundwater availability due to saltwater intrusion processes, an accurate representation of the initial (current) groundwater salinity distribution in the modelling area was of major importance. There are several ways to express

salinity; the two most widely-used being chloride concentration and total dissolved solids (TDS) content. In this report, salinity was defined as the latter and will be also referred to as salinity or salt concentration throughout the remainder of this report. In the model, the maximum and minimum TDS concentrations were set to 35.0 kg/m^3 (seawater salinity) and 0.01 kg/m^3. Data on groundwater salinity was available and derived from the U.S. Geological Survey (USGS, 2019b). However, the salinity measurements for each model layer did not cover the entire study area, but were often clustered in specific regions. Especially data of brackish to saline groundwater was unavailable for large parts of the study area. Therefore, a threefold approach was used to estimate the initial TDS concentration distribution as accurately as possible. Firstly, a distinction was made between regions containing respectively fresh groundwater and brackish to saline groundwater based on the transects published by Griffith (2003) and Tomaszewski (2003), as explained in more detail in Section 3.1.5.1. This way, an initial estimate of the salinity distribution was created for the entire modelling area. Secondly, the available groundwater quality data was collected and interpolated for each aquifer (Section 3.1.5.2). The interpolated salinity distribution was then assigned to the initial distribution from transect interpolation wherever groundwater quality data was available. Thirdly, a mixing zone was created to eliminate sharp interface between fresh and saline groundwater based on a linear concentration gradient and the distribution of the confining layers was recalculated by averaging the values of the surrounding aquifers (Section 3.1.5.3).

3.1.5.1. Interpolation of Aquifer Transects

The initial estimate of the salinity distribution was based on the transects provided by Griffith (2003) and Tomaszewski (2003). The study of the former covered the Southern Hills regional aquifer system and the top aquifer of the Catahoula equivalent aquifer system in southeastern Louisiana from the Louisiana-Mississippi state border in the north to the furthest extent of fresh groundwater in the south, slightly south of New Orleans. The study by Tomaszewski (2003) was focussed on the aquifers present in the New Orleans area along the Mississippi River. In both studies, no chloride concentrations were given, but distinction was made between fresh ($c_{cl-} \leq 250$ mg/l) and saline ($c_{cl-} > 250$ mg/l) water, corresponding to a TDS concentration of approximately 0.45 kg/m^3. As a first step, the altitude of the interfaces between fresh and saline groundwater was estimated from the boreholes depicted in the cross sections. The cross sections only contained information on the presence of fresh and saline groundwater in the aquifers, and not in the confining layers. Therefore, in the case that two subsequent aquifers contained respectively fresh and saline groundwater or vice versa, the interface elevation was estimated as the midpoint of the intermediate confining layer. Each interface depth was labelled either 'fresh' or 'saline' to store the salinity of the water in the column beneath the interface.

A total number of 141 depicted wells were extrapolated, including 15 present in both studies. Every single borehole from the study conducted by Tomaszewski (2003) was used, while some of the boreholes in the north-western part of the research by Griffith (2003) were omitted, as they were outside of the study area. Coordinates of the well logs were either retrieved from the U.S. Geological Survey (USGS, 2019b) or estimated from the overview map provided by (Griffith, 2003). The locations of the used boreholes are depicted in Fig. 3.5.

To estimate of the distribution of fresh and saline groundwater outside of the study areas of Tomaszewski (2003) and Griffith (2003), nine additional 'boreholes' were created (Fig. 3.5). Eight of these boreholes contained only saline groundwater and their location was based on different groundwater resources reports published by the USGS. One of these artificial boreholes was located in each of Jefferson Parish (based on Prakken & Lovelace, 2014), Lafourche Parish (Prakken & Lovelace, 2013b), Terrebonne Parish (Prakken et al., 2014b) and Plaquemines Parish (Prakken, 2013a), while two were located in both Assumption Parish (Prakken & Lovelace, 2013a) and Saint Bernard Parish (Prakken, 2013b). The last artificial borehole was located in Assumption Parish and the interface depth of this borehole was based on the fresh groundwater depth given by Prakken & Lovelace (2013a).

The acquired borehole information was converted into an iMOD Point File (or ipf-file), which enabled visualisation of the boreholes in iMOD 4.3 (Fig. 3.6). The iMOD Solid Tool (Vermeulen et al., 2017) was used to connect boreholes using a set of cross sections. In these cross sections, the interfaces between fresh and saline groundwater layers were drawn by using 10 elevation lines, the odd lines (1,3,5,7,9) representing the top of fresh groundwater layers and therefore the bottom of saltwater layers, while the even lines (2,4,6,8,10) represented the bottom of fresh groundwater layers. These lines were always ordered top-down from 1 to 10.

Fig. 3.5. IPF well locations used for the interpolation of the aquifer transects including the source of information stored in the IPF-files. The blue line represents the location of the transect depicted in Fig. 3.7.

Fig. 3.6. 3D visualisation of the IPF-boreholes used for transect interpolation. Sources of the boreholes are given in Fig. 3.5.
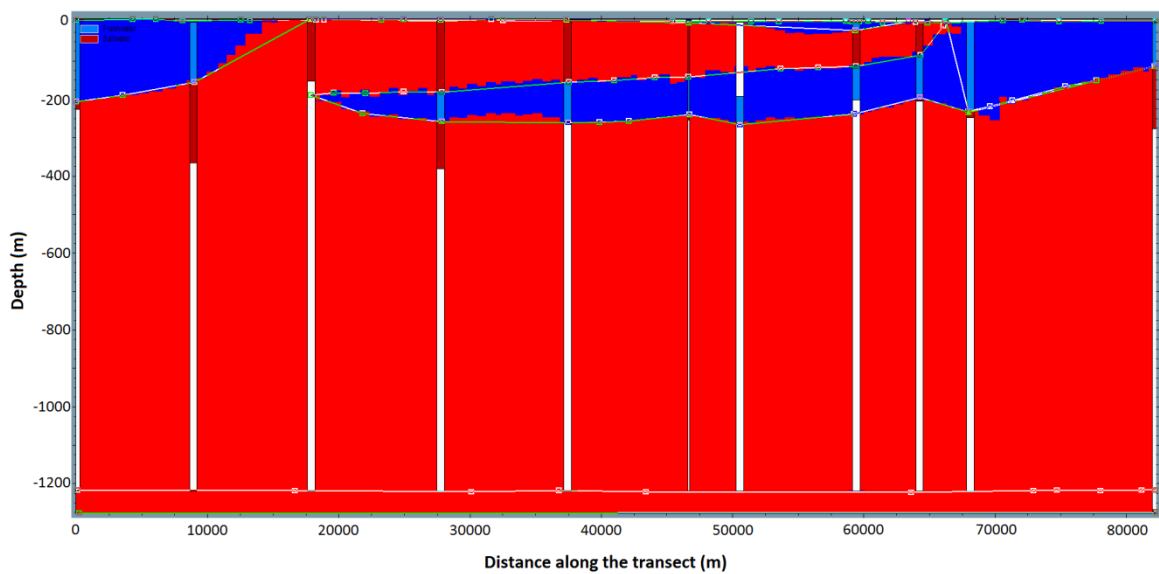
Fig. 3.7. Example transect of the interpolated 3D salinity distribution based on the information in the depicted wells. The transect location is depicted in Fig. 3.5.

33

The interpolation of the cross sections into a three-dimensional solid was done using ordinary kriging. The semivariogram properties were calibrated until the general pattern of the created distribution of fresh and saline groundwater corresponded to the patterns found in the transects by Griffith (2003) and Tomaszewski (2003). Interpolation led to a distribution corresponding the most to the transects using a spherical semivariogram with a sill of 1.0 x 10^5 m, a range of 5.0 x 10^6 m and nugget of 0.0 m. One of the transects used for interpolation is given in Fig. 3.7, blue and red representing respectively fresh and saline groundwater. 15 additional cross sections were created to validate the created solid and to deal with some clear errors resulting from the interpolation, leading to a total of 40 transects used. The elevation lines in the cross sections were redrawn and interpolated multiple times, until the remaining major flaws visible in the solid were eliminated.

The created distribution of fresh and saline groundwater was used to assign initial TDS concentrations and groundwater density values to the model grid. For saline water, these values were respectively set to 35 kg/m^3 and 1025 kg/m^3, representing seawater, and for freshwater to 0.1 kg/m^3 and 1000 kg/m^3. These values were assigned to the model geology (Section 3.1.3) by looking at the nearest interface of the created salinity distribution solid underlying the centre of each model layer for each model cell. An even interface number corresponded to fresh groundwater values and an odd interface number to saline groundwater water values, as explained previously. The resulting distribution of fresh and saline groundwater in model layer 11 (resembling the 1200-foot aquifer) is depicted in Fig. 3.8a.

3.1.5.2. Interpolation of Groundwater Quality Data

After the initial estimation of the distribution of fresh and saline groundwater as derived from the transects was completed, it was improved using the available groundwater quality data for the Southern Hills regional aquifer system and the top aquifer of the Catahoula equivalent aquifer system, which was derived from the U.S. Geological Survey (USGS, 2019b). Data on the groundwater salinity (or TDS concentration) was not readily available. Therefore, the TDS concentration was based on the available specific conductance data and then converted to TDS concentration using Eq. (2.1). For some aquifers, the availability of recent water quality data was limited. Hence, all available specific conductance values, dating back to the 1940s, were used. A total number of 8320 observations were acquired for the aquifer system, ranging between 207 for model layer 23 or the Slidell aquifer to 1076 for model layer 19 or the Abita aquifer. No salinity measurements were available for the southern and easternmost parts of the study area. In general, the data points of deeper aquifers were clustered in the more northern parts of the study area, while the observations of the shallower aquifers were largely available around the latitude of New Orleans. For some aquifers, the data availability was extending to the west and north beyond the model area boundaries. Data points outside of the model boundaries were also incorporated for interpolation.

The gathered salinity point values were stored in a single IPF-file for each aquifer and subsequently converted to a raster (IDF-) file by two-dimensional interpolation per model layer using the iMOD interpolation tool. For the sake of consistency, the interpolation method and settings were equal to these used for transect interpolation (Section 3.1.5.1). The interpolation boundaries for each aquifer were set to 5 km outside the outer measurement locations. The interpolated salinity data raster fields, each only covering part of the modelling area, where then superimposed on the initial

estimation based on the transect interpolation. The salinity fields derived from the observation points were converted to density fields using Eq. (2.2) and then added to the density fields derived from transect interpolation. The salinity distribution of the 1200-foot aquifer (model layer 11) after this step is depicted in Fig. 3.8b.

3.1.5.3. Mixing Zone and Salinity of Confining Units

As stated before, data on groundwater salinity is severely lacking in areas containing brackish to saline groundwater. Therefore, most of the saline parts of the aquifer system were assumed to contain seawater salinity (35 kg/m³), being a known quantity. Moreover, seawater salinity was assumed to be the maximum salinity present in the system and assigning seawater salinity to model cells where the absolute value was unknown could be considered as the most conservative (worst-case) estimate. Because of this assumption, cells containing very small fresh groundwater concentrations were adjacent to fully saline (35 kg/m³) model cells at this point.

Due to hydrodynamic dispersion, transition zones are generally present in coastal aquifers at the boundary between fresh and saline groundwater. In these dispersion zones, the salinity of the groundwater increases from freshwater to seawater values (Sherif et al., 1990). The length of this zone varies from a few meters to over 50 km (Sherif & Singh, 1999; Sherif et al., 1990). As in large parts of the study area, this mixing zone was missing as a result of the transect interpolation (Section 3.1.5.1), this mixing zone was added in this study to the initial TDS distribution of the model after the transect interpolation and the addition of the interpolated groundwater salinity data fields. In this study, the mixing zone length was assumed to be 15 km.

The mixing zone for each aquifer was assumed to be present in the model cells currently containing seawater salinity (C = 35 kg/m³) and located within 15 km of the closest model grid cell with a concentration smaller than seawater salinity. The concentration gradient in the mixing zone was considered to be linear and the salinity value of a model cell located in the mixing zone was therefore determined by the groundwater salinity in the nearest non-seawater cell and the distance to this cell. The salinity values of the dispersion zone cells were then calculated by:
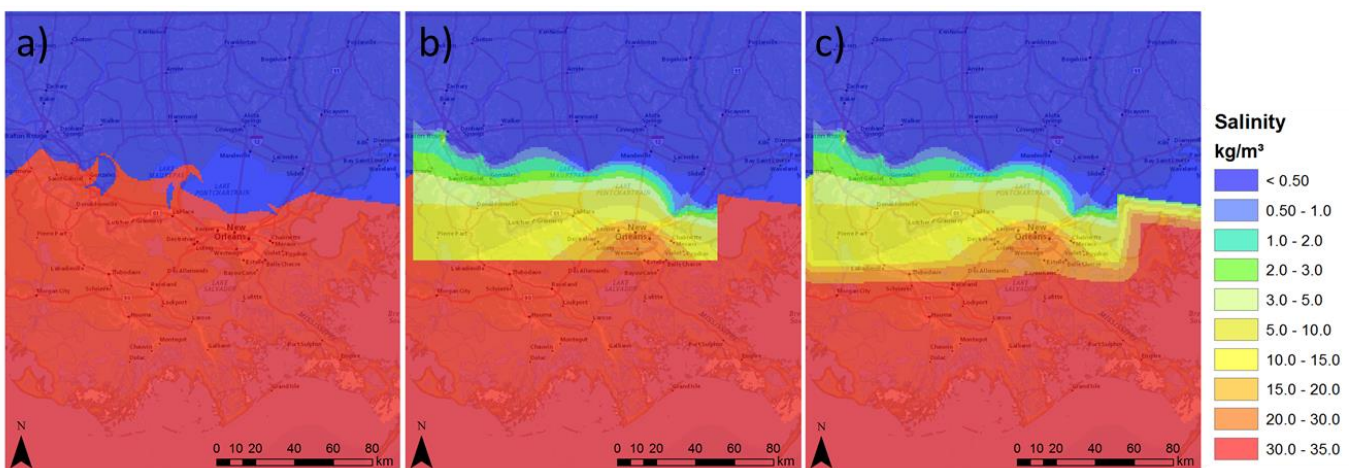
Fig. 3.8. The initial TDS concentration distribution in model layer 11 after (a) transect interpolation, (b) groundwater quality data interpolation and (c) addition of the mixing zone.

35

$$C_m = C_s - \frac{15 - d_{mc}}{15} * (C_s - C_c) \tag{3.6}$$

Where:
- o C_m = TDS concentration of the mixing zone cell (kg/m^3)
- o C_s = TDS concentration of seawater (35 kg/m^3)
- o C_c = concentration (kg/m^3) in the model cell closest to the mixing zone cell with $C < 35$ kg/m^3
- o d_{mc} = distance (km) between mixing zone cell and closest cell with $C < 35$ kg/m^3

Determination of the distance to and location of the closest model cell with $C < 35$ kg/m^3 and calculation of mixing cell values was executed using a Python 3.6 tool. The resulting salinity distribution for model layer 11 is shown in Fig. 3.8c.

Apart from the aquifers, this method was also applied to the top confining layer (model layer 1 through 4). The TDS concentration of the other confining layers was recalculated, thereby disregarding the result of the transect interpolation, by averaging the salinity values of the vertically adjacent model cells in the aquifers directly above and below that layer using a Python 3.6 tool. In the bottom model layer, the salinity was kept at seawater level. Conversion of salinity to density values to create the input groundwater density raster layers was done using Eq. (2.2).

3.1.6. River Systems

3.1.6.1. River Width, Depth and Conductance
The outline, width and depth of the river systems in the modelling area were obtained from the global river database created by Andreadis, Schumann, & Pavelsky (2013), who made use of simple geometric equations relating river width and depth to discharge, derived from the HydroSHEDS global river network dataset (Lehner et al., 2008). Although significant uncertainties existed in the river database (Andreadis et al., 2013), the width and depth data still provided useful approximations that could be used for the calculation of several model input variables.

In MODFLOW, and therefore in iMOD-SEAWAT, river leakage into the underlying model layer is determined by the head difference between a certain river system cell and the corresponding (top) model layer cell, and by a riverbed conductance value, following Eq. (2.7). The riverbed conductance of a model cell is defined as (Guo & Langevin, 2002):

$$COND = \frac{L \, w \, K_s}{b_s} \tag{3.7}$$

Where:
- o $COND$ = riverbed conductance (m^2/d)
- o L = river segment length in model grid cell (m)
- o w = width of the river (m)
- o K_s = hydraulic conductivity of the river bed (m/d)
- o b_s = thickness of river bottom sediments (m)

The fraction K_s/b_s is the reciprocal of the riverbed resistance (R_s). As both parameters determining the riverbed resistance were unknown and the required data was not readily accessible, the value of R_s was assumed to be 100.0 d throughout the model. As a result, the riverbed conductance was considered to be equal to the width (w) multiplied by the river segment length (L) divided by the riverbed resistance value (100.0 d). Data on the river width was received from the global river data base (Andreadis et al., 2013). The river segment length was estimated to be equal to 2000 m. This value was obtained by multiplying the model cell size (1000 m) by an approximate river sinuosity value of 2.0, which was based on values used and found in several studies (Assine & Silva, 2009; Paz et al., 2008; Timár, 2003). Implementation of these values in Eq. (3.7) led to an estimated value of the river bed conductance equal to twenty times the river width.

3.1.6.2. River Salinity

Similar to the initial groundwater salinity distribution, the salt concentrations and water densities of the river systems were based on specific conductance data. All available data for the study area from 2000 onwards were used. Data for the Mississippi River and the remainder of the streams in the study area were separated as they were considered different river systems in the model (Section 3.2.5). Two additional observations located respectively northwest and northeast of the study area and two points with the concentration of seawater (35 kg/m^3) southwest and southeast of the model boundaries were added to ensure that the entire modelling extent was covered. The data was
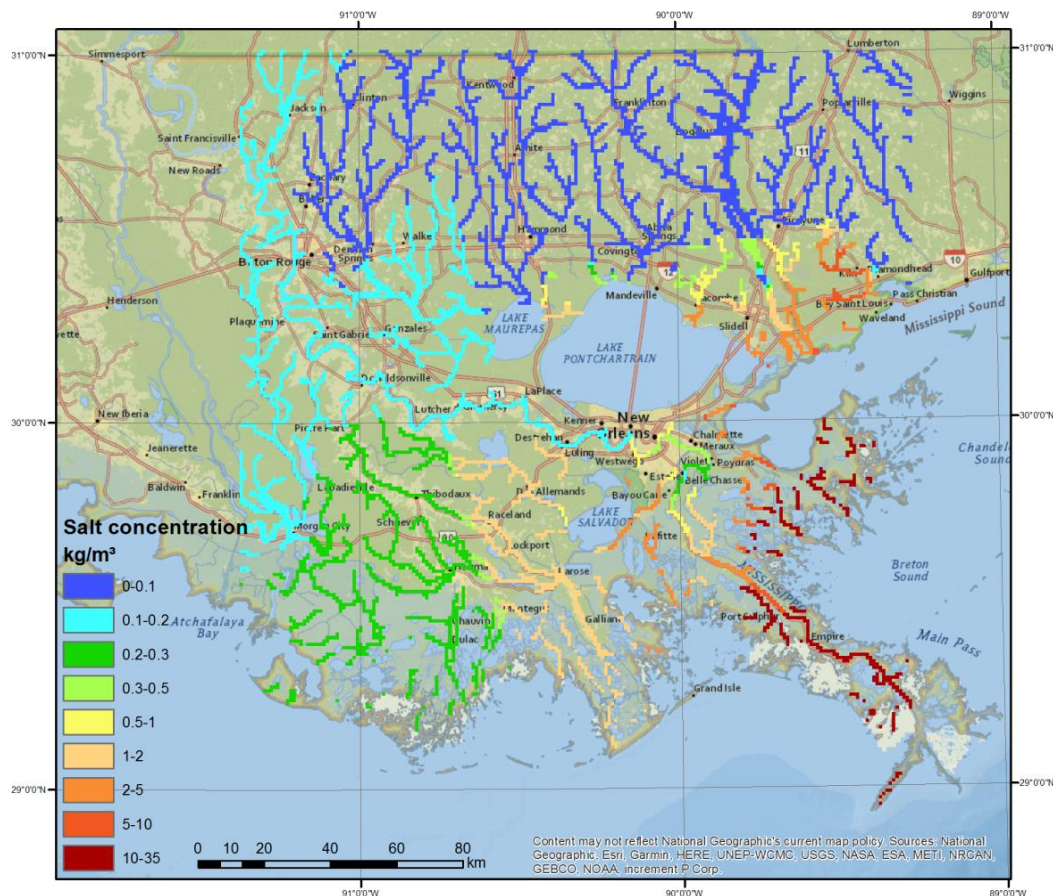
Fig. 3.9. Salinity of the main river systems in southeastern Louisiana used in the model. Salinity values derived from specific conductance values provided by the USGS (USGS, 2019b and USGS, 2019c).

provided by the USGS for both Louisiana (USGS, 2019b) and Mississippi (USGS, 2019c). Specific conductance was converted to salinity (TDS concentration) using Eq. (2.1). Based on the observation points, the river salinity values for both the Mississippi River and the remainder of the river systems were determined using inverse distance weighted interpolation in ArcMap 10.5.1. Concentration values were converted to density values using Eq. (2.2). The river systems and river salinities used in the model are depicted in Fig. 3.9.

3.1.7. Groundwater Extraction Wells

As discussed in Section 2.3.4, groundwater extraction occurs throughout southeastern Louisiana. Data on the exact locations and extraction rates of different pumping wells in the area were unavailable for this study. Therefore, extraction rates were based on the information provided by the USGS in fact sheets published between 2011 and 2017 on the available freshwater resources for each parish. In most of these reports, total extraction rates were provided per subsystem of the Southern Hills regional aquifer system. These values were converted to rates per single aquifer based on the subdivisions within the aquifer system as summarized in Table 3.1.

As the locations and amount of extraction wells was unknown for most parishes, extractions were lumped into one single well for each aquifer in the centre of each parish (Fig. 3.10). However, the central parts of Plaquemines Parish, Ascension Parish, Saint James Parish, Saint Charles Parish and Assumption Parish contained (partly) saline groundwater. Therefore, the location of the wells in
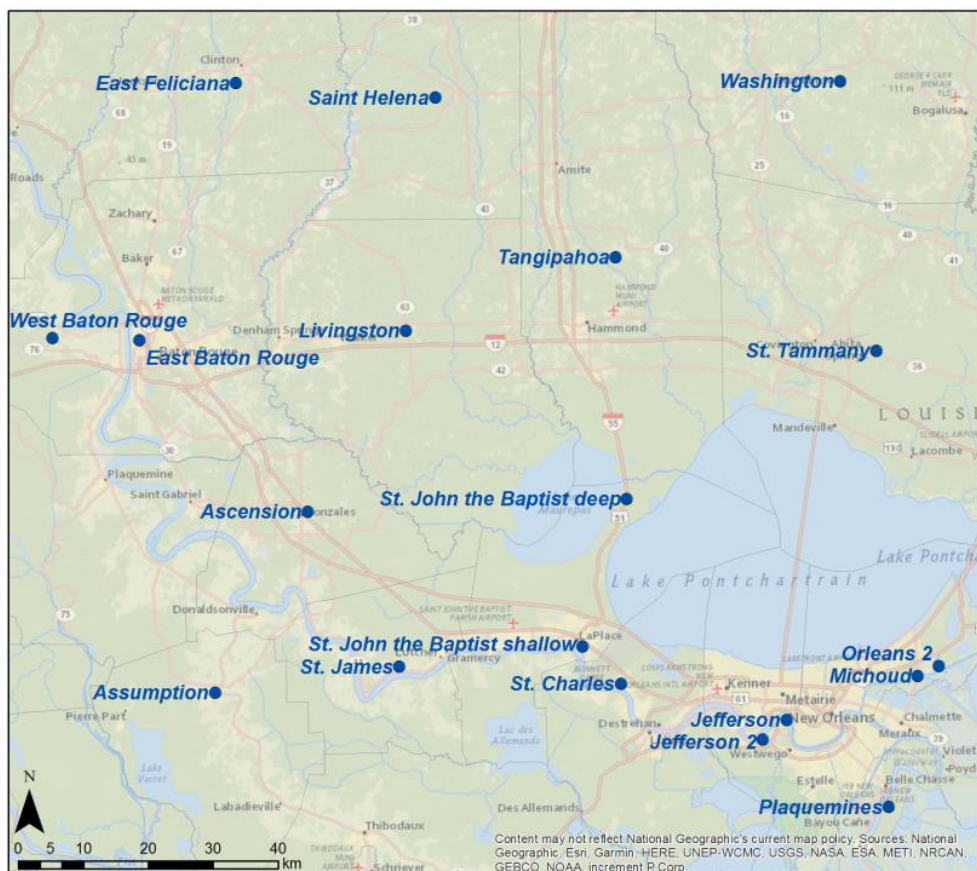
Fig. 3.10. Pumping well locations used in the base model. Parish boundaries are shown in the background image. The pumping wells in Orleans and Jefferson Parish are depicted with more detail in Fig. 3.14.

38

these parishes was adjusted to a location where fresh groundwater was present following the initial distribution of fresh and saline groundwater (Section 3.1.5). For the same reason, two wells were used for Saint John the Baptist Parish (Fig. 3.10), the southern one for the shallow aquifers and the northern one for the deep aquifers. Furthermore, the well in layer 23 of East Feliciana Parish was moved southwards, to prevent it from being located in a confining layer. The location of the wells in East Baton Rouge Parish was based on more detailed information provided by (Tomaszewski, 1996) and was assumed to be equal to the location of the 'Industrial District' well depicted in Fig. 3.12.

In the New Orleans area, four major withdrawal centres were present, two of which were located in Orleans Parish and two in Jefferson Parish. The majority of the groundwater extractions in the New Orleans area were in the Gonzales-New Orleans aquifer, in which all four wells were active. As extraction rates at other locations in the New Orleans area were considered to be negligible compared to these four, the rate used in the model were based on the total amounts per parish given in the corresponding water resource reports and the relative amount pumped at these wells in 2007 as provided by Prakken (2009) compared to the other major well in the parish the given well was located in. The locations of all extraction wells used in this study are depicted in Fig. 3.10 and the rates per aquifer and parish, and the water resource reports they were based on, are summarized in Appendix B.

3.2. Model set up

In this section, the input variables and model parameters collected in the iMOD run-files used to run the model are discussed, following the categorisation of the used input packages of iMOD-SEAWAT. An example of a run-file is attached in Appendix C. This run-file was used for model scenario FS2, which was used to predict the effects of groundwater extraction on the freshwater availability in the New Orleans area in the coming century (Section 3.4.3).

3.2.1. [GEN] General Settings and [DIS] MODFLOW Discretization Package

The spatial properties of the model and time discretization of the desired model runs were assigned in these packages. The modelling extent and model layering were assigned using the collected and created data according to the discussion in Section 3.1.1 through Section 3.1.3. The used modelling timespan and starting year depended on the purposes of a certain model run, but most cases covered a 100-year modelling scenario (Section 3.4.1 – Section 3.4.4). These modelling runs were subdivided into eleven stress periods, starting from present (2019). The first stress period consisted of a single time step of 10^{-4} d (or 8.64 s) and was used to create an initial steady-state hydraulic head distribution based on the input variables. Then, the 100-year modelling period was divided into 10 stress periods of equal length (± 10 years). The input variables used during a stress period could be altered at the start of each stress period. Each stress period was divided into 15 time steps used for variable-density flow calculations. Convergence of the model solution was improved by starting with a small time step at the start of a stress period and doubling it for each subsequent time step within each stress period.

In SEAWAT, the solute transport equation (Eq. (2.5)) was solved as transient (Guo & Langevin, 2002). The variable-density groundwater flow equation (Eq. (2.4)), however, could be solved assuming either steady-state or transient conditions. In steady-state conditions, the head distribution can be assumed to be constant over time for the given set of input parameters, i.e., an equilibrium based on the model input parameters is assumed. Therefore, in steady-state, if a model variable is changed, the hydraulic head is recalculated for the new equilibrium state of the model. In transient conditions, the time it takes to reach this new equilibrium is also incorporated. As the stress-period duration of 10 years used in this model was assumed to be long enough for the model to reach a new equilibrium after perturbations at the beginning of the stress period, each stress period was assumed to be steady-state.

3.2.2. [BAS6] MODFLOW Basic Package

The role of each model cell in the calculation of the variable-density groundwater flow equation (Eq. 2.5) in iMOD-SEAWAT is determined by their so-called IBOUND-value. Model cells are considered to contain a constant hydraulic head (IBOUND = -1), no flow conditions (IBOUND = 0) or a variable hydraulic head (IBOUND = 1). In this study, all model cells were assumed to contain a variable hydraulic head, therefore the IBOUND value of each model cell in each model layer was assumed to be equal to 1.

The first estimate of the initial hydraulic head distribution was created by assuming the head in a given model cell to be equal to the DEM elevation at the same coordinate (Section 3.1.2) for elevations equal to or above mean sea level and equal to 0 m for elevations below mean sea level. Large initial flow velocities reduced the model performance of iMOD-SEAWAT, leading to longer runtimes or in the worst case to no model convergence. Therefore, initial vertical flow was assumed to be non-existent by creating a hydrostatic initial head distribution. To create these conditions, a density correction was applied to the initial head following the discussion in Section 2.2.5. A more detailed description of the implementation of this correction will be given in Section 3.2.4.

3.2.3. [LPF] MODFLOW Layer-Property Package

The horizontal and vertical hydraulic conductivity values for both the aquifers and the confining layers were assigned in this package. The used horizontal hydraulic conductivity values were discussed in Section 3.1.4. The ratio between vertical and horizontal hydraulic conductivity, or the vertical anisotropy, was assumed to be 0.3 for the aquifers. The vertical hydraulic conductivity of the confining layers was assumed to be equal to the horizontal conductivity. No vertical anisotropy was assumed because the horizontal conductivity values of the confining layers in the model were small, in the order of 10^{-4} to 10^{-5} m/d, compared to similar studies (e.g. Giambastiani, Antonellini, Oude Essink, & Stuurman, 2007; Huyakorn, Anders, Mercer, & White, 1987; Oude Essink, 2001; Oude Essink, Van Baaren, & De Louw, 2010). Furthermore, the study by Dial & Sumner (1989), from which the method to determine the hydraulic conductivity of the confining layers was derived, did not specify whether their method was used for calculating the vertical or horizontal hydraulic conductivity values.

3.2.4. [GHB] General Head Boundary Package

Groundwater flow at the general head boundaries is calculated in iMOD-SEAWAT according to Eq. (2.7). The model presented here contained a general head boundary at the edges of the model extent for each layer. In model layer 1, the general head boundary was extended towards the major surface water bodies, which included the Gulf of Mexico, Lake Pontchartrain, Lake Maurepas, Lake Salvador and Lake Cataouatche (Fig. 3.11).

Initially, the input general head boundary hydraulic heads were assumed to be on the elevation of the DEM on land and at 0 m at the major water bodies, except for Lake Maurepas, which is located 2 m above mean sea level. In the hilly northern part of the study area, large elevation differences exist between adjacent model grid cells, which led to large head gradients and therefore high horizontal flow velocities between adjacent general head boundary cells, which negatively affected the model performance. This effect was reduced by averaging the hydraulic head of each GHB model cell with GHB head values in the four adjacent cells, two on each side, using a Python 3.6 tool. This led to a more smoothened GHB head distribution and therefore smaller horizontal flow velocities at the general head boundaries.

In addition, hydrostatic conditions were assumed at the general head boundaries, i.e., vertical
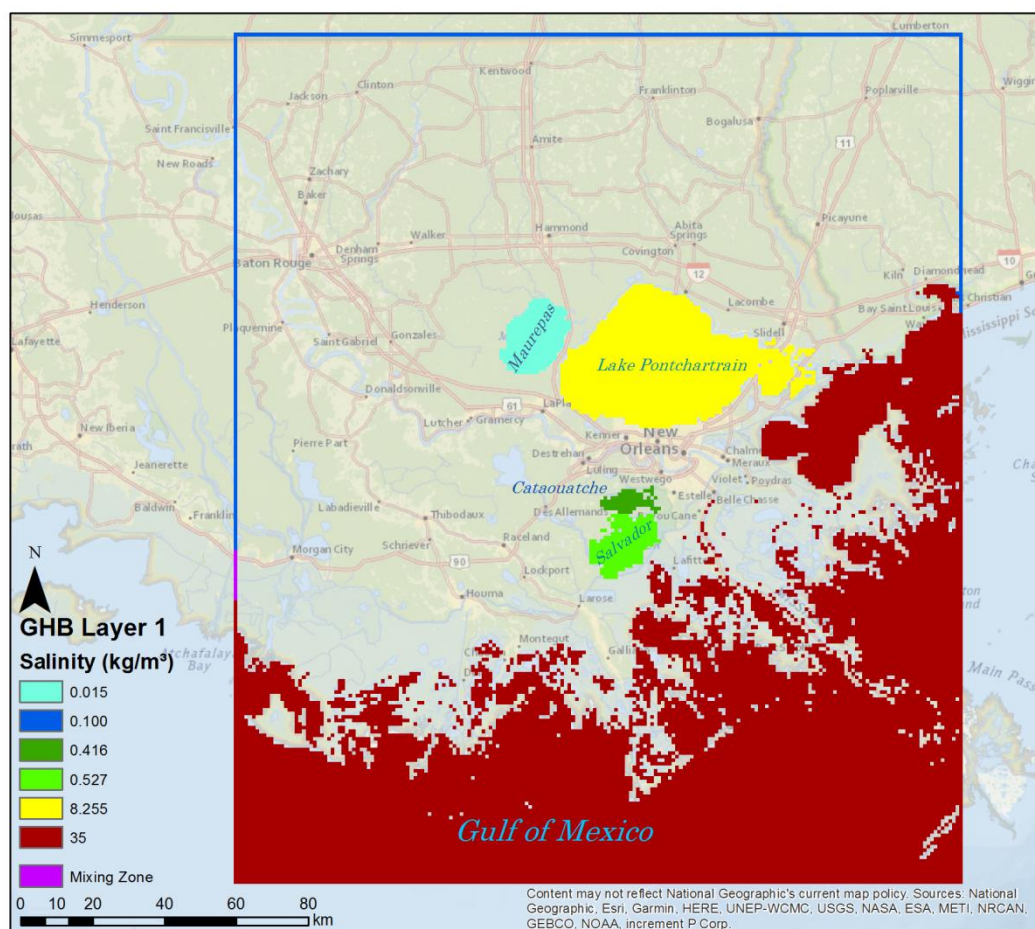
Fig. 3.11. Salinities used for the general head boundary of model layer 1. Values on land derived from the initial distribution of fresh and saline groundwater (Section 3.1.5), values of the lakes from USGS data as summarized in Table 3.2 and the values at the Gulf of Mexico were assumed to resemble seawater.

Table 3.2. Calculated salinity and density of the major lakes in southeastern Louisiana based on USGS data from the given observation period.

Lake	Observation period	Salinity (kg/m^3)	Density (kg/m^3)
Pontchartrain	2005	8.255	1005.90
Maurepas	1975-1981	0.015	1000
Salvador	2007-2012	0.527	1000.38
Cataouatche	2000-2019	0.416	1000.30

groundwater flow was considered to be non-existent. To acquire the needed hydrostatic conditions, the input hydraulic heads were recalculated using a Python 3.6 tool based on the density correction equation (Eq. (2.14)), starting from the initial hydraulic heads (h_0) as described above. The new input point water heads were calculated per boundary cell for the centre of each model layer. To achieve this, half of the correction term Δh_0 (Eq. (2.14)) of the model layer for which the point water head needed to be calculated was assigned before calculation of the new point water head, while the other half was added to the correction term afterwards to be incorporated in the calculations for the next layer.

The water level at the boundaries resembling the major water bodies was assumed to be independent of hydrogeological processes. Therefore, constant head conditions were resembled at the corresponding boundary cells by using a very large conductance ($COND$ = 5.0 x 10^6 m^2/d). The general head boundary on land was allowed to adjust to the hydrogeological conditions and therefore a much smaller conductance value ($COND$ = 100 m^2/d) was assigned to these boundary cells.

Apart from the hydraulic head and conductance, TDS concentration and groundwater density values were allocated to the general head boundary cells. These values were derived from the initial distribution of fresh and saline groundwater, which was discussed in Section 3.1.5. However, this was not the case for the major water bodies. The Gulf of Mexico and the adjacent estuaries and estuarine lakes were assumed to contain seawater values (C = 35 kg/m^3 and ρ = 1025 kg/m^3). Salt concentrations and densities for the major lakes were estimated based on specific conductance sample values provided by the U.S. Geological Survey (USGS, 2019a). Subsequently, specific conductance values were converted to TDS concentrations using Eq. (2.1) and concentrations into groundwater densities using Eq. (2.2). The data availability for the lakes was limited and usually measurements occurred only during a certain timespan. The observation periods, and average concentration and salinity values of these lakes were summarized in Table 3.2. The GHB salinity distribution of model layer 1 is depicted in Fig. 3.11.

3.2.5. [RIV] River Package

Three different river systems were used in the model, the first one being the Mississippi River and the second one the other major streams in the study area as depicted in Fig. 3.9. The hydraulic heads, or the river stages, of these river systems were assumed to be equal to the elevation of the corresponding grid cell derived from the DEM, using a minimum elevation of 0 m. The river bottom elevation was then derived by subtracting the river depth, which was provided by the HydroSHEDS

global database (Section 3.1.6.1), from the river stage. River conductance of these two river systems was assumed to be twenty times the river width, as explained in Section 3.1.6.1.

A third river system was created to mimic the effect of small streams and ditches not included in the HydroSHEDS database. The river bottoms of these streams were assumed to be located 0.5 m below the hydraulic heads, which were set at the DEM elevation. The river conductance of the third river system was set to 250 m^2/d. Following Eq. (3.7), this value corresponded to an area of 25,000 m^2 being covered by these small streams and ditches per model cell, or 2.5% of the cell area. This third river system was present in each model cell on land. All three river systems were assigned to the top model layer. River water densities were assigned based on the discussion in Section 3.1.6.2, using the same interpolation raster field for the second (other major streams) and the third (small streams and ditches) river systems, but a different one based on the available data for the Mississippi River only for the first river system.

3.2.6. [DRN] Drainage Package

The drainage package was used to resemble drainage systems such as agricultural drainage pipes and sewerage. As drainage systems are generally located in the shallow subsurface, the drainage elevation was set to 0.5 below the DEM. The drains were assumed to be present in each model cell on land. Furthermore, this package was used to prevent the hydraulic head in the top model layer from rising above the land surface elevation, resulting from possible model errors. To prevent this seepage of groundwater to the land surface, a large drainage conductance value, equal to 50,000 m^2/d, was applied.

3.2.7. [RCH] Recharge Package

Recharge in the study area was estimated based on the average value of potential recharge found by Beigi & Tsai (2015) for southwestern Mississippi and southeastern Louisiana. This value was equal to 227.5 mm/y or 6.23 x 10^{-4} m/d. Baseflow should be subtracted from the potential recharge to get the actual recharge. However, baseflow values were unknown. As, in the study of Beigi & Tsai (2015), potential recharge in southeastern Louisiana was significantly higher than the average value of their study area, their average value of 6.23 x 10^{-4} m/d was assumed to be valid as the actual recharge rate for southeastern Louisiana. As the used (potential) recharge value included evaporation, the evapotranspiration package ([EVP]), also included in iMOD-SEAWAT, was not used.

3.2.8. [WEL] Well Package

One IPF-file was created for each odd model layer containing the coordinates and rates of the extraction wells in the corresponding aquifer following the discussion in Section 3.1.7. The reference model well locations were shown in Fig. 3.10 and initial extraction rates, used for future groundwater extraction scenario FS1 as discussed in Section 3.4.3, were summarized in Appendix B. The modification and addition of several extraction and infiltration wells used in the different modelling scenarios will be discussed in Section 3.3 and Section 3.4.

3.2.9. [OC] Output Control Options and [PCG] Preconditioned Conjugate-Gradient Package

The model output files and solver conditions for the variable-density groundwater flow equations were assigned in these packages. As a model output, both IDF-files and TEC-files were created to display the results in respectively iMOD 4.3 and TECPLOT 10. The groundwater flow equations were solved using the preconditioned conjugate-gradient package. The used head change criterion (HCLOSE) and residual criterion (RCLOSE) were set to respectively 0.005 m and 10,000 m^3/d. More details on the PCG solver package can be found in Hill (1990).

3.2.10. [BTN] MT3DMS Basic Transport and [SSM] MT3DMS Sink Source Mixing Packages

The BTN package dealt with some basic tasks needed for the MT3DMS solute transport code. It required the model layer thickness as geometry input and these model layer thickness files needed to correspond with the DEM and model layer bottom files defined in the MODFLOW Discretization [DIS] Package (Section 3.2.2) Therefore, the model layer thicknesses were directly derived from the layer tops and bottoms. Other input variables included the initial TDS concentration values (Section 3.1.5), the effective porosity, assumed to have a constant value of 0.3, and the ICBUND boundary. The function of the ICBUND boundary was similar to the IBOUND boundary in the Discretization Package (Section 3.2.1), but this time used for solving the solute transport equation (Eq. 2.5). An ICBUND value of -1, corresponding to constant salinity conditions, was assigned to the GHB cells at the edges of the modelling grid underlying the Gulf of Mexico. The bottom model layer (model layer 34) was assumed to fully saline at all times, therefore the ICBUND of this entire layer was also set to -1. All other model cells were assumed to be active (variable salinity) during the model runs and therefore contained and ICBUND value of 1.

Source concentration for several MODFLOW packages were assigned in the SSM package, including the River and General Head Boundary packages for which the input concentrations were explained in respectively Section 3.1.6 and Section 3.2.4. The input concentration of recharge was assumed to be 0.05 kg/m^3 and the concentration at the drains was determined by the initial TDS concentration in model layer 1 following the discussion in Section 3.1.5.

3.2.11. [ADV] MT3DMS Advection Package and [DSP] Dispersion Package

These packages were used to set conditions for solving the solute-transport equation (Eq. (2.5)). The total-variation-diminishing (TVD) solver was used for the solving the advection part of this equation, as it is known to provide accurate solutions when sharp fresh-saltwater interfaces are present (Guo & Langevin, 2002). The required longitudinal dispersivity value is both site-specific and scale-dependent in groundwater modelling (Schulze-Makuch, 2005; Zech et al., 2015). Site-specific information on the dispersivity value was not available, while the modelling scale was assumed to be in the order of 10^3 m, equal to the model cell size. In the model, a longitudinal dispersivity value of 1.0 m was used, which was estimated based on the values proposed by Zech et al. (2015). Both horizontal and vertical transverse dispersivity values were considered to be 0.1 m or 10% of the longitudinal dispersivity. The diffusion coefficient generally used in for modelling of porous media is approximately 10^{-9} m^2/s or 8.64 x 10^{-5} m^2/d (Hassanizadeh, 2017).

3.2.12. [GCG] Generalized Conjugate Gradient Solver and [VDF] Variable-Density Flow Package

The GCG solver was used to implicitly solve the dispersion and sink/source terms of the solute transport equation (Zheng & Wang, 1999). Package parameters included iteration loop constraints and the used iterative algorithm. The Symmetric Successive Over Relaxation (SSOR) was used as it requires relatively little memory to operate (Zheng & Wang, 1999). The VDF package was used to set the constraints for solving the variable-density groundwater flow equation (Eq. (2.4)). Groundwater density was restricted to values between freshwater density (1000 kg/m^3) and seawater density (1025 kg/m^3). The slope that relates fluid density to solute concentration was assumed to be 0.7143, corresponding with the conversion equation (Eq. (2.2)).

3.3. Calibration and Initial Model Stability

3.3.1. Hydraulic Conductivity Calibration

The hydraulic conductivity values of the aquifers in this model (Section 3.1.4) were based on estimates or averages of a single or a few observation points as summarized by Griffith (2003). Furthermore, the hydraulic conductivity was assumed to be constant for each aquifer throughout the entire model, therefore not taking heterogeneity into account. As the formation of each aquifer was a result of multiple processes which were not happening simultaneously throughout the entire modelling area (Section 2.3.2), it could be assumed that the hydraulic conductivity varied spatially. Therefore, the initial hydraulic conductivity values had to be revised.

To compensate for the largest errors following the use of a single estimated hydraulic conductivity value per aquifer, the hydraulic conductivity values were reconsidered by relating observed and model output head differences corresponding to known extraction rates to a varying hydraulic conductivity rate. The head differences resulting from groundwater extraction, also known as the drawdown, is inversely related to the transmissivity (Theis, 1935), which is defined as the product of the hydraulic conductivity and aquifer thickness (Fitts, 2013). Therefore, a decrease of the hydraulic conductivity should lead to an increase of the drawdown and vice versa.

As data on the absolute drawdown due to groundwater extraction was unknown, the hydraulic conductivity was calibrated for several aquifers using the approximate hydraulic head differences as depicted in the studies by Prakken (2009) and Tomaszewski (1996). The study of the latter provided approximate extraction rates (Table 3.3) and head contours for several aquifers in East Baton Rouge Parish. The work of Prakken (2009) provided the same information for the Gonzales-New Orleans aquifer in the New Orleans area. As the Gonzales-New Orleans aquifer is the main focus of the local case study that will be presented further on in the research, it was evaluated separately. Absolute drawdown could not be used, as 'natural' hydraulic heads prior to extraction were unknown. The used observed head difference was the maximum contour difference depicted in different figures of these studies, the lowest hydraulic head often corresponding to the main extraction well.

Fig. 3.12. Well locations in the Baton Rouge area used for hydraulic conductivity calibration, acquired from Tomaszewski (1996). Extraction rates per location are listed in Table 3.3.

For the Gonzales-New Orleans aquifer (model layer 9), head differences were estimated for the main extraction wells in both Orleans Paris (Michoud in Fig. 4.14) and Jefferson Parish (Jefferson 1). The used extraction rates were equal to the reference case extraction rates as summarized in Appendix B. For the Baton Rouge area, a separate extraction scenario was created, by calibrating the conductivity based on the observations in seven aquifers. The approximate pumping rates for East Baton Rouge Parish, as derived from Tomaszewski (1996), are summarized in Table 3.3, and the used extraction well locations are depicted in Fig. 3.12. Pumping rates in all other parishes remained unchanged relative to the reference case scenario (Appendix B).

Table 3.3. Extraction wells and corresponding rates used for calibration of the hydraulic conductivity for several aquifers in East Baton Rouge Parish. The rates are based on the information provided by Tomaszewski (1996). The pumping locations are displayed in Fig. 3.12.

Aquifer	Model Layer	Extraction rate per pumping location (m³/d)					
		Industrial District	Lula	Government	Zachary	Bankston	Conv. Station
1200-foot	11	11,356	-	-	-	-	-
Upper Ponchatoula	13	7,571	-	-	2,839	-	-
Big Branch	17	20,820	-	-	-	9,464	-
Abita	19	-	28,391	87,06	-	-	-
Tchefuncte	25	75,708	-	-	41,640	-	-
Hammond	27	9,464	-	10,599	-	-	7,571
Ramsay	31	51,103	-	-	58,674	-	-

The calibration runs were steady-state runs using only the first, 10^{-4} day long, model stress period discussed in Section 3.2.1. As the initial test model results showed an underestimation of the drawdown due to groundwater extraction, the hydraulic conductivity was varied by multiplying the original values, both horizontal and vertical, for each aquifer by 0.75, 0.5 and 0.3. For the Gonzales-New Orleans aquifer, an additional run using a multiplication factor of 0.25 was created. After running the model for each of the adjusted hydraulic conductivity rates, the resulting head differences were estimated from the resulting head distribution between the main extraction well for each layer and two seemingly representative locations on the outer head contours displayed in the studies of Tomaszewski (1996) for East Baton Rouge Parish and Prakken (2009) for the New Orleans area. Two observation points were used for each aquifer to lower the error margin. The resulting new hydraulic conductivity estimations (Section 4.1) were implemented in the model and therefore used for the remainder of this study.

3.3.2. Model Stabilization

The initial state of a complex, large-scale groundwater model such as the one presented here is affected by a range of variables. The concentration distribution and the different Cauchy boundaries (GHB, rivers and drains) influence the variable-density groundwater flow of the modelled groundwater system and uncertainties arise with each of these variables. Therefore, the initial model configuration might give rise to large initial changes of fresh and saline water volumes caused by instabilities of the model itself rather than reflecting any natural salinization or freshening of the modelled groundwater system.

To properly study the effect of different processes (e.g. extractions or climate change) on fresh groundwater resources, large fresh groundwater volume changes due to model instabilities are undesirable. In this case, the model was assumed to be stable when the total fresh groundwater volume present in the modelled groundwater system remained either more or less constant or changed at a constant rate. Therefore, the approximate moment of model stability was determined by running the model without wells until the (changes of) fresh groundwater volume seemed to stabilize. The output salinity distribution for the corresponding time-step was then used as the starting point for the different model scenarios (Section 3.4) and was therefore assumed to be the new initial distribution of fresh and saline groundwater.

3.4. Research scenarios

3.4.1. Regional Aquifer System

Currently, large abundances of fresh groundwater are present in the Southern Hills regional aquifer system. To find out whether these fresh groundwater volumes are currently sustainably managed, the effects of groundwater extraction on the groundwater resources in southeastern Louisiana during the coming century were studied. This projection was made for a 100-year period, between 2019 and 2119. During this time span, groundwater was extracted following the discussion in Section 3.1.7 and as listed in Appendix B. The only exception was the extraction well at Michoud, for which the value was set to 10% of the original value, as this was assumed to be the most likely future scenario following the discussion in section 2.3.4. To estimate the effects of groundwater extraction on saltwater intrusion and the available freshwater volumes, the results were then compared to a full natural flow scenario without any withdrawals.

In each research scenario, fresh groundwater volume will be expressed as the total volume of water with a TDS concentration less than 0.5 kg/m^3 and the total volume of water with a TDS concentration smaller than 1.0 kg/m^3. The former meets the drinking water standards of the USA (USEPA, 2017). Although the latter does not meet this criteria, freshwater with up to his concentration is still potable in most cases and should therefore not be fully excluded. To distinguish between the two upper freshwater limits, water with a TDS concentration less than 0.5 kg/m^3 will be referred to as 'drinking water', while water with $C \leq 1.0$ kg/m^3 will be referred to as 'useable water'. For the regional case studies, discussed in the current section and Section 3.4.2, freshwater volumes were expressed in terms of the total freshwater resources present in the aquifers. Groundwater volumes in confining layers ($K_h < 1.0$ m/d) were omitted, as they are not readily available for use.

3.4.2. Sea Level Rise, Subsidence and Flooding

Both sea level rise and subsidence could induce enhanced saltwater intrusion and therefore deteriorate fresh groundwater resources (Section 2.1.6). As both processes were expected to be of major importance in southeastern Louisiana during the coming century (Section 2.3.6), the consequences of both issues on the fresh groundwater resources was studied in this research. Additionally, the effects of a short-term flooding of the coastal regions of the study area were subject of interest. The used extraction rates in these simulations were equal to the ones used in the New Orleans future extraction scenario FS2 as explained in Section 3.4.3. This scenario was therefore used as the reference case to which the changes due to sea level rise, subsidence and flooding were compared.

The used rates of sea level rise and subsidence were based on the worst-case scenario in the study conducted by Blum & Roberts (2009), which was discussed in Section 2.3.6. The corresponding eustatic sea level rise and subsidence rates were respectively 6.0 mm/y and 8.0 mm/y. Sea level rise was simulated by increasing the head of the seaward general head boundary for each layer by 6.0 cm at the beginning of each stress period of ten years, starting from the third stress period (2029). Because deeper model layers were not in direct contact with the Gulf of Mexico within the extent of study area, the increase in head at the seaward (southern) general head boundary due to sea level rise was expected to be smaller than the used rate of 6.0 cm per decade and decreasing with depth.

Since the actual representative values were unknown, the aforementioned rates were still used and could be considered as a worst-case scenario.

As a very extensive drainage system was used in the model to keep the hydraulic head in the top model layer below the surface level, lowering of the ground surface level and the resulting lowering of the water table could be resembled by lowering the drain elevation. Therefore, the drain elevation was lowered by 8.0 cm each stress period to simulate subsidence, starting from the third stress period (2029). Three model simulations were done to study the consequences of sea level rise and subsidence, one for both processes separately and one combining them. Possible inundation resulting from sea level rise and subsidence was ignored. Therefore, the coastline remained at its initial location throughout the modelling runs.

To simulate the impact of a short-term flooding, such as the one following hurricane Katrina in 2005, model boundary conditions were altered for a 10-day period, starting at the onset of the 100-year modelling period (2019). During these ten days, it was assumed that all land located two meters or less above sea level and somewhat close to the coast was inundated by seawater. Fig. 3.13 shows the location of the flooded areas during this 10-day period. To resemble the flooding, the general head boundary conditions of the top model layer were altered for model cells located in the flooded area. The hydraulic head of the general head boundary was set to 2 m and the GHB conductance to

Fig. 3.13. Area flooded (purple) for 10 days to study the effect of flooding on the fresh groundwater resources.

50 x 10^6 m/d^2, equal to the conductance of the major water bodies. As the Holocene confining layer was present in the entire inundated area, the 10-day inundation period was considered to be too short for seawater to fully penetrate the top model layer. Therefore, the salinity in the flooded areas of the top model layer was assumed to be 17.5 kg/m^3 or half of the seawater salinity during the flooding period, thereby assuming the seawater to have intruded to the middle of the top model layer at most, or to 12.5% of the total depth of the Holocene confining layer, as it was represented by four model layers. An exception was made for the model cells which already contained a higher salinity than 17.5 kg/m^3 in the initial TDS distribution (Section 3.1.5). These model cells kept their initial TDS concentration value. The corresponding GHB densities were calculated from the TDS concentrations using Eq. (2.2).

3.4.3. Future Extraction Scenarios

Fresh groundwater volume changes and saltwater intrusion in the Gonzales-New Orleans aquifer of the New Orleans area during the coming century (2019-2119) were estimated based on four withdrawal (FS) scenarios. Here, the New Orleans area was spatially defined by the area depicted in Fig. 3.14. The study area covered the entire urban area of New Orleans itself and multiple adjacent settlements including Metairie and Kenner. Apart from large chunks of Orleans Parish and Jefferson Parish, the study area also covered a small part of Saint Bernard Parish. It was bounded in the north by Lake Pontchartrain, to the west by Saint Charles Parish and to the south and east by Plaquemines Parish and the remaining parts of Saint Bernard Parish, Orleans Parish and Jefferson Parish.

The four extraction scenarios were created by varying the withdrawal rates at the four major pumping stations in the New Orleans area (Fig. 3.14). In the first future scenario (FS1), the reference case extraction rates were used as summarized in Appendix B and described in Section 3.1.7. For the second scenario (FS2), the extraction rate at the Michoud Power Plant was decreased to 10% of the initial value, in line with the maximum rate that will be extracted in the newly planned power plant at that location (CK Associates Environmental Consultants, 2016). The third scenario (FS3) covered the case that no new electrical facility would be opened at Michoud, while in the fourth scenario (FS4), all four major wells in the New Orleans area were abandoned. The withdrawal rates used in the New Orleans area for the four different scenarios can be found in Table 3.4. FS2 was considered to be the most probable future scenario and will therefore be used as the base case for the other regional and local projections described in Section 3.4.1, Section 3.4.2 and Section 3.4.4.

Table 3.4. Future withdrawal scenarios (FS) for the Gonzales-New Orleans aquifer in the New Orleans area. Well locations are depicted in Fig. 3.14.

Scenario	Extraction rate (m³/d)			
	Michoud	Orleans 2	Jefferson 1	Jefferson 2
FS1	41261	8475	18363	7117
FS2	4126	8475	18363	7117
FS3	0	8475	18363	7117
FS4	0	0	0	0
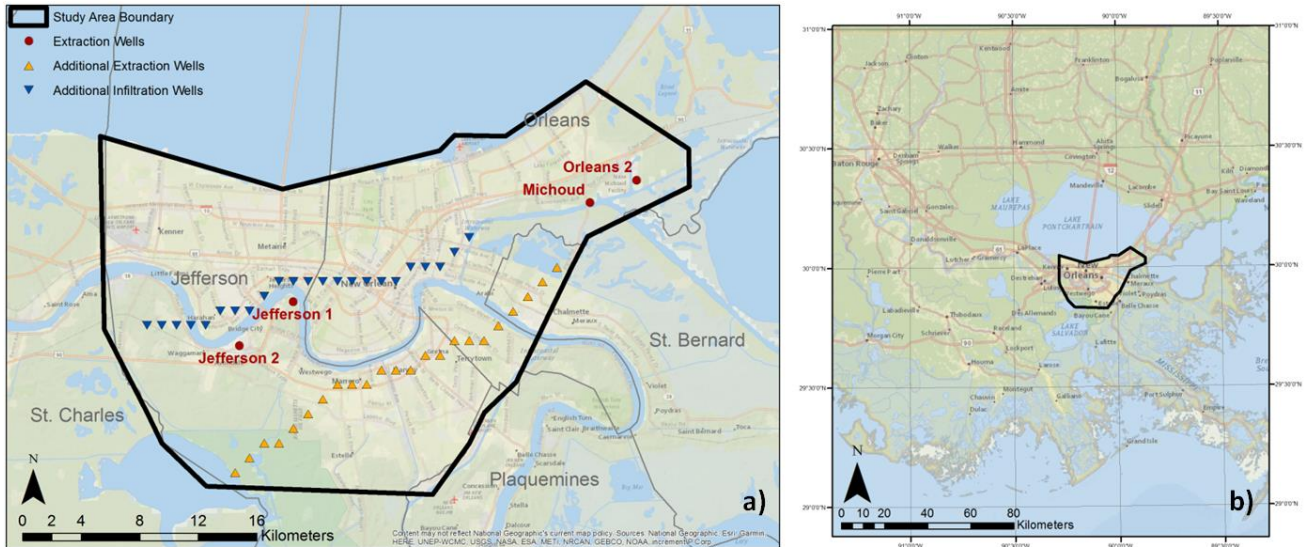
Fig. 3.14. (a) Study area location in the New Orleans area. The four major withdrawal centres in the New Orleans area are depicted, as well as the additional extraction and infiltration wells. (b) Location of the New Orleans study area in the regional modelling area.

3.4.4. Artificial Recharge and Saltwater Extraction

Several methods to enlarge or sustain fresh groundwater resources were discussed in section 2.1.5. The effects on the available fresh groundwater volumes during the coming century in the Gonzales-New Orleans aquifer of two of these methods, artificial recharge and the extraction of saltwater, were tested by implementing a set of additional extraction wells and a set of infiltration wells. Both of these sets consisted of 23 individual wells covering one model cell each. The location of the additional saltwater extraction wells (Fig. 3.14a) was based on the location of the interface between fresh and saline groundwater in the Gonzales-New Orleans aquifer derived from the initial modelling results. These extraction wells were located approximately 4 kilometres south of the interface between useable water ($C \leq 1.0$ kg/m^3) and saline water ($C > 1.0$ kg/m^3). The infiltration wells (Fig. 3.14a) were located in the fresh groundwater zone on the boundary between water with a TDS concentration less than 0.5 kg/m^3 (drinking water) and water with a concentration in the range 0.5-1.0 kg/m^3.

Moreover, the infiltration wells were purposely located close to the Mississippi River, as the river was assumed to be the source of freshwater for the infiltration wells. Infiltration salinity was therefore set to 0.235 kg/m^3, based on the most recent (1987-1988) salinity data from the USGS (USGS, 2019b) available for the Mississippi River near New Orleans. The total infiltration and extraction rates were set to 50 million cubic metres per year, which is equal to approximately 0.14 x 10^6 m^3/d in total or 6.0 x 10^3 m^3/d for each well. This rate was equal to 0.078% of the lowest Mississippi River discharge at Belle Chasse, located at the northern tip of Plaquemines Parish, between October 2008 and March 2019 (USGS, 2019a). Other sources of fresh water that could be used for artificial recharge in the New Orleans area are excess rainfall and desalinized brackish water.

The effect of smaller extraction and infiltration rates of ten million cubic meters per year (or 1.2 x 10^3 m^3/d) in total was also tested. For both the larger and the smaller rates, the effects of artificial recharge and saltwater extraction were studied both separately and combined, as well as an

51

additionally scenario combining the large infiltration rate with the small extraction rate. The effects of these measures were calculated relative to extraction scenario FS2 (Section 3.4.3), which was used as a reference case. The extraction wells used in the reference case were still active during the simulation alongside with the extraction and infiltration wells used for mitigation. The simulated mitigation scenarios are summarized in Table 3.5. Both infiltration and extraction wells were implemented in model layer 9, representing the Gonzales-New Orleans aquifer.

Table 3.5. Infiltration and extraction rates per well used for different mitigation scenarios. Infiltration and extraction well locations are depicted in Fig. 3.14. (I = Infiltration, E = Extraction, 10/50 = ten/fifty million cubic meters per year).

| Scenario | Pumping rate per well (m³/d) | |
	Infiltration	Extraction
I-50	5955.9	0
E-50	0	5955.9
I-E-50	5955.9	5955.9
I-10	1191.2	0
E-10	0	1191.2
I-E-10	1191.2	1191.2
I-50-E-10	5955.9	1191.2
FS2	0	0

4. Results

4.1. Calibration of the Hydraulic Conductivity

The initial estimates of the horizontal hydraulic conductivity of the aquifers, based on Griffith (2003), were calibrated using a simple trial-and-error method, as explained in Section 3.3.1. Note that similar results could have been achieved by changing the aquifer thicknesses, as drawdown is inversely related to aquifer transmissivity (Theis, 1935), which is defined as the horizontal hydraulic conductivity times the aquifer thickness. In this study, the transmissivity term was only altered by changing the hydraulic conductivity, as the layer thicknesses were kept constant.

4.1.1. Gonzales-New Orleans Aquifer

The results of the empirical calibration of the hydraulic conductivity for the Gonzales-New Orleans aquifer are shown in Fig. 4.1. The crosses represent the drawdown produced by the model for a certain relative hydraulic conductivity ($k/k_{original}$). For both drawdown data points, the head differences provided by the steady-state model were almost identical. Therefore, only the result at one data point was displayed in Fig. 4.1 for each run. The solid lines represent the exponential trend line through these data points and the horizontal dashed lines the observed contour differences derived from Prakken (2009). The vertical dashed lines represent the relative hydraulic conductivity values for which the model approximated the observed values.
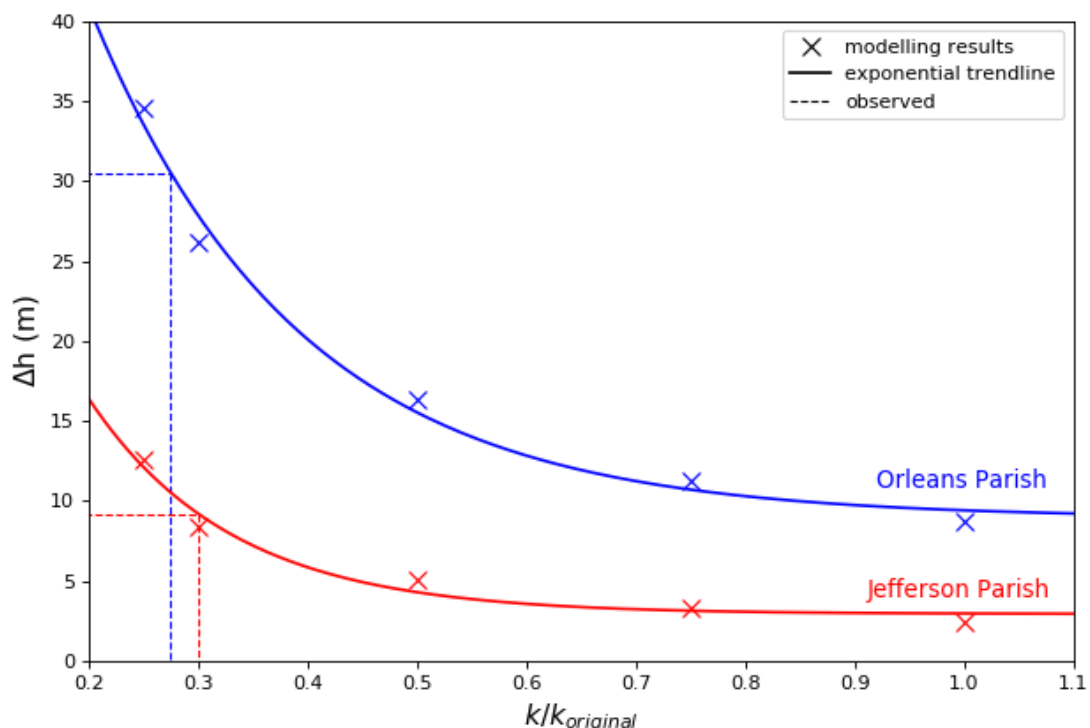
Fig. 4.1. Head difference versus hydraulic conductivity as a fraction of its original value in the Gonzales-New Orleans aquifer. Head differences are given between the main well location and the outer contour as displayed by Prakken (2009) for Orleans Parish (blue) and Jefferson Parish (red). The crosses represent the modelling results and solid lines the trend lines through the modelling results. The dashed lines illustrate (horizontal) the observed head difference and (vertical) the relative k-value for corresponding to the observed head difference.

Based on Fig. 4.1, observed drawdowns are represented by the model using a horizontal and vertical hydraulic conductivity of approximately 0.3 times the original value. As the Gonzales-New Orleans aquifer in the New Orleans area is the main focus of this study and both observation points were located in this area, the hydraulic conductivity of the Gonzales-New Orleans was adjusted according to these findings to a horizontal hydraulic conductivity value of 11.4 m/d, which is equal to 0.3 times the original value of 38.1 m/d (Table 2.1).

4.1.2. Baton Rouge Area

The results of the hydraulic conductivity calibration of the seven aquifers in the Baton Rouge are depicted in Fig. 4.2. As discussed in Section 3.3.1, the information used was provided by Tomaszewski (1996). Details on the contents of the graph are provided in section 4.1.1, with the main difference that two observation points are displayed for each aquifer and hydraulic conductivity instead of one, as a wider range of values was observed.

Unlike the results for the Gonzales-New Orleans aquifer, a large range of apparent relative hydraulic conductivity values is observed for the aquifers in the Baton Rouge area. These varying values might be explained by the simplified model geology, which was based on observations in the New Orleans area and Eastern Florida parishes rather than the Baton Rouge area. As drawdown is inversely related to transmissivity (Theis, 1935), the head differences are both susceptible for changes in hydraulic conductivity and model/geological layer thickness.
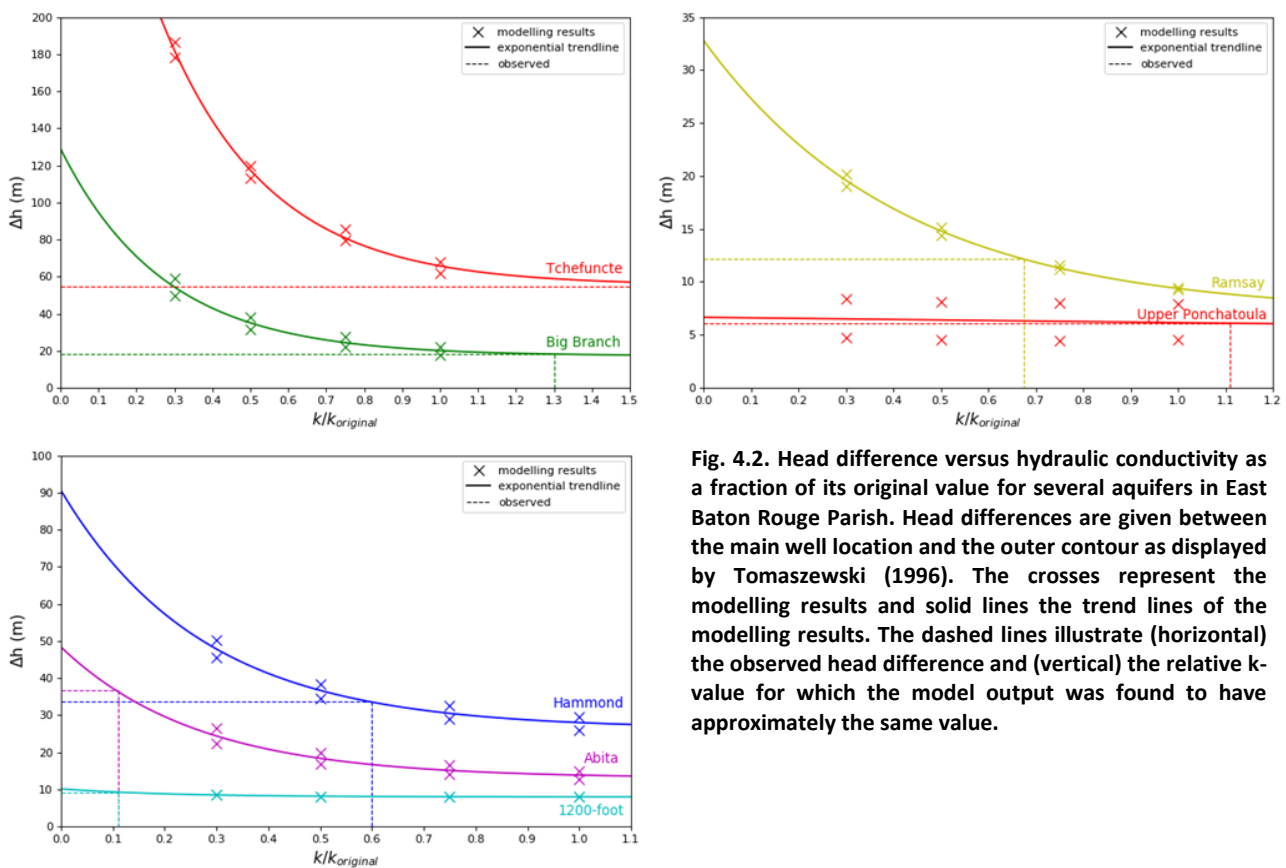
Fig. 4.2. Head difference versus hydraulic conductivity as a fraction of its original value for several aquifers in East Baton Rouge Parish. Head differences are given between the main well location and the outer contour as displayed by Tomaszewski (1996). The crosses represent the modelling results and solid lines the trend lines of the modelling results. The dashed lines illustrate (horizontal) the observed head difference and (vertical) the relative k-value for which the model output was found to have approximately the same value.

The Tchefuncte aquifer (Fig. 4.2a) is an outlier in the sense that the exponential curve through the modelling results never seems to reach the observed head difference value but rather seems to run parallel to it. For the six other aquifers, the relative hydraulic conductivity corresponding to the observed head difference also varied up to an order of magnitude. However, most of the modelled aquifers reach the observed value at a hydraulic conductivity smaller than the initial value ($k/k_{original} <$ 1). On average, the 'real' hydraulic conductivity of these six aquifers is equal to 0.65 times the original value, which can therefore be assumed to be the best estimate correction factor for the hydraulic conductivity values in the model. Therefore, both the horizontal and the vertical initial hydraulic conductivity values for all aquifers, except the Gonzales-New Orleans aquifer, were multiplied by 0.65. The resulting new hydraulic conductivity values were assigned to the corresponding model layers and used during the model scenarios that will be discussed in the following sections.

4.2. Regional Aquifer System Analysis

4.2.1. Initial Model Stability

The variable-density groundwater model was assumed to be unstable initially due to the large variety of important input variables (Section 3.3.2) and model stability was assumed when fresh groundwater volumes were more or less constant or changing at a constant rate. Fig. 4.3 shows the changes of fresh groundwater volume over time for the entire modelled groundwater system, including both aquifers and confining layers, in full natural conditions, without any extractions. The figure shows that changes of the total fresh groundwater volumes are relatively small in the first 100 years relative to the initial volumes, with the maximum deviation within 1% of the initial value. Therefore, the model was assumed to be stable from its starting point and the input heads and concentrations could be used as the initial values for the different research scenarios that will be discussed in the next sections.
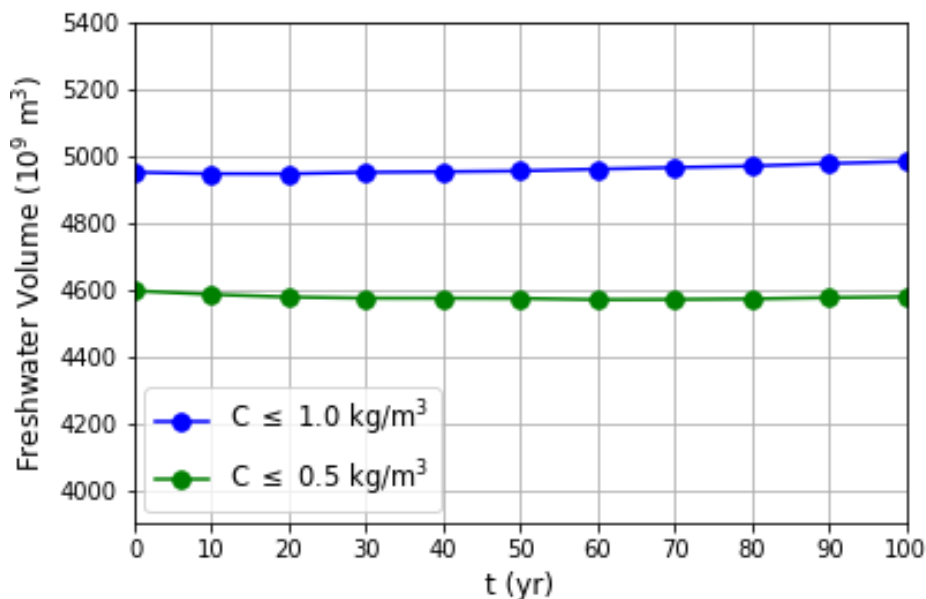
Fig. 4.3. Total fresh groundwater volumes in the groundwater system over time for full natural flow (no extractions) starting from initial model input.

55

4.2.2. Initial Distribution of Fresh and Saline Groundwater

The initial distribution of fresh and saline groundwater was estimated using the available measurements in the USGS-database and the transects provided by Griffith (2003) and Tomaszewski (2003), as explained in Section 3.1.5. This distribution was assumed to be the current or 2019 state and used as a starting point for the different future scenarios. The full initial TDS-concentration distribution is displayed in Fig. 4.4. The availability of fresh groundwater decreases going southwards (negative y-direction) towards the Gulf of Mexico, as freshwater is available nearly throughout the entire depth of Southern Hills regional aquifer system in the area north of the latitude of Lake Pontchartrain and almost fully absent to the south of the latitude of the New Orleans area. In general, (fully) saline groundwater intrudes further into the aquifer system in deeper aquifers. Nevertheless, the transition zone between fresh and saline water is fairly vertical throughout the depth of the modelled aquifer system in the Baton Rouge area (Fig. 4.4b), where groundwater flow is hampered by the presence of the Baton Rouge fault system (Section 2.3.3.1). This effect is less visible at the transition zone in the New Orleans area, in accordance with the smaller influence of the fault system on groundwater flow in this area (Section 2.3.3.1). The transition zone between fresh and saline groundwater is generally located in the central part of the study area, around the latitude of New Orleans and the area just south of Baton Rouge.

The initial fresh groundwater volume (Fig. 4.3) in the entire modelled groundwater system, including both aquifers and confining units, is equal to 4594.3 x 10^9 m^3, or 17.9% of the total groundwater volume, for $C \leq 0.5$ kg/m^3 (drinking water) and 4949.0 x 10^9 m^3 (19.4%) for $C \leq 1.0$ kg/m^3 (useable water). From these volumes, only the freshwater present in the aquifers is readily available for groundwater extraction. The fresh groundwater volume initially present in the aquifers, thereby excluding the volumes in the confining layers, are 3129.5 x 10^9 m^3 and 3359.5 x 10^9 m^3 for respectively drinking and useable water.
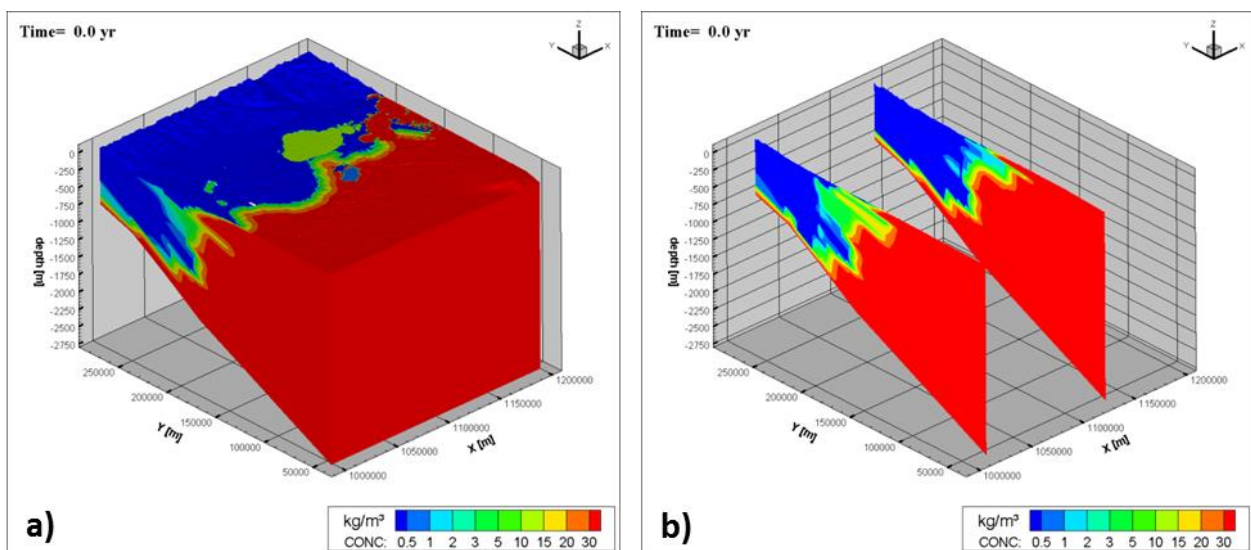
Fig. 4.4. Initial salinity distribution in the study area, based on the methods described in Section 3.1.5, given as (a) a 3D-overview and (b) two north-south transects through the study area, one dissecting the Baton Rouge area (bottom left) and the other dissecting the New Orleans area (top right).

56

4.2.3. Consequences of Groundwater Extraction

The effects of groundwater extraction on the groundwater resources of the Southern Hills regional aquifer system was studied by comparing the changes of fresh groundwater volumes for full natural flow and extraction scenario FS2 (Section 3.4.3). Fig. 4.5 shows the total fresh groundwater volumes present in the aquifers (confining layers were excluded) for these scenarios. The figure shows that only a small fraction of the fresh groundwater volume is lost due to groundwater extraction compared to the scenario without groundwater extraction, approximately 0.3% (10.2 x 10^9 m^3) and 0.4% (12.4 x 10^9 m^3) in 2119 for a freshwater concentration limit of respectively 0.5 kg/m^3 (drinking water) and 1.0 kg/m^3 (useable water). The relative changes of fresh groundwater resources are therefore relatively small on the scale on the total modelled groundwater system, following the large initial volume of freshwater present in the system. Moreover, groundwater recharge seems to overtake extraction rates by the end of the coming century, as both figures show growing fresh groundwater volumes for both natural flow and with groundwater extractions from 2100 onwards.

Although on a regional scale, fresh groundwater resources are not significantly affected by groundwater extraction, it might have implications on a more local scale. Especially areas where extraction rates are high and which are located close to the transition zone between fresh and saline groundwater, such as the Baton Rouge area, are susceptible to saltwater intrusion. The groundwater TDS concentration of a north-south transect passing through the extraction area in East Baton Rouge Parish is shown in Fig. 4.6 for the initial (2019) situation (Fig. 4.6a), and the final situation in 2119 for full natural flow (Fig. 4.6c) and the FS2-scenario (Fig. 4.6e). Furthermore, the 2119 north-south flow velocity for natural flow (Fig. 4.6d) and FS2 (Fig. 4.6f) are depicted. The figure shows that near the transition zone between fresh and saline water, groundwater flow is generally reversed from the southwards (negative) direction for full natural flow (Fig. 4.6c & Fig. 4.6d) to the northwards (positive) direction towards the extraction well in East Baton Rouge Parish (Fig. 4.6e and Fig. 4.6f). The location of the well system (approximately at Y = 200,000 m) can be distinguished in Fig. 4.6f as a sharp vertical boundary between southward and northward flow. The reversed groundwater flow leads to the movement of saline groundwater towards the extraction well throughout the aquifer depth, leading to the intrusion of saltwater into the fresh groundwater resources for several kilometres, as can be seen in Fig. 4.6e.
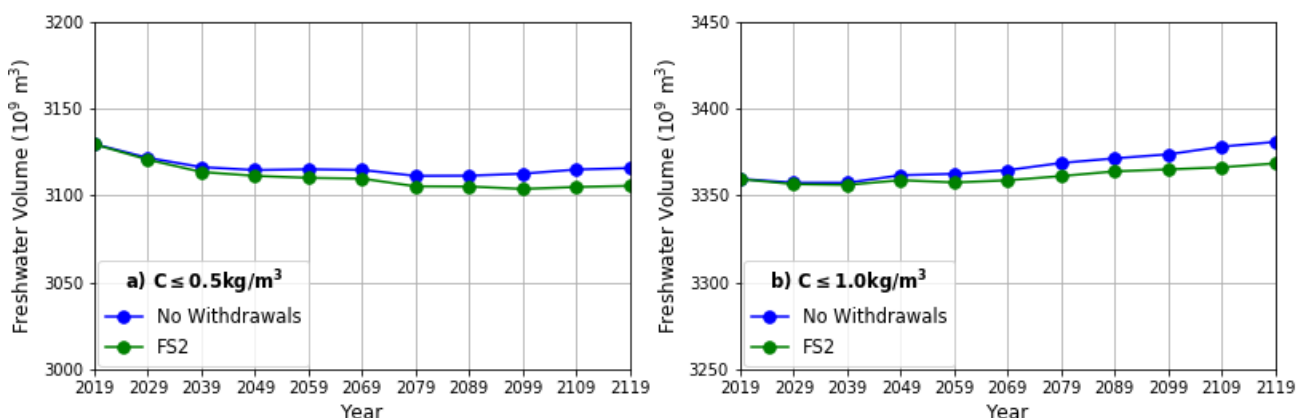
Fig. 4.5. Fresh groundwater volumes in the aquifers of the Southern Hills regional aquifer system over time for the coming century without groundwater extraction and for Future Scenario 2 using a upper TDS concentration boundary of (a) 0.5 kg/m^3 and (b) 1.0 kg/m^3.
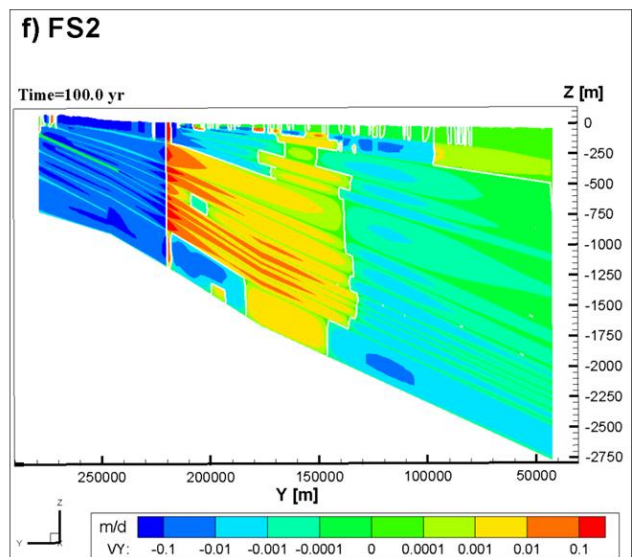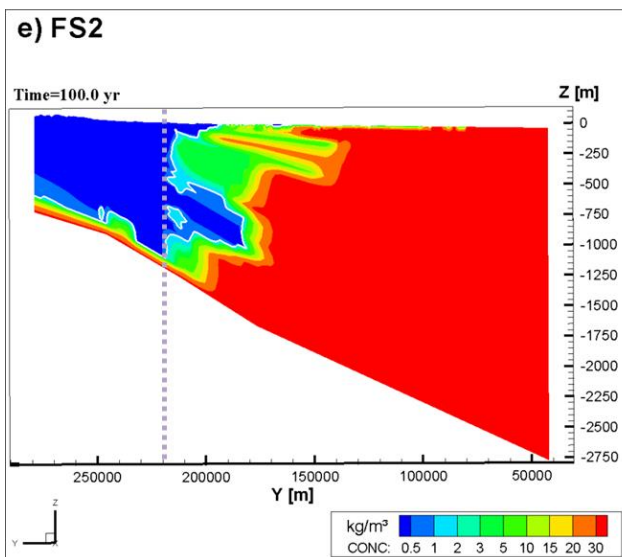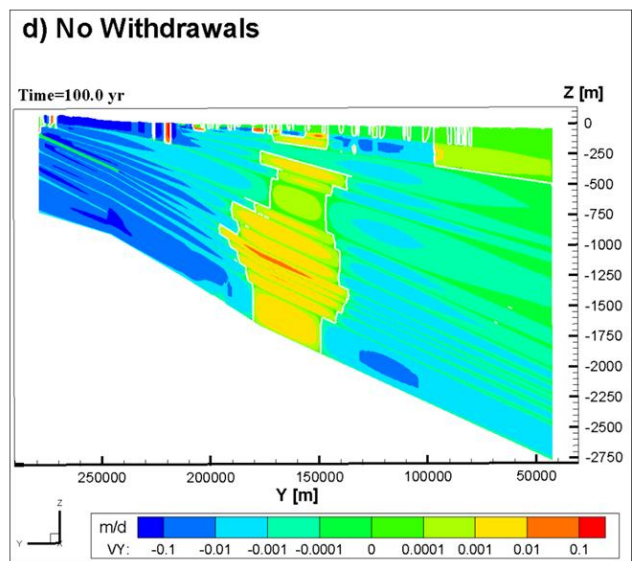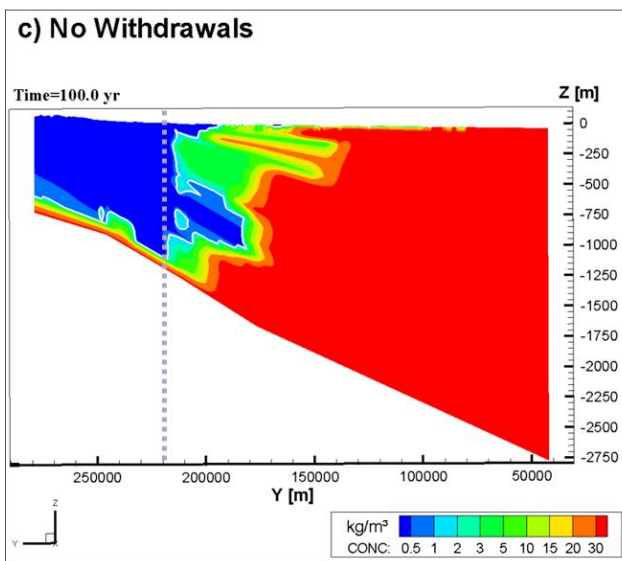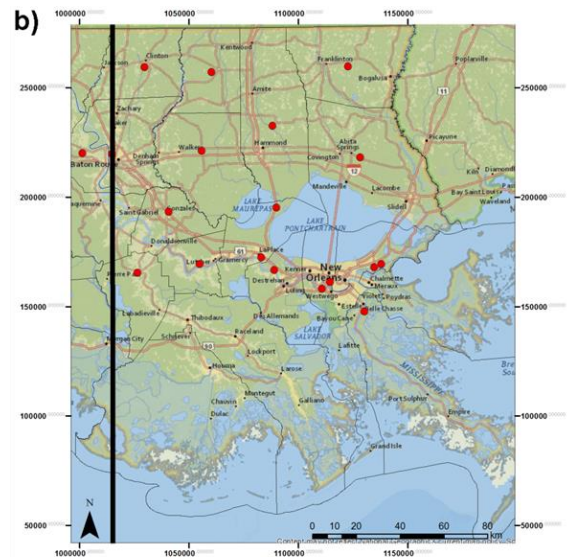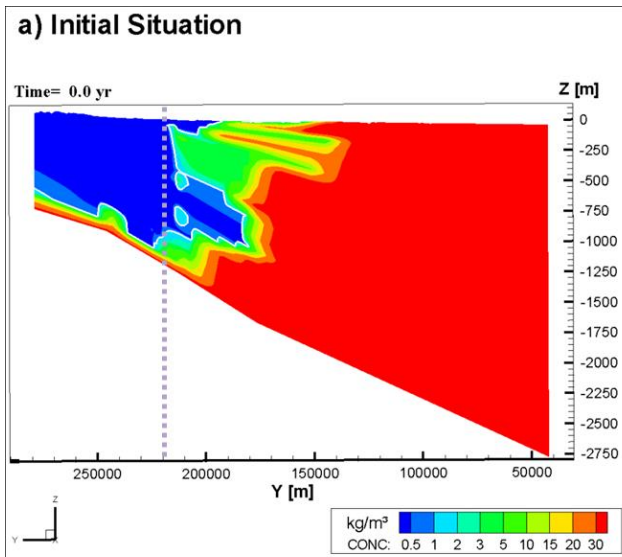
Fig. 4.6. North-south transects through the western part of the study area including the Baton Rouge area: (a) Initial distribution of fresh and saline groundwater (b) Transect location (c) Distribution of fresh and saline groundwater in 2119 for full natural flow (d) North-south velocity in 2119 for full natural flow (e) Distribution of fresh and saline groundwater in 2119 for full natural flow for FS2 (f) North-south velocity in 2119 for FS2. Flow velocities are positive to the north and negative to the south. The white lines represent the interface between fresh (C ≤1.0 kg/m^3) and saline groundwater in the subfigures on the left and the boundary between positive and negative groundwater flow velocity in the subfigures on the right. The dashed purple line is approximately located at the wells in East Baton Rouge Parish, but was mainly created as a guideline for figure comparison.
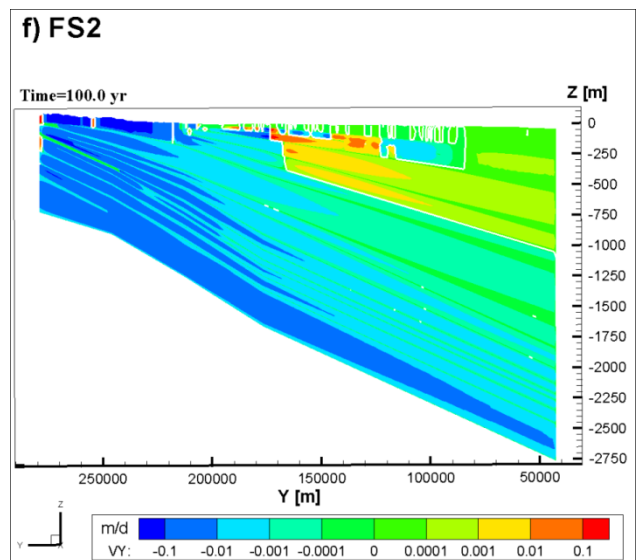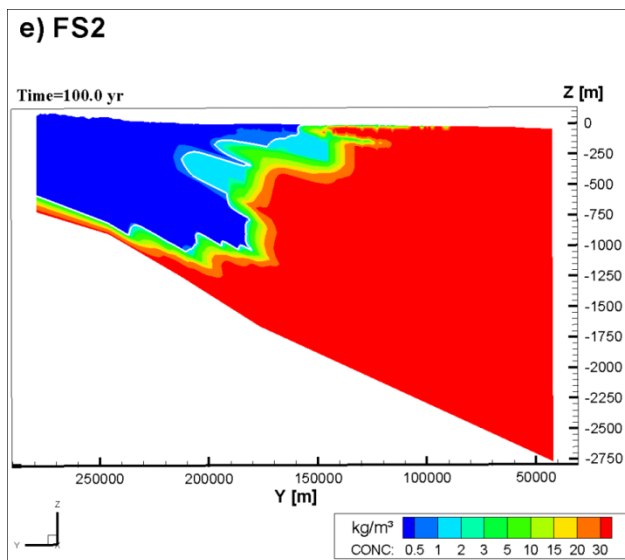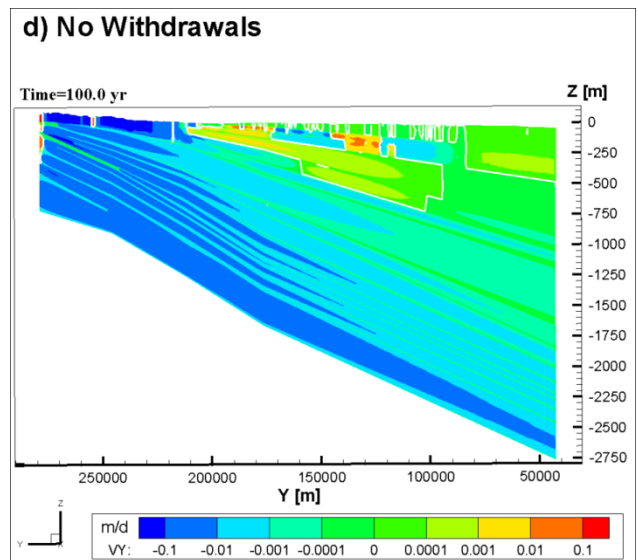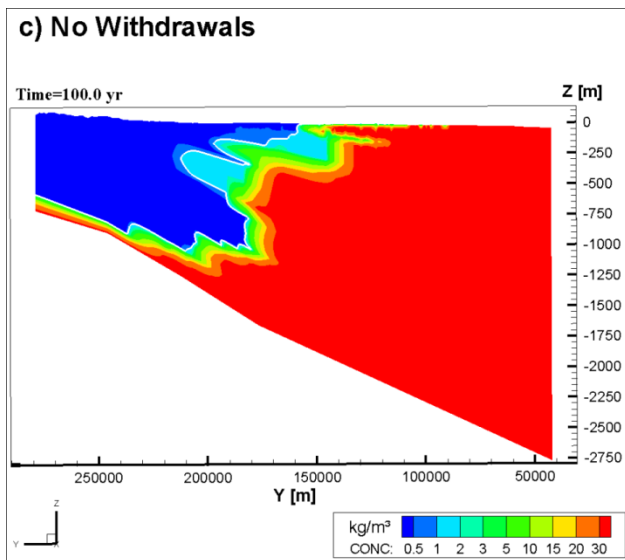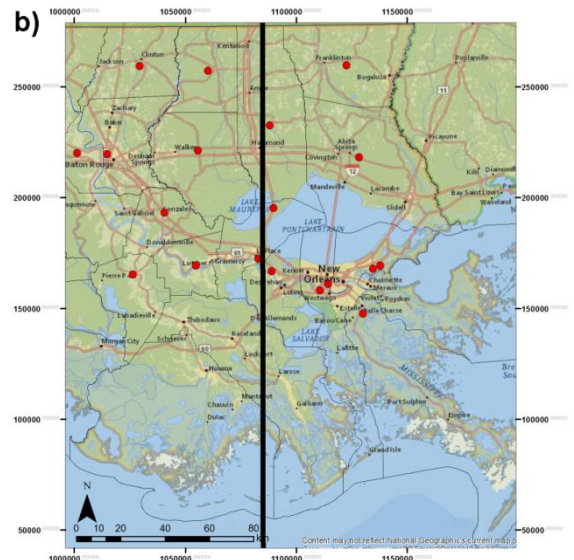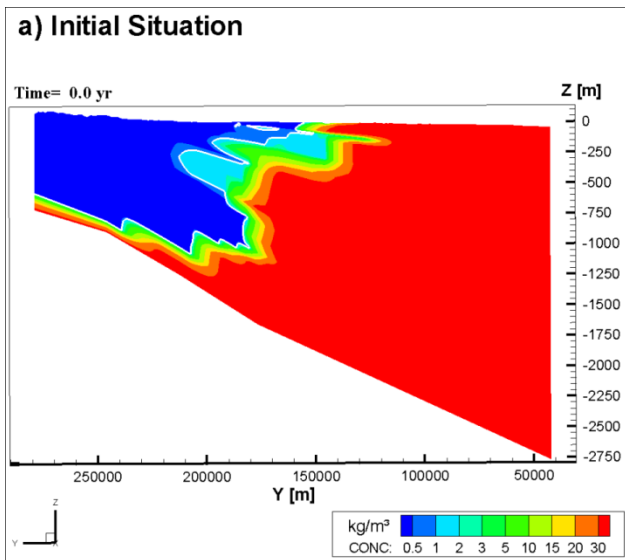
Fig. 4.7. North-south transects through central part of the study area: (a) Initial distribution of fresh and saline groundwater (b) Transect location (c) Distribution of fresh and saline groundwater in 2119 for full natural flow (d) North-south velocity in 2119 for full natural flow (e) Distribution of fresh and saline groundwater in 2119 for full natural flow for FS2 (f) North-south velocity in 2119 for FS2. Flow velocities are positive to the north and negative to the south. The white lines represent the interface between fresh (C ≤1.0 kg/m^3) and saline groundwater in the subfigures on the left and the boundary between positive and negative flow velocity in the subfigures on the right.

59

Fig. 4.7 shows similar cross sections passing through the central part of the study area close to the extraction wells in Saint Charles Parish, Saint John the Baptist Parish and Tangipahoa Parish. Although groundwater is being extracted at relatively high rates from deeper aquifers in both Saint John the Baptist and Tangipahoa Parish (Appendix B), groundwater flow is generally southwards in each aquifer below the "1200-foot" aquifer (model layer 11). In the shallower aquifers, groundwater flow is affected by the wells in Saint Charles Parish and Saint John the Baptist Parish, causing enhanced northward groundwater flow in the areas south of the extraction wells (Y < 16,000) towards the transition zone of fresh and saline groundwater near the extraction wells. Nevertheless, only the extraction well in the Norco aquifer (model layer 7) in Saint Charles Parish salinizes due to ongoing groundwater extraction. On a regional scale, no large changes of the groundwater salinity distribution are visible (compare Fig. 4.7d to Fig. 4.7f).

4.2.4. Effects of Sea Level Rise, Subsidence and Flooding

The future impacts of sea level rise, subsidence and flooding on the fresh groundwater resources of Southeastern Louisiana were studied following the discussion in Section 3.4.2. Subsidence and sea level rise were expected to influence the head distribution in the aquifers. Fig. 4.8 depicts the 2119 hydraulic head changes relative to FS2 versus latitude for sea level rise, subsidence and these processes combined. The effect of sea level rise decreases approximately linearly from the seaward general head boundary (Y = 42500) towards the northern parts of the study area (Fig. 4.8a). Note that it was assumed that the hydraulic head at the seaward model boundaries increased with the same rate as the sea level, which is a worst case scenario since the effects of sea level rise are likely to be attenuated due to the fact that the deeper model layers are not in direct contact with the sea. The influence of subsidence on the hydraulic head generally decreases with depth (Fig. 4.8b), being
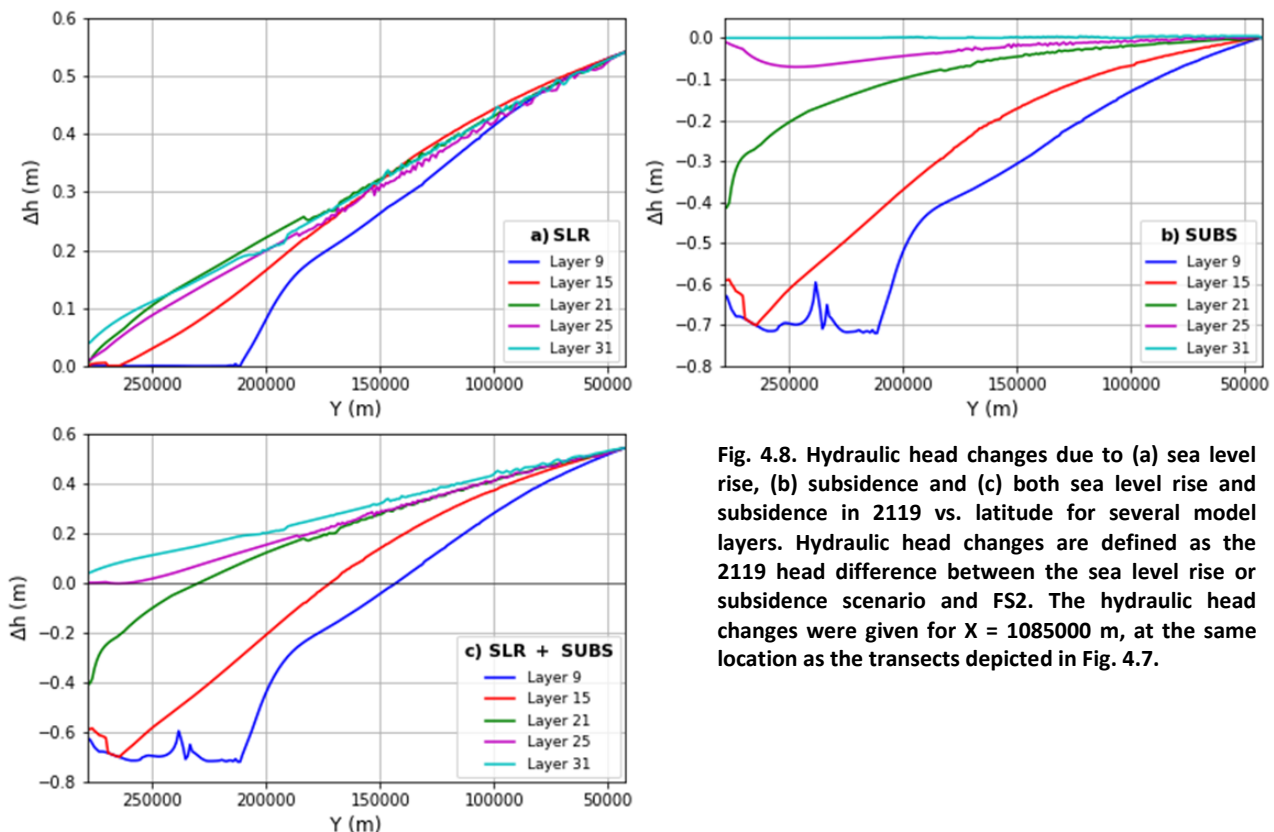
Fig. 4.8. Hydraulic head changes due to (a) sea level rise, (b) subsidence and (c) both sea level rise and subsidence in 2119 vs. latitude for several model layers. Hydraulic head changes are defined as the 2119 head difference between the sea level rise or subsidence scenario and FS2. The hydraulic head changes were given for X = 1085000 m, at the same location as the transects depicted in Fig. 4.7.

at most -0.72 m, or the total amount of subsidence in 2119, in shallower layers, to approximately zero in the deepest model layers. The hydraulic head changes as a result of sea level rise and subsidence combined are more or less equal to the sum of both processes separately, leading to larger hydraulic head gradient change as it is dominated by the positive effects due to sea level rise in the south and the negative effects due to subsidence in the north (Fig. 4.8c).

Fig. 4.9 shows the changes of fresh groundwater volume in the aquifers for the four scenarios relative to FS2. The FS2 future scenario was used as the reference case and is therefore represented by the line $\Delta V = 0$. Note that for sea level rise and subsidence, model boundary conditions were not changed before 2029 and therefore the scenario up until that point was equal to FS2. The 10-day flooding has virtually no effect on the fresh groundwater resources in the study area. The freshwater volume change resulting from flooding relative to the reference case (FS2) fluctuates between 0.002% and -0.002% of the total freshwater volume for both drinking water and useable water. The influence of sea level rise is also very small, as the maximum fresh groundwater volume decrease caused by sea level rise is 0.12 x 10^9 m^3 or 0.0036% of the total useable (C ≤ 1.0 kg/m^3) groundwater volume at that point in time.

Subsidence results in a significantly larger decrease of fresh groundwater resources. For drinking water (C ≤ 0.5 kg/m^3), it leads to a reduction of 2.73 x 10^9 m^3 or 0.088% relative to FS2 by 2119 and for useable water 2.62 x 10^9 m^3 or 0.078%. The decrease of fresh groundwater availability resulting from relative sea level rise (sea level rise + subsidence) is therefore mainly determined by subsidence, although sea level rise causes a slightly larger decrease of the available fresh groundwater volume compared to subsidence alone (Fig. 4.9). The volume decrease relative to FS2 for sea level rise and subsidence combined is 2.83 x 10^9 m^3 or 0.091% for drinking water and 2.92 x 10^9 m^3 or 0.087% for useable water by 2119.

Fig. 4.9 also depicts the near-surface fresh groundwater volume that was drained from the aquifers due to subsidence. Apparently, a large part of the fresh groundwater volume decrease due to subsidence can be explained by drainage of the aquifers cropping in the northern part of the study area rather than saltwater intrusion. In fact, respectively 93.9% and 98.1% of the volume decrease
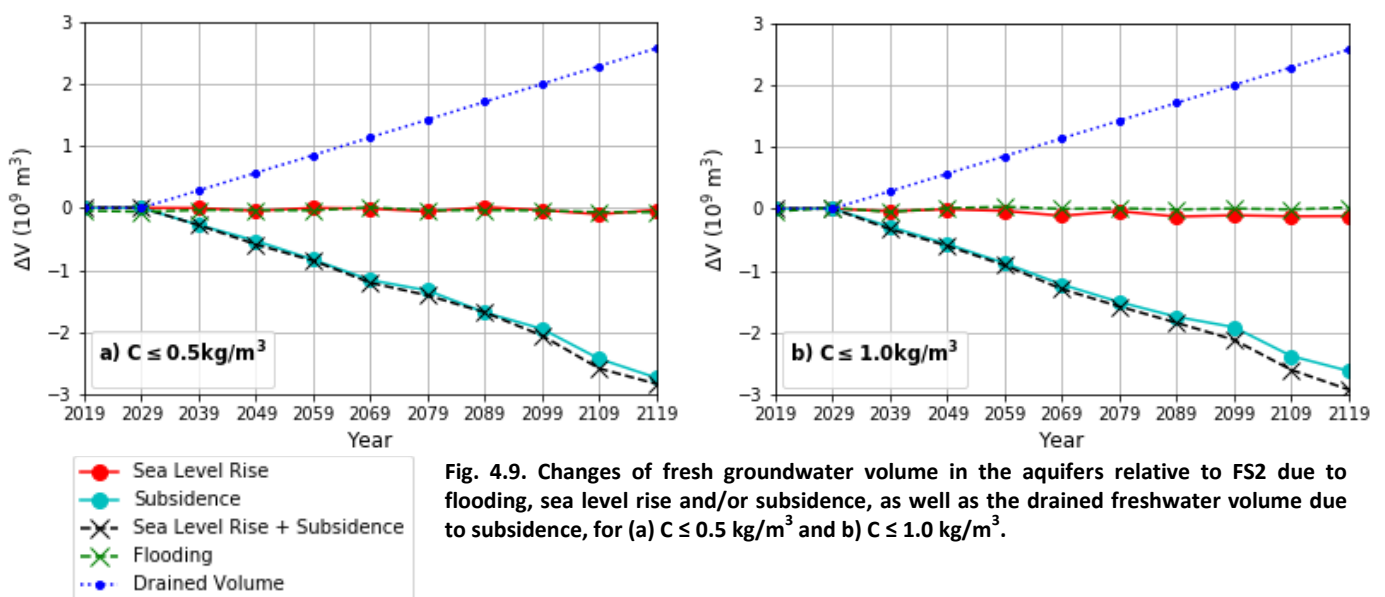
Fig. 4.9. Changes of fresh groundwater volume in the aquifers relative to FS2 due to flooding, sea level rise and/or subsidence, as well as the drained freshwater volume due to subsidence, for (a) C ≤ 0.5 kg/m^3 and b) C ≤ 1.0 kg/m^3.

by 2119 for respectively drinking and useable water is due to drainage at surface level. For the scenario with both sea level rise and subsidence, this is respectively 90.7% and 88.0%. Therefore, the role of saltwater intrusion in the decrease of the fresh groundwater volumes due to subsidence is very small, amounting to a volume loss of at most less than 0.01% of the total freshwater volume present in the modelled aquifers.

4.3. Projections for the New Orleans Area

4.3.1. Initial Fresh Groundwater Resources

The estimated drinking water volume ($C \leq 0.5$ kg/m^3) present in the Gonzalez-New Orleans aquifer is equal to 5.58×10^9 m^3 or 27.0% of the total groundwater volume. The fresh groundwater is concentrated in northwestern Orleans Parish and northern Jefferson Parish (Fig. 4.11b) An additional 5.95×10^9 m^3 (28.8%) of the groundwater has a salinity between 0.5 and 1.0 kg/m^3, which surrounds the fresher groundwater to the west, south and east. Thus, over half of the groundwater present in the study area is considered fresh. Saline groundwater is present in the southern parts of the New Orleans area. The transition zone between fresh and saline groundwater intersects the study area from the southwest to the northeast, meaning that saline groundwater has intruded further in the eastern parts of the study area. In addition, saline groundwater is present in the northwest corner of Jefferson Parish.

4.3.2. Effects of Groundwater Extraction on the Fresh Groundwater Resources

The effects of the four extraction scenarios as described in Section 3.4.3 on the available fresh groundwater volumes in the Gonzales-New Orleans aquifer of the New Orleans area during the coming century are depicted in Fig. 4.10. The projected 2119 distributions of fresh and saline groundwater in the New Orleans area following from the four extraction scenarios are depicted in Fig. 4.11c-f. For all four scenarios, the fresh groundwater availability decreases between 2019 and 2119. Moreover, the rate at which fresh groundwater volumes decrease seems to grow with time. The rate of decrease, however, heavily depends on the scenario. If all four major extraction wells are to be abandoned at present (FS4), the decrease of fresh groundwater availability between 2019 and

Fig. 4.10. Volume of freshwater present in Gonzalez-New Orleans aquifer over time for the coming century following the different future extraction scenarios explained in Section 3.4.3. The upper limit of freshwater was assumed to be (a) 0.5 kg/m^3 and (b) 1.0 kg/m^3. The volumes were calculated for the study area depicted in Fig. 4.11.

2119 will be relatively small. In that case, approximately 0.79 x 10^9 m^3 or 14% of the initial drinking water volume (C ≤ 0.5 kg/m^3) is lost. The most noticeable losses occur at the south-central part of the initial volume (compare Fig. 4.11b to 4.11f), indicating saltwater intrusion from the south. Using an upper limit for freshwater of 1.0 kg/m^3 (useable water), losses were only 0.54 x 10^9 m^3 or 5% of the initial volume. Therefore, groundwater volume with a TDS concentration in the range 0.5-1.0 kg/m^3 was actually increasing, as the lost volumes of drinking water were partly replaced by water with salinity in that range instead of more saline (C > 1.0 kg/m^3) groundwater.

Similar increases of groundwater with a TDS concentration between 0.5 and 1.0 kg/m^3 are observed for FS1, FS2 and FS3 (Fig. 4.11c-e). However, due to the extensive groundwater withdrawals in these
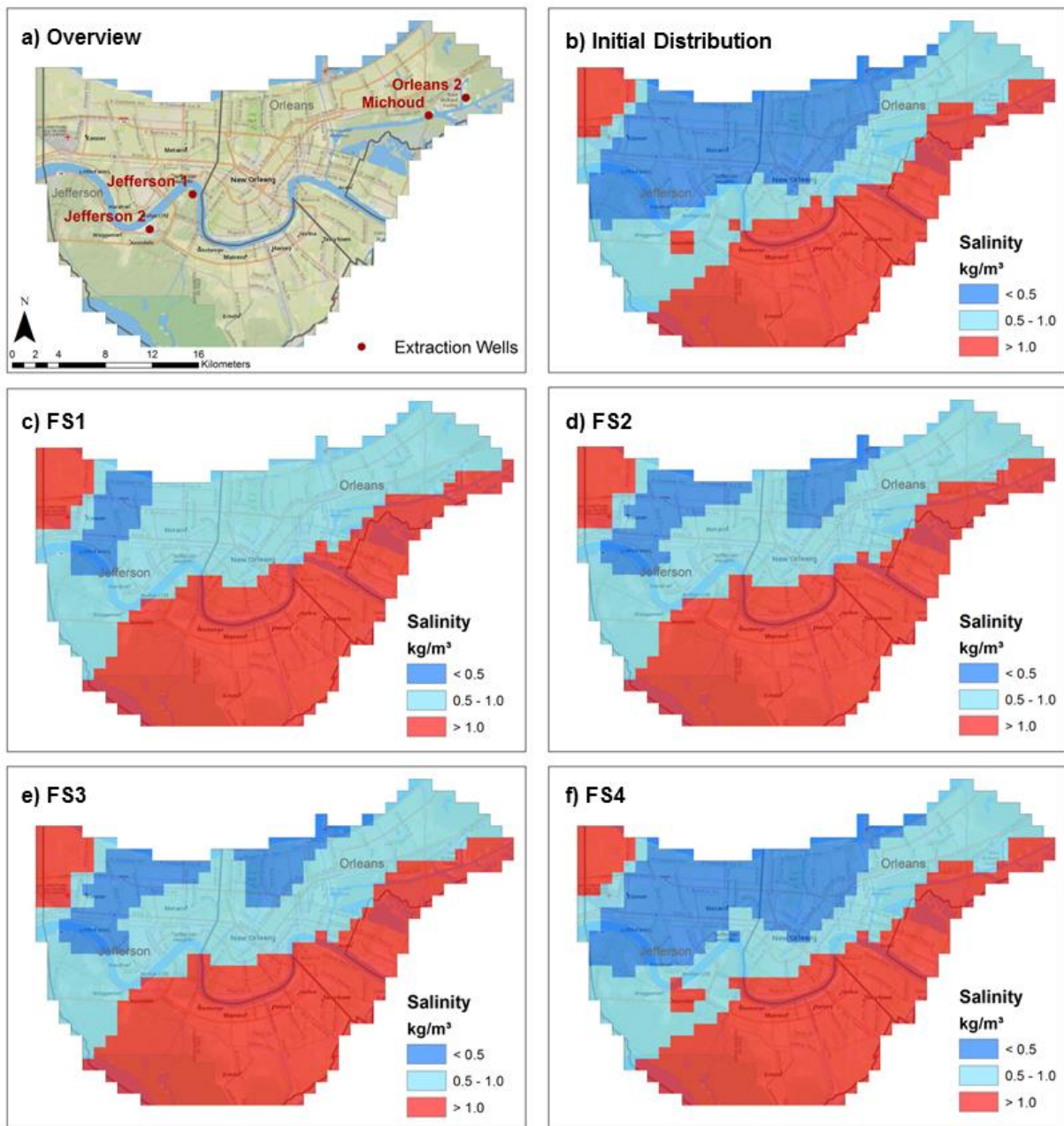
Fig. 4.11. (a) Overview of the study area in New Orleans including pumping well locations relevant for the different extraction scenarios discussed in Section 3.4.3 (b) The present distribution of fresh and saline groundwater in the Gonzales-New Orleans aquifer. The other subfigures depict the 2119 distribution of fresh and saline groundwater for the following future scenarios: (c) FS1 (d) FS2 (e) FS3 (f) FS4.

scenarios, the total fresh groundwater volumes significantly decrease in these scenarios. The decrease of the amount of useable water between 2019 and 2119 is similar for the three pumping scenarios, ranging between 1.96 x 10^9 m^3 (17.0%) for FS1 to 1.82 x 10^9 m^3 (15.8%) for FS2 and FS3. The projected volume changes of the last two scenarios are indistinguishable with respect to useable water (Fig. 4.10b). Compared to the initial situation (Fig. 4.11b) and the final situation without pumping (4.11f), saltwater intrusion resulting from groundwater pumping (Fig. 4.11c-e) especially occurs in the southwestern part of the study area, in the area surrounding the well systems in Jefferson Parish (Fig. 4.11a). For each of FS1-FS3, saltwater has intruded up to the four major withdrawal centres by 2119.

The extraction rate at Michoud does have a significant effect on the future availability of drinking water volumes (C ≤ 0.5 kg/m^3) in the New Orleans area. If extraction rates at that location are kept at pre-closure values (FS1), drinking water volume in 2119 would be decreased by 4.57 x 10^9 m^3 or 81.8% relative to its initial value (Fig. 4.10a). In that case, the presence of drinking water in the Gonzales-New Orleans aquifer would be limited to northwestern Jefferson Parish (Fig. 4.11c). This is a result of a significantly decreased hydraulic heads due to the extraction well at Michoud, up to 34.8 m relative to FS4 near the well itself. Reduction of the drinking water resources in the FS2 and FS3 scenarios is less than in FS1, but still significant. FS2 and FS3 would lead to a decrease of drinking water volume between 2019 and 2119 of respectively 3.35 x 10^9 m^3 (59.9%) and 3.24 x 10^9 (58.1%). Reopening of the Michoud power plant with a pumping rate of 10% of the pre-closure value would therefore lead to an extra drinking water volume reduction of 1.8%. In both FS2 and FS3, the initial drinking water volume present is split into two smaller parts (Fig. 4.11d-e), one located in northern Jefferson Parish and the other in northwestern Orleans Parish.

4.3.3. Effects of Artificial Recharge and Saltwater Extraction

Different measures to secure or enlarge the future availability of fresh groundwater in the Gonzales-New Orleans aquifer were proposed (Section 3.4.4). The resulting changes of fresh groundwater volumes in the New Orleans area are depicted in Fig. 4.12. According to the figure, using only saltwater extraction has adverse effects on the available amount of both drinking water ($C ≤ 0.5$ kg/m^3) and useable water ($C ≤ 1.0$ kg/m^3) compared to the reference case (FS2). Larger extraction rates (E-50) lead to a large reduction of the fresh groundwater resources than smaller rates (E-10). For the E-50 scenario, drinking water resources are fully depleted by the end of the century (Fig. 4.12a).

Implementation of the infiltration and/or extraction wells leads to an expansion of the fresh groundwater resources, relative to FS2, in all other scenarios (Fig. 4.12). The projected final (2119) distributions of fresh and saline groundwater in the Gonzales-New Orleans aquifer in the New Orleans area for these scenarios are depicted in Fig. 4.13d-h. The amount of volume increase relative to FS2 is strongly correlated with the infiltration rate. A relatively small total infiltration rate of 10 x 10^6 m^3/y (I-10) causes the fresh groundwater volumes to remain approximately constant throughout time (Fig. 4.12c-d). In this scenario, the spatial distribution of fresh and saline groundwater changes very little in the coming century (compare Fig. 4.13b to Fig. 4.13e). By 2119, 1.1% of the initial drinking water volume is lost, compared to 59.9% for FS2. The amount of useable water decreases by 5.3% for I-10 and 15.8% for FS2. Application of both infiltration and extraction at a rate of 10 x
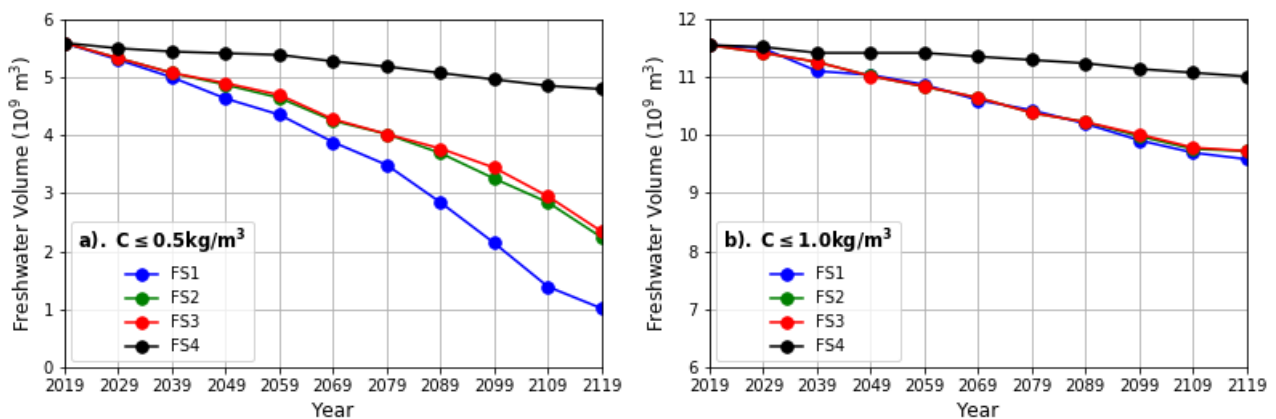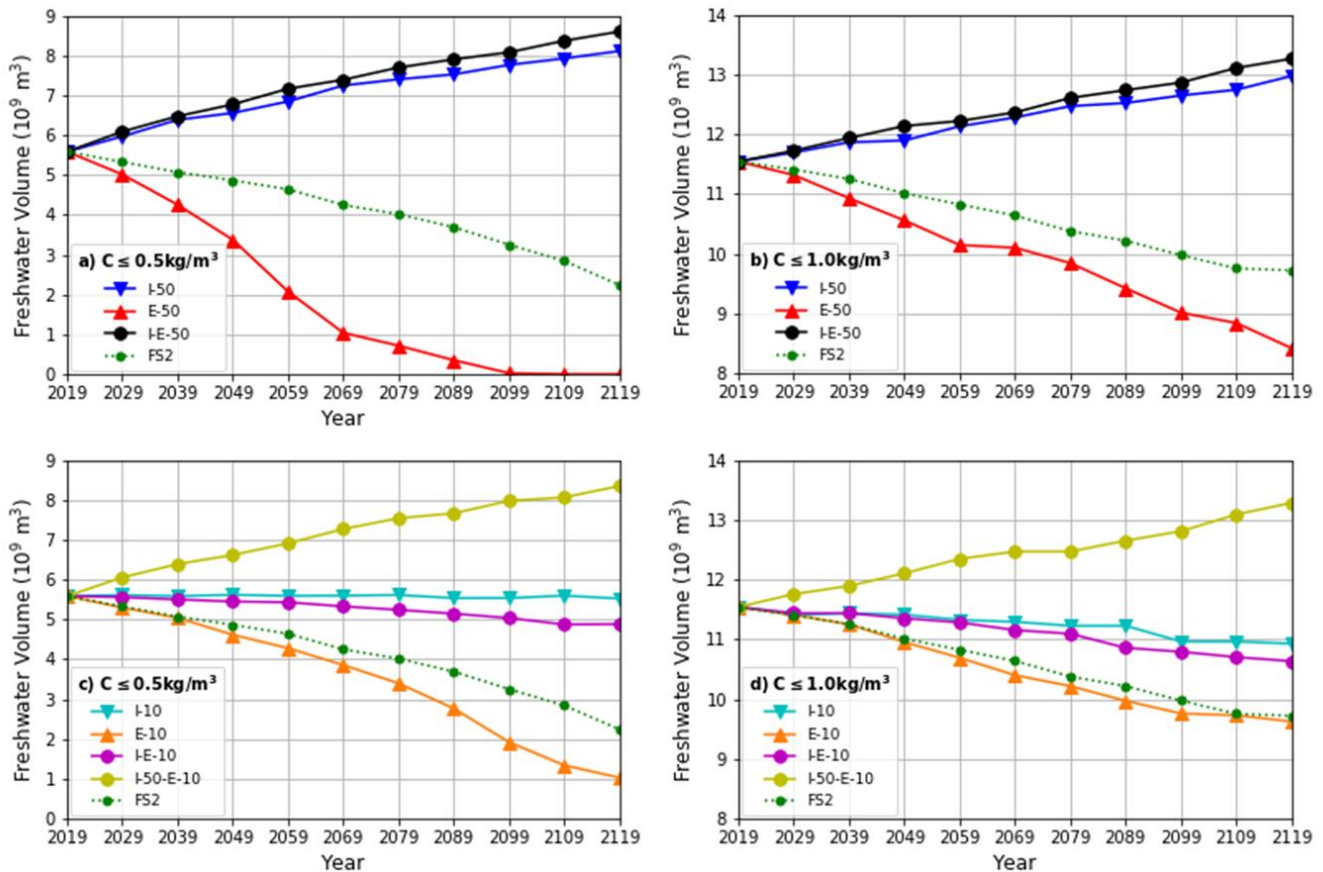
Fig. 4.12. Volume of fresh groundwater present in the Gonzalez-New Orleans aquifer over time for the coming century following the different future mitigation scenarios explained in Section 3.4.4. (a) and (c) depict the results for drinking water, (b) and (d) for useable water. The volumes were calculated for the study area depicted in Fig. 4.13a.

10^6 m³/y (I-E-10) is unfavourable relative to the infiltration-only scenario, leading to a volume loss of for 11.6% for drinking water and 7.9% for useable water.

A total artificial recharge rate of fifty million cubic meters per year leads to increasing fresh groundwater volumes over time (Fig. 4.12). This is the case for all three scenarios containing this rate (I-50, I-E-50 and I-50-E-10). Drinking and useable water volumes increase by respectively 45.2% and 13.0% for I-50, 49.5% and 15.1% for I-50-E10 and 54.0% and 14.9% for I-E-50 between 2019 and 2119. Therefore, unlike the adverse effects of saltwater extraction found for no infiltration or smaller infiltration rates, additional saltwater extraction actually slightly increases fresh groundwater volumes relative to the case without additional extraction (I-50). Moreover, the scenario with larger extraction rates (I-E-50) leads to a slightly larger increase of the available drinking water resources then the scenario with a smaller rate (I-50-E-10), although the reverse is true for useable water.

The distribution of fresh and saline groundwater in the year 2119 of the three high-rate infiltration rate cases are depicted in Fig. 4.13 d, f and h. In each of these cases, artificial recharge causes a southward expansion of the drinking water volume. Additionally, saltwater extraction leads to a southward retreat of the interface between useable and saline groundwater. In the case of a large extraction rate (I-E-50), fresh groundwater is extending southward to such an extent that is being extracted at some of the additional extraction wells by 2119 (Fig. 4.13f). The saltwater front in the northwest of Jefferson Parish is also pushed backwards by the infiltration of freshwater. In the
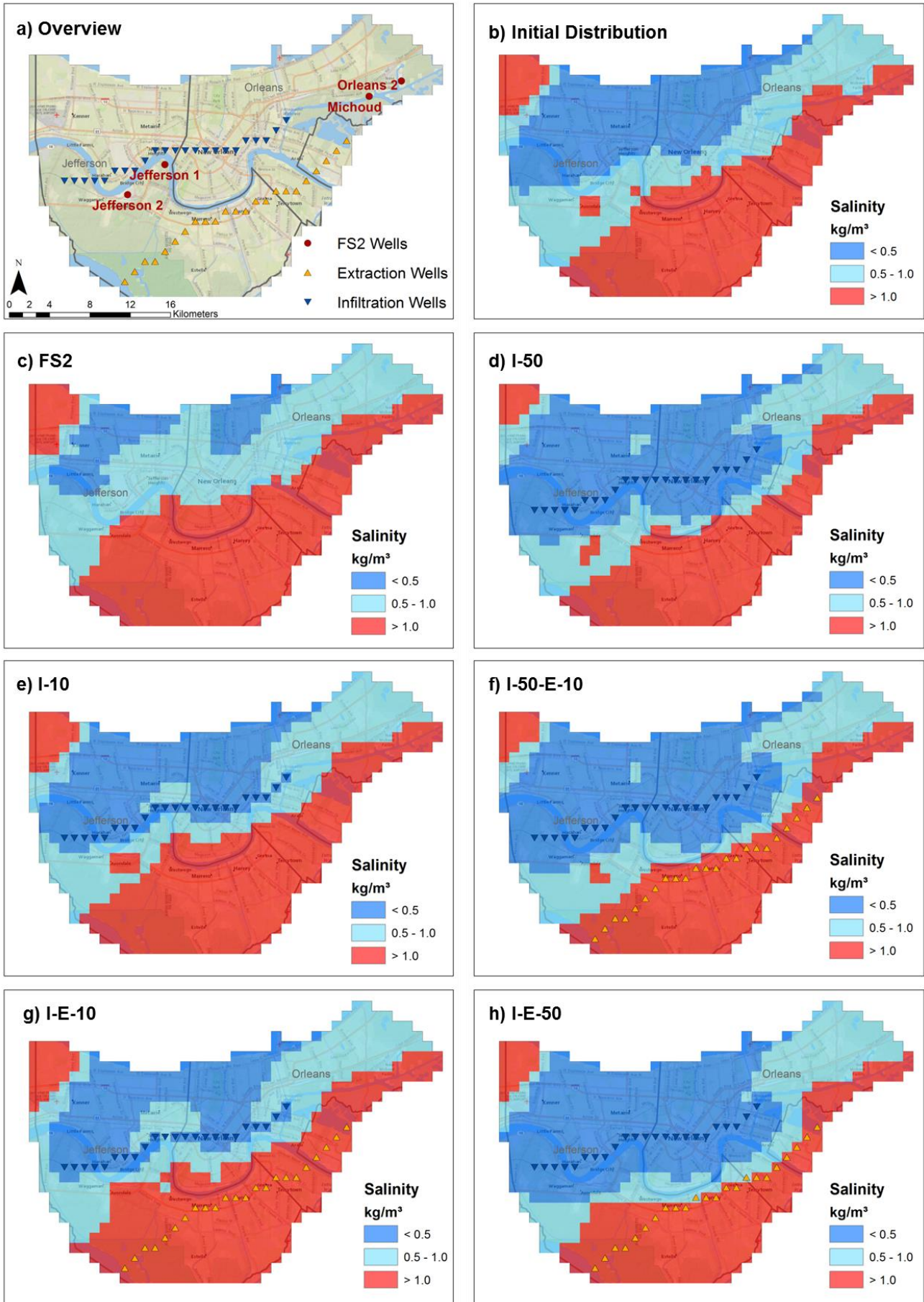
Fig. 4.13. (a) Overview of the study area in New Orleans including the locations of the major withdrawal centres and the additional extraction and infiltration wells. **(b)** The present distribution of fresh and saline groundwater in the Gonzales-New Orleans aquifer. **(c)** 2119 fresh-salt distribution for FS2. The other subfigures depict the 2119 the fresh-salt distribution for the following mitigation scenarios: **(d)** I-50 **(e)** I-10 **(f)** I-50-E-10 **(g)** I-E-10 and **(h)** I-E-50.

southwestern part of the study area, saltwater seems to intrude further inland in the I-E-50 scenario, but not in the I-50 and I-50-E-10 scenarios. Nonetheless, the resulting spatial distribution of fresh and saline water is generally similar for the three cases and dominated by the artificial recharge.

The effects of the different mitigation methods on the groundwater salinity at the groundwater extraction wells Jefferson 1 and Jefferson 2 (Fig. 4.13a) are depicted in Fig. 4.14. Initially, the groundwater salinity values at both wells are in the range 0.5 kg/m^3 $\leq C \leq$ 1.0 kg/m^3, and the extracted groundwater could therefore be categorized as useable water but not as drinking water. These values are in accordance with the findings of Prakken (2009), stating that no water was withdrawn in the areas with $C \leq$ 0.45 kg/m^3 (Section 2.3.4). Ongoing groundwater extraction (FS2) leads to salinization of both extraction wells. The changes of the salinities at the wells over time for the different mitigation scenarios are in line with the findings earlier in this section. For example, the use of groundwater extraction (E-50 and E-10) as sole mitigation methods leads to increased salinization at the extraction wells compared to the reference case FS2. At Jefferson 1, the useable water limit (C = 1.0 kg/m^3) is exceeded by 2109 for the E-50 scenarios, while at Jefferson 2, this limit is exceeded around 2039 for the E-50, E-10 and reference FS2 scenarios. The E-50 scenario leads to a slight decrease of the salinization at Jefferson 2 until approximately 2109.

Similar to the changes in groundwater volume (Fig. 4.12), both the I-10 and the I-E-10 scenarios lead to an approximate stabilization of the salinity at the depicted extraction wells, although the significant freshening occurs at Jefferson 2 from 2059 onwards for both scenarios. The three
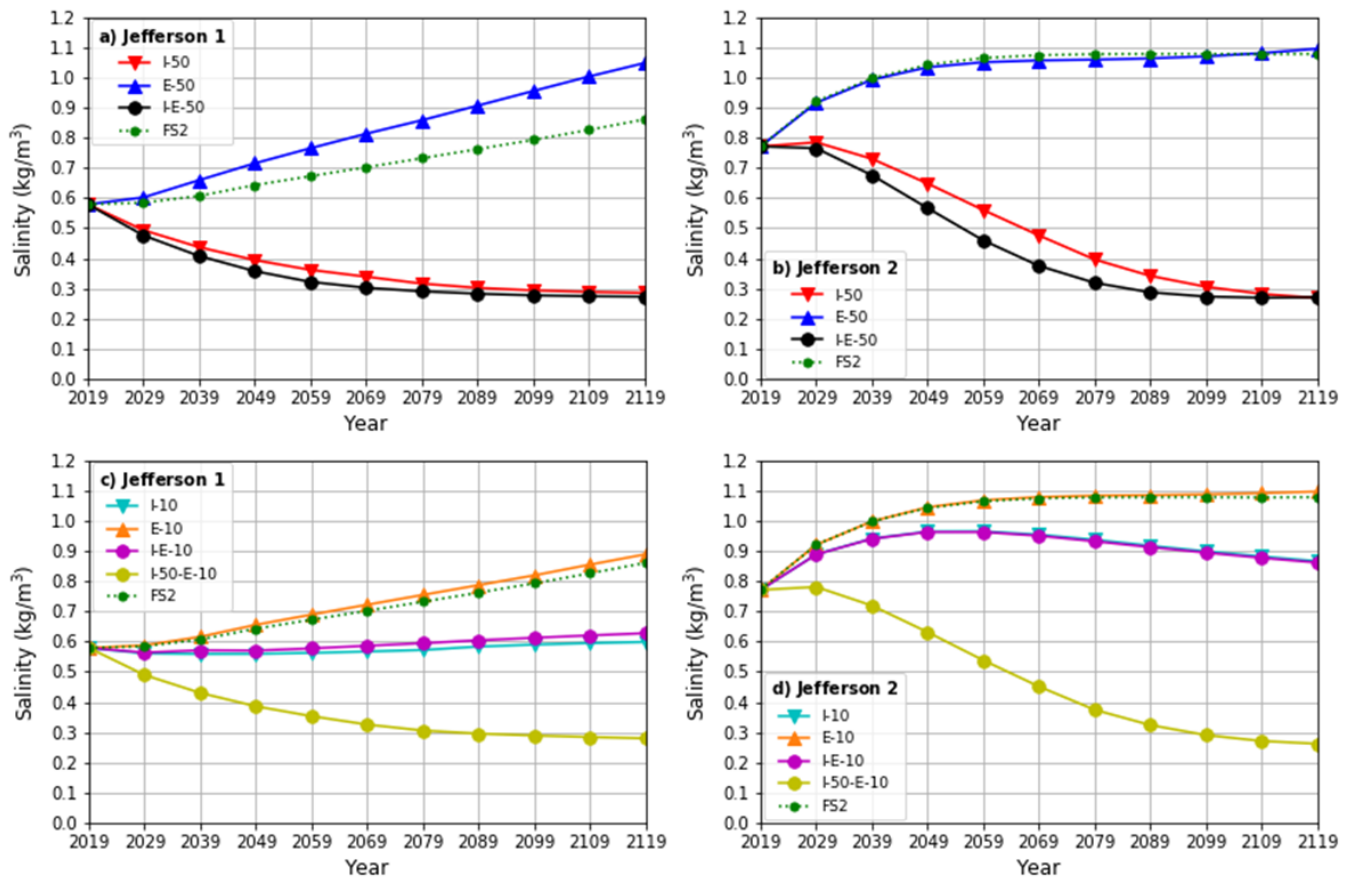
Fig. 4.14. Salinity projections following different mitigation scenarios for the coming century in the Gonzales-New Orleans area at the extraction wells Jefferson 1 (a and c) and Jefferson 2 (b and d). Well locations are depicted in Fig. 4.13a. Details on the different scenarios are provided in section 3.4.4

scenarios using a total infiltration rate of 50 x 10^6 m^3 year (I-50, I-E-50 and I-50-E-10) lead to a significant freshening of the groundwater at the two extraction wells in Jefferson Parish, down to less than 0.3 kg/m^3 by 2119, thereby enabling the production of drinking water ($C \leq 0.5$. kg/m^3) at these wells. All three mitigation methods would lead to the availability of drinking water at Jefferson 1 by 2029. At Jefferson 2, drinking water would be available around 2067, 2055 and 2063 for respectively scenario I-50, I-E-50 and I-50-E-10.

4.3.4. Comparison of FS2 vs. I-E-50

Large scale infiltration and extraction rates as proposed in this study largely influence the behaviour of the groundwater system in the area. Therefore, a comparison of the system behaviour between the base-case (FS2) scenario and the scenario with the largest infiltration and extraction rates (I-E-50) will be made in this section. Fig. 4.15 depicts the initial hydraulic head distribution in the Gonzales-New Orleans aquifer (model layer 9) for both scenarios, as well as the head difference between the scenarios and the minimum and maximum head differences per layer. Fig. 4.16 shows the distribution of fresh and saline groundwater, the hydraulic head distribution, and north-south velocity distribution for the Gramercy, Norco, Gonzales-New Orleans and 1200-foot aquifers in a schematic north-south transect through the New Orleans area. In the FS2 scenario, the hydraulic heads throughout the New Orleans area are approximately between 0.0 m and 5.0 m. Near the withdrawal centres, the head is lowered due to groundwater extraction (Fig. 4.15a), down to -9.0 m at the largest well in Jefferson Parish (Jefferson 1). Groundwater flow in the Gonzales New-Orleans aquifer is also largely determined by the presence of the extraction wells, as groundwater flow is southward north of the same well in Jefferson Parish and northward to the south of that well (Fig. 4.16e).

Groundwater flow patterns are substantially altered by the implementation of artificial recharge and saltwater extraction. The hydraulic head distribution of the Gonzales-New Orleans aquifer is now dominated by the location of the infiltration and extraction wells (Fig. 4.15b), leading to significantly higher hydraulic heads in the northwestern part of the area and lower heads in the southeastern parts. Relative to the FS2 scenario, the head has increased up to 16.7 m at the infiltration front and decreased down to 12.4 m at the extraction front (Fig. 4.15c-d). Flow velocities are also largely influenced by the presence of the additional wells (Fig. 4.16f), leading to large velocities relative to the FS2 scenario directed towards the extraction wells and away from the infiltration wells. Note that the initial extraction wells also cause a larger northward flow of saline water from the south, at rates up to 0.1 m/d or approximately 36.5 m/y.

The additional well systems also lead to a considerable amount of hydraulic head change in the confining layers directly above and below the Gonzales-New Orleans aquifer (Fig. 4.15d). The hydraulic heads in the Norco aquifer (model layer 7) and the 1200-foot aquifer (model layer 11) change up to 1.0 m relative to FS2 (Fig. 4.15d). Although these differences are relatively small, it causes the groundwater flow to reverse in these aquifers in the area between the infiltration and the extraction wells (Fig. 4.16f). In the Gramercy and Upper Ponchatoula aquifers, or model layers 5 and 13, head differences due to the mitigation measures are a few centimetres at most, and are therefore not expected to significantly influence groundwater flow.
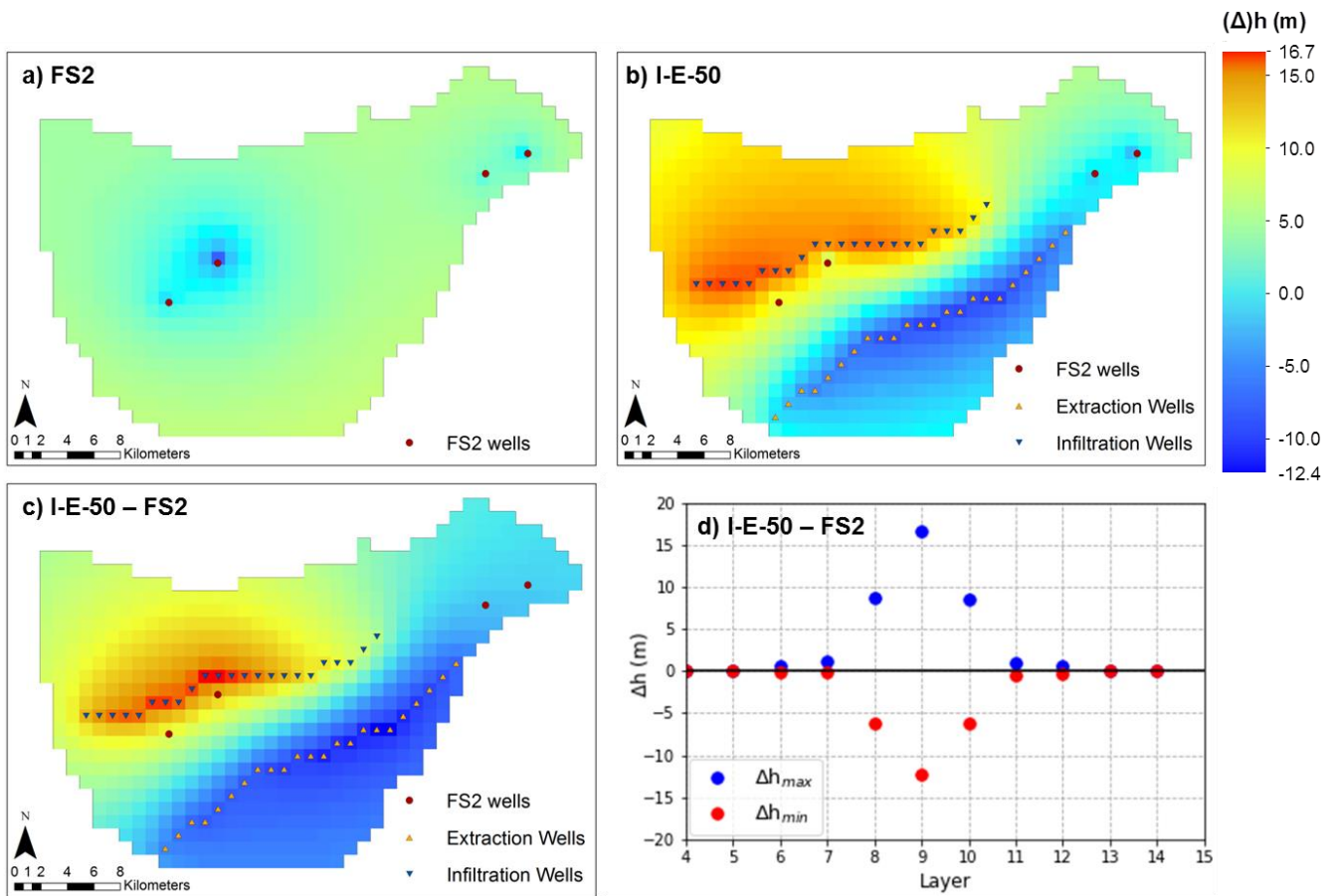
Fig. 4.15. 2019 hydraulic head distribution in the Gonzales-New Orleans aquifer for (a) FS2 and (b) I-E-50. (c) Hydraulic head difference between I-E-50 and FS2 in the Gonzales-New Orleans aquifer. (d) Maximum hydraulic head increases and decreases for I-E-50 relative to FS2 in different model layers. The legend given on the top right is valid for subfigures (a), (b) and (c).

69
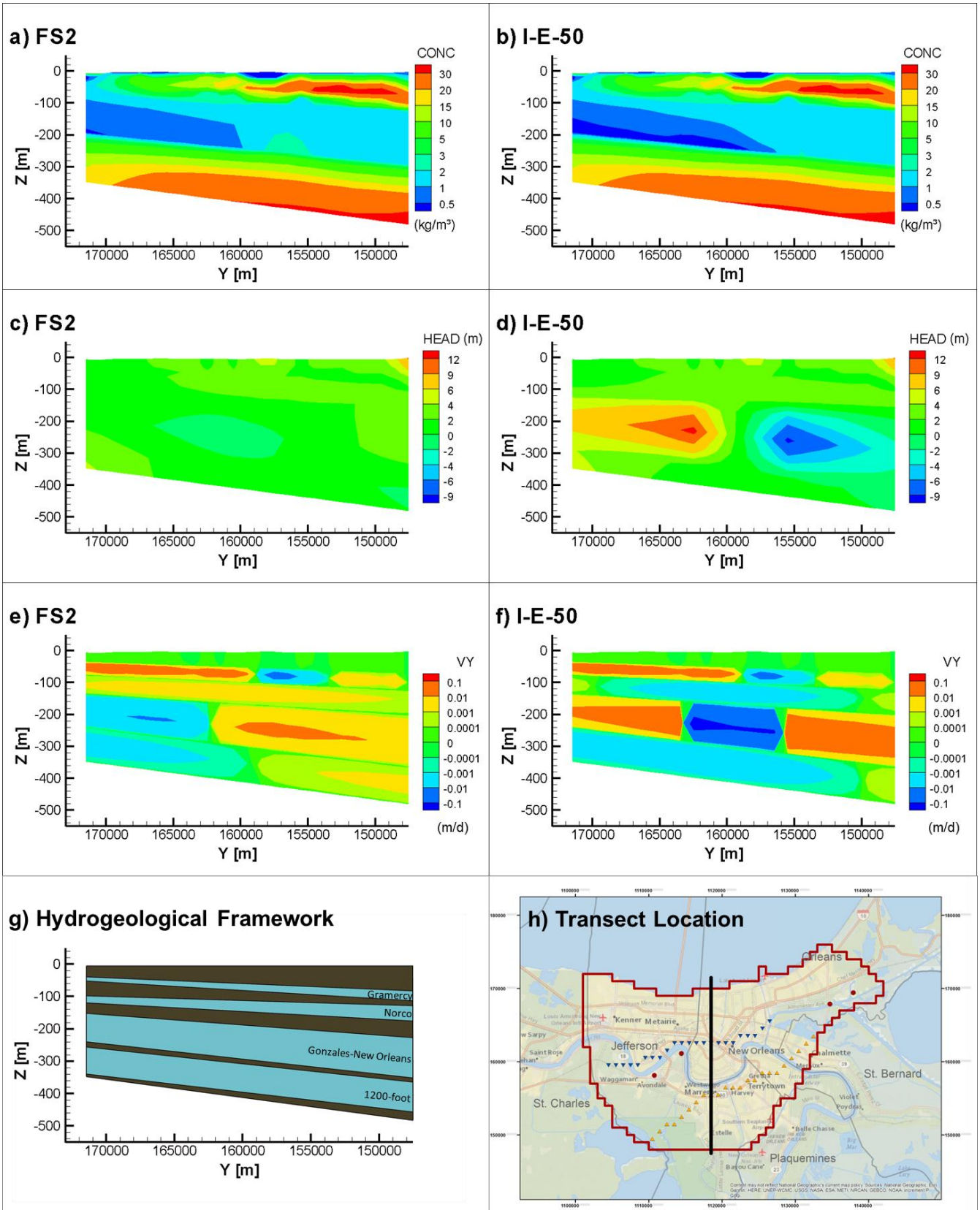
Fig. 4.16. Schematic north-south transects through the New Orleans area depicting the 2119 fresh-salt distribution for (a) FS2 and (b) I-E-50, the hydraulic head distribution for (c) FS2 and (d) I-E-50, the north-south groundwater flow velocities for (e) FS2 and (f) I-E-50. (g) Schematic representation of the hydrogeology in the study area. (h) Transect location (black line) in the study area (red polygon).

5. Discussion

5.1. Synthesis of the Modelling Results

Currently, large abundances of fresh groundwater are present in the Southern Hills regional aquifer system in the northern parts of Southeastern Louisiana, distributed among fifteen major aquifers. Although sea level rise, subsidence and short-term flooding were found to trigger saltwater intrusion in coastal aquifers in several studies (Section 2.1.6), these processes are expected to have little to no influence on the total fresh groundwater volumes of Southeastern Louisiana, although some local effects might occur. Salinization of the aquifers due to flooding is presumably hampered due to the presence of the confining Holocene top layer in the areas close to the coastline.

In the groundwater model, the hydraulic head increase due to sea level rise was found to decrease linearly from the southern seaward general head boundary towards 0 m at the aquifer outcrop area or model boundary. Thereby, sea level rise caused the hydraulic head difference between adjacent model cells to increase by a few millimetres at most. As natural gradients and gradients due to groundwater extraction are much larger, the effect of sea level rise on groundwater flow is negligible. Note that a worst-case scenario was used in determining the head changes at the seaward boundary of the aquifers, using the rate of sea level rise as head increase over time. However, the hydraulic head change due to sea level rise is likely to be attenuated at the seaward boundary as the aquifers are not in direct contact with the Gulf of Mexico. Therefore, the head gradient changes on land due to sea level rise are probably even smaller as the values presented in this study. The negligible consequences of sea level rise for the freshwater resources of the confined aquifer system presented here are in line with the findings by Chang et al. (2011), who found no long-term influence of sea level rise on the location of the saline groundwater front, and by Sherif & Singh (1999), who concluded that the saltwater intrusion for a 0.5 m sea level rise was limited to 0.4 km, which is smaller than the model cell size used in this study.

The hydraulic head changes due to subsidence are in the same order of magnitude than the changes due to sea level rise, causing similar small effects on the distribution of fresh and saline water in the aquifer system, not leading to considerable saltwater intrusion. The only significant losses of fresh groundwater resources were found in the northern part of the study area due to direct drainage following lowering of the land surface. Effects of permanent inundation due to sea level rise and subsidence were not taken into account. Inundation is known to significantly induce saltwater intrusion in unconfined aquifers (Ataie-Ashtiani et al., 2013; Ketabchi et al., 2016), but is expected to have less effect on confined aquifers as no direct infiltration of saline water into the fresh groundwater resources occurs.

Groundwater extraction induces saltwater intrusion to a much larger extent than sea level rise or subsidence, leading to groundwater flow reversals and enhanced northward flow in the areas south of the extraction wells. However, the fresh groundwater volume losses are still only 0.3% to 0.4% of the total fresh groundwater volume present in the Southern Hills regional aquifer system. On the other hand, adverse consequences of fresh groundwater withdrawals occur on a more local scale, in areas with large extraction rates located close to the transition zone between fresh and saline groundwater. In both the Baton Rouge area and the New Orleans area, saltwater is expected to

intrude several kilometres into the fresh groundwater resources in the coming century as a result of the high extraction rates in these areas. For the Baton Rouge area, extraction induced saltwater intrusion has already been observed (Lovelace, 2007; Tomaszewski, 1996) and is expected to continue in the future (Tsai & Li, 2008).

Continued groundwater extraction has deteriorating effects on the fresh groundwater resources in the New Orleans area. Past withdrawals already caused saltwater intrusion into the freshwater containing parts of the Gonzales-New Orleans aquifer (Tomaszewski, 2003) and although pumping rates have declined in the past decades, this process is expected to continue during the coming century. According to the findings in this study, the amount of drinking water (C ≤ 0.5 kg/m^3) will decrease by 58% to 82% in the coming century, depending on the extraction rate at the Michoud power plant facility. Nevertheless, the proposed reopening of the power plant with a groundwater use of 10% of the initial withdrawal rate would not cause a significant increase of salt water intrusion relative to the scenario without extractions at Michoud. In the case that extraction rates at Michoud would stay at pre-closure values, drinking water volumes in the Gonzales-New Orleans aquifer would be limited to a small area in the northwestern part of Jefferson Parish in 2119. The two wells in Jefferson Parish have the largest impact on the intrusion of saline water (C > 1.0 kg/m^3) into the useable water (C ≤ 1.0 kg/m^3) volumes, as saline water moves several kilometres northward between 2019 and 2119 in the southwestern parts of the New Orleans area. The wells in Orleans Parish already extract saline water from the start. Therefore, these wells have little impact on the northward movement of the saltwater front.

The possibilities of ensuring or enlarging future fresh groundwater volumes in the New Orleans area were explored by implementing artificial recharge, saltwater extraction or a combination of both in the model. Using only saltwater extraction to enlarge fresh groundwater resources turned out to be unsuccessful at it decreased the future fresh groundwater volumes relative to the base-case rather than increasing it. The use of artificial recharge using water from the Mississippi River for infiltration can significantly reduce the effects of saltwater intrusion or even increase the fresh groundwater volumes in the Gonzales-New Orleans aquifer, depending on the applied infiltration rate. If an infiltration rate of ten million cubic meters per year is applied, the total fresh groundwater volume stabilizes and groundwater extraction can be continued at the FS2-rate without triggering significant intrusion of saltwater or further salinization of the extraction wells in Jefferson Parish.

If the infiltration rate is increased to fifty million cubic meters per year, fresh groundwater volumes significantly increase over time, pushing the saltwater front southwards and leading to freshening of the groundwater extraction wells. Drinking water volumes then increases by 45% between 2019 and 2119. In this case, saltwater extraction actually slightly enhances the fresh groundwater volume increase up to an extra 9%. The I-E-50 scenario was thereby the case for which fresh groundwater volume increased the most. However, the additional groundwater extraction also led to an increased groundwater flux towards the well from the south, where groundwater with a higher salinity is located. Movement of high salinity groundwater towards the study area is unwanted as it might enhance saltwater intrusion once the extraction wells are abandoned. Moreover, large-scale groundwater extraction can induce large subsidence rates in the New Orleans area (Section 2.3.6), which is already prone to flooding. Furthermore, extra costs are created by the implementation of the well systems and the treatment and/or discharging of the extracted saline groundwater. As the

increase of fresh groundwater volume of I-E-50 relative to I-50 is relatively small, the use of solely artificial recharge might be the most advantageous and viable measurement to improve the available fresh groundwater resources in the New Orleans area.

5.2. Model Uncertainties

As the availability of model input data is often limited and increasing the model complexity might have adverse consequences on the model performance, simplifications and assumptions regarding the model input variables in a large-scale groundwater model such as the one presented here are often inevitable. As such, a simplified model geology was used in this study, based on several transects provided by (Griffith, 2003) and focussing on the information that could be derived for the New Orleans area and the Eastern Florida Parishes. The established hydrogeology was assumed to be representative for the entire model domain, assuming constant layer thicknesses and depths in the east-west direction. Furthermore, aquifers were considered to be continuous and homogeneous throughout the study area. However, local studies in the Baton Rouge area (Chamberlain, 2012; Elshall et al., 2013; Pham & Tsai, 2017) and the New Orleans area (Ayrer, 2013; Ayrer & Wicks, 2013) revealed that the subsurface of Southeastern Louisiana is highly heterogeneous and complex. Moreover, the effects of flow impeding structures such as the Baton Rouge fault were also neglected. The uncertainties arising with these simplifications were partly compensated by means of reallocation of the hydraulic conductivity values for model cells with a very small layer thickness (Section 3.1.4), causing several aquifers to be connected which is in line with the available literature (Chamberlain, 2012; Griffith, 2003). Furthermore, uncertainties regarding the hydraulic conductivity values of the aquifers were partly reconsidered by using a simple calibration method (Section 3.3.1 and Section 4.1).

Additional uncertainties arise due to the model cell size and the amount of model layers used, especially when studying processes on a local scale as was the case here for the New Orleans area, which consists of only 697 model cells of 1000 x 1000 meters. In this case, a very slight salinity increase might cause the TDS concentration of a model grid cell to be pushed just above a certain threshold, leading to a relatively large decrease of the total fresh groundwater volumes. Furthermore, each aquifer was represented by a single model layer. Therefore, vertical salinity differences within aquifers were not included in the model and vertical migration of saline water due to groundwater extraction, which can be a relevant process within the Gonzales-New Orleans aquifer (Prakken, 2009), was disregarded.

The longitudinal dispersivity value used in the model is also subject large uncertainties. Dispersivity, in itself, is used as an upscaling parameter and is both scale-dependent and site-specific (Schulze-Makuch, 2005; Zech et al., 2015). The value used here (α = 1.0 m) was based on the values given by Zech et al, (2015). However, larger dispersivity values for model scales in the order of kilometers have been proposed in the past (e.g. Pickens & Grisak (1981); Schulze-Makuch (2005)). Fig. 5.1 depicts the effect of different dispersivity values on the initial model stability assumed in this study (Section 4.2.1). The figure shows that fresh groundwater volumes in the modelled groundwater system decrease significantly over time for larger dispersivity values, thereby omitting the initial model stability. The aforementioned uncertainties might be subject of future research to improve and verify the performance of model used in this study.
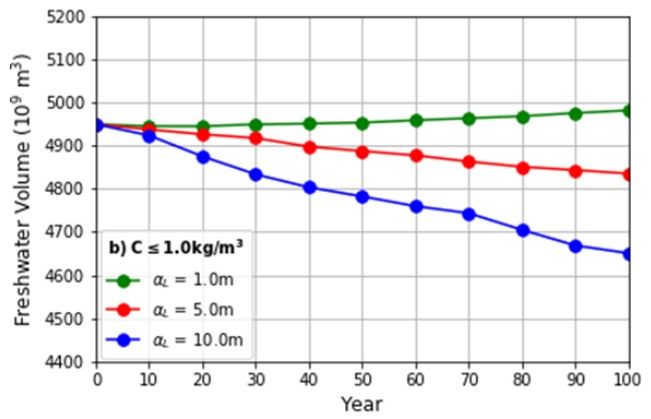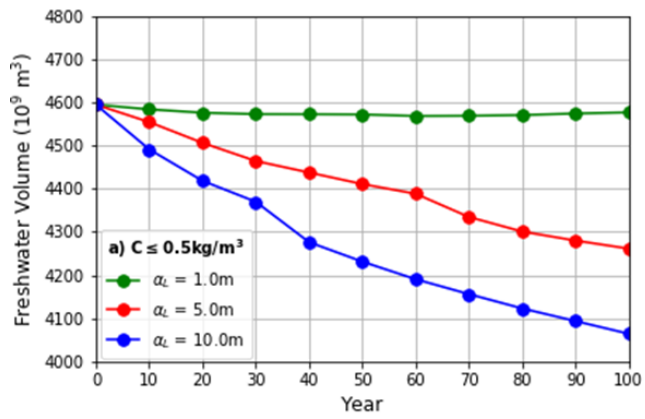
Fig. 5.1. Freshwater volume over time for full natural flow using different longitudinal dispersivity values for an upper freshwater limit of (a) 0.5 kg/m^3 and (b) 1.0 kg/m^3.

6. Conclusions & Further Research

6.1. Conclusions

The effects of saltwater intrusion on the fresh groundwater resources in southeastern Louisiana were studied based on a regional 3D variable-density groundwater flow and solute transport model established using the iMOD-SEAWAT software. The input variables required in the model were collected from several data sources. As the available data for several variables was insufficient or not fully covering the study area, interpolation techniques and literature based assumptions were used to fill these knowledge gaps. The created model covered an area of nearly 50,000 km^2 and consisted of 34 model layer including 15 aquifers, covering the entire Southern Hill regional aquifer system. Based on several future scenarios, the behaviour of the groundwater system was projected for the coming century to answer the research questions posed in Section 1.

Fresh groundwater is present in great abundances in the northern part of the aquifer system. Therefore, both natural and man-made saltwater intrusion enhancing mechanisms were found to have only a small effect on the total fresh groundwater volume in the Southern Hills regional aquifer system in the next 100 years. Saltwater intrusion resulting from short-term flooding, sea level rise and/or subsidence was found to be negligible, which was expected for a confined aquifer system as presented here, leading to a decrease of the fresh groundwater resources of less than 0.01% during the coming century. The effect of groundwater extraction on the total fresh groundwater volume present in the aquifer system was also found to be small, as less than 0.5% of the total freshwater volume was lost by 2119 following ongoing groundwater extraction.

On a more local scale, withdrawals can have large consequences for the fresh groundwater resources and lead to salinization in areas which are both subject to large extraction rates and located close to the transition zone between fresh and saline groundwater, such as the Baton Rouge area and the New Orleans area. Flow reversals and increased northward flow from saline groundwater containing areas towards fresh groundwater containing areas was found to be a consequence of groundwater extraction throughout the study area. In the Baton Rouge area, ongoing groundwater extraction was found to cause significant encroachment of saltwater towards the extraction wells. On the other hand, despite the presence of extraction wells, no significant saltwater intrusion occurred in the transition zone between fresh and saline groundwater in Saint James Parish and Saint John the Baptist Parish.

Continued groundwater extraction during the coming century has large implications for the availability of fresh groundwater in the Gonzales-New Orleans aquifer, the most important source of fresh groundwater in the New Orleans area. Continued withdrawals would lead to a decrease of the available drinking water volumes between 58% and 82% by 2119, depending on the amount that is withdrawn at the Michoud power plant. The proposed opening of a new power plant at Michoud with an extraction rate amounting to 10% of the pre-closure value would have a relatively small effect on the groundwater resources, leading to an extra drinking water volume loss of 2%. Saltwater intrusion into the fresh groundwater resources is expected to mainly occur in Jefferson Parish and the westernmost part of Orleans Parish.

The application of artificial recharge, using water from the Mississippi River, and saltwater extraction to ensure or increase the future fresh groundwater availability in the Gonzales-New Orleans aquifer has been studied. Using solely saltwater extraction was found to have adverse effects on the future fresh groundwater resources, leading to further salinization of the groundwater extraction wells. Artificial recharge, on the other hand, was proven to be an effective countermeasure to saltwater intrusion and led to freshening at the two groundwater extraction wells in Jefferson Parish. Infiltrating 10×10^6 m^3/y would cause the available fresh groundwater volume to stay more or less constant, while an infiltration rate of 50×10^6 m^3/y would cause the 2119 drinking water volume to grow by 45.9% relative to the present volume. For the latter infiltration rate, combining it with saltwater extraction would actually lead to a slightly larger fresh groundwater volume increase. However, the downsides of large extraction rates, including subsidence, attraction of highly saline water and higher operation costs, might cause the use of solely artificial recharge to be the most viable option to obtain enlarged groundwater volumes for the future.

6.2. Recommendations for Future Research

- o Conducting extended research on the hydrogeology of the Southern Hills aquifer system to gain more insight in the distribution of aquifers and confining layers, and achieve better estimates of the hydraulic conductivity values.
- o Verifying and calibrating the groundwater model using past and present observations on groundwater salinity and hydraulic heads, for example by creating an initial TDS concentration based on the salinity measurements for a certain period in the past and comparing the resulting changes of groundwater salinity to more recent observations.
- o Using a finer model resolution to include transport process within aquifers such as upward movement of saline water due to groundwater extraction.
- o Gathering additional groundwater measurements in the saline parts of the aquifer system to get a better estimate of the thickness of the transition zone between fresh groundwater and fully saline seawater.
- o Using a paleo-reconstruction of the formation of the Mississippi Delta to fully understand the processes that led to the current distribution of fresh and saline groundwater.
- o Implementing and studying the effect of a variable recharge rate, both spatially and temporally, based on determining factors such as precipitation rates and land use.
- o Further investigating the possibilities of saltwater extraction and artificial recharge to counteract saltwater intrusion by altering the well locations, numbers of wells and extraction rates.

References

AAE, L. &. (2016). *Groundwater for power plants: A big risk to New Orleans East*. Retrieved from https://www.all4energy.org/uploads/1/0/5/6/105637723/michoud-hia-groundwater-final-report.pdf

AAPA. (2016). U.S. Port Ranking by Cargo Tonnage 2016. Retrieved February 1, 2019, from https://www.aapa-ports.org/unifying/content.aspx?ItemNumber=21048#Statistics

Abd-Elhamid, H. F., & Javadi, A. A. (2011). A Cost-Effective Method to Control Seawater Intrusion in Coastal Aquifers. *Water Resources Management*, *25*(11), 2755–2780. https://doi.org/10.1007/s11269-011-9837-7

Abdalla, O. A. E., & Al-Rawahi, A. S. (2013). Groundwater recharge dams in arid areas as tools for aquifer replenishment and mitigating seawater intrusion: example of AlKhod , Oman. *Environmental Earth Sciences*, *69*, 1951–1962. https://doi.org/10.1007/s12665-012-2028-x

Anderson, C. E. (2012). *Sources of salinization of the Baton Rouge aquifer system : southeastern Louisiana*. Louisiana State University and Agricultural and Mechanical College. Retrieved from https://digitalcommons.lsu.edu/gradschool_theses/4078

Andreadis, K. M., Schumann, G. J. P., & Pavelsky, T. (2013). A simple global river bankfull width and depth database. *Water Resources Research*, *49*(10), 7164–7168. https://doi.org/10.1002/wrcr.20440

Antonellini, M., Mollema, P., Giambastiani, B., Bishop, K., Caruso, L., Minchio, A., … Gabbianelli, G. (2008). Salt water intrusion in the coastal aquifer of the southern Po Plain, Italy. *Hydrogeology Journal*, *16*, 1541–1556. https://doi.org/10.1007/s10040-008-0319-9

Assine, M. L., & Silva, A. (2009). Contrasting fluvial styles of the Paraguay River in the northwestern border of the Pantanal wetland, Brazil. *Geomorphology*. https://doi.org/10.1016/j.geomorph.2009.03.012

Ataie-Ashtiani, B., Werner, A. D., Simmons, C. T., Morgan, L. K., & Lu, C. (2013). How important is the impact of land-surface inundation on seawater intrusion caused by sea-level rise? *Hydrogeology Journal*, *21*, 1673–1677. https://doi.org/10.1007/s10040-013-1021-0

Ayrer, J. (2013). *Subsurface stratigraphic architecture of Pleistocene sediments in the greater New Orleans area*. Louisiana State University and Agricultural and Mechanical College. Retrieved from https://digitalcommons.lsu.edu/gradschool_theses/1710/

Ayrer, J., & Wicks, C. M. (2013). Geologic Model of Quaternary and Tertiary Deltaic Stratigraphy and the Impacts on Saltwater Encroachment in the Greater New Orleans Area. *Gulf Coast Association of Geological Societies Transactions*, 79–90.

Bear, J., & Cheng, A. . . . D. (1999). Introduction. In J. Bear, A. H. D. Cheng, S. Sorek, D. Ouazar, & I. Herrera (Eds.), *Seawater Intrusion in Coastal Aquifers – Concepts, Methods and Practices* (Vol. 14, pp. 1–8). Dordrecht: Kluwer Academic Publishers.

Bear, J., Zhou, Q., & Bensabat, J. (2001). Three dimensional simulation of seawater intrusion in heterogeneous aquifers, with application to the coastal aquifer of Israel. *First International Conference on Saltwater Intrusion and Coastal Aquifers: Monitoring, Modeling, and Management. Maroc, Essaouira, Morocco.*, *13*.

Beigi, E., & Tsai, F. T. C. (2015). Comparative study of climate-change scenarios on groundwater recharge, southwestern Mississippi and southeastern Louisiana, USA. *Hydrogeology Journal*, *23*(4), 789–806. https://doi.org/10.1007/s10040-014-1228-8

Blum, M. D., & Roberts, H. H. (2009). Drowning of the Mississippi Delta due to insufficient sediment supply and global sea-level rise. *Nature Geoscience*, *2*, 488–491. https://doi.org/10.1038/ngeo553

Buono, A. (1983). The Southern Hills Regional Aquifer System of Southeastern Louisiana and Southwestern Mississippi. *U.S. Geological Survey Water-Resources Investigations Report 83-4189*.

Burkett, V. R., Ziklkoski, D. B., & Hart, D. A. (2003). Sea-Level Rise and Subsidence: Implications for Flooding in New Orleans, Louisiana. *U.S. Geological Survey Subsidence Interest Group Conference: Proceedings of the Technical Meeting, Galveston, Texas, November 27-29, 2001*, 63–70.

Chamberlain, E. L. (2012). Depositional Environments of Upper Miocene Through Pleistocene Siliciclastic Sediments, Baton Rouge Aquifer System, Southeastern Louisiana. *LSU Master's Theses. 4062*.

Chamberlain, E. L., Hanor, J. S., & Tsai, F. T. (2013). Sequence Stratigraphic Characterization of the Baton Rouge Aquifer System , Southeastern Louisiana. *Gulf Coast Association of Geological Societies Transactions*, *63*, 125–136.

Chang, S. W., Clement, T. P., Simpson, M. J., & Lee, K. K. (2011). Does sea-level rise have an impact on saltwater intrusion?

Advances in Water Resources, *34*(10), 1283–1291. https://doi.org/10.1016/j.advwatres.2011.06.006

CK Associates Environmental Consultants. (2016). *TECHNICAL REPORT - EVALUATION OF GROUNDWATER WITHDRAWAL AND AIR QUALITY*. Retrieved from http://www.entergy-neworleans.com/powertogrow/power_station/JEL6CKTechnicalReport.pdf

Coleman, J. M., Roberts, H. H., & Stone, G. W. (1998). Mississippi River Delta: an Overview. *Journal of Coastal Research*, *14*(3), 698–716.

Copeland, C. (2005). Hurricane-Damaged Drinking Water and Wastewater Facilities: Impacts, Needs, and Response. *Congressional Research Service, Library of Congress*, *1*, 1–6. Retrieved from https://digital.library.unt.edu/ark:/67531/metadc824633/

D'Arconte, P. (2002). Land and Resource Uses of the Acadian-Pontchartrain NAWQA. Retrieved March 2, 2019, from https://la.water.usgs.gov/nawqa/resource.htm

Dial, D. C., & Kilburn, C. (1980). Ground-water resources of the Gramercy Area, Louisiana. *Louisiana Department of Transportation and Development, Office of Public Works Water Resources Technical Report No. 24, 39 P.*

Dial, D. C., & Sumner, D. M. (1989). Geohydrology and simulated effects of pumpage on the New Orleans aquifer system at New Orleans, Louisiana. *Louisiana Department of Transportation and Development Water Resources Technical Report No. 46, 54 P.* Retrieved from https://la.water.usgs.gov/publications/pdfs/TR46.pdf

Dial, D. C., & Tomaszewski, D. J. (1988). Geohydrology, water quality, and effects of pumpage on the New Orleans aquifer system, northern Jefferson Parish, Louisiana. *U.S. Geological Survey Water-Resources Investigations Report 88-4097, 34 P.* Retrieved from http://pubs.usgs.gov/%0Awri/1988/4097/report.pdf. %0D

Dickinson, G. (1953). Geological aspects of abnormal reservoir pressures in the Gulf Coast region of Louisiana, USA. *American Association of Petroleum Geologists Bulletin*, *37*(2), 410–432. https://doi.org/10.1306/5CEADC6B-16BB-11D7-8645000102C1865D

Diersch, H.-J. G., & Kolditz, O. (2002). Variable-density flow and transport in porous media: approaches and challenges. *Advances in Water Resources*, *25*, 899–944.

Dokka, R. K. (2011). The role of deep processes in late 20th century subsidence of New Orleans and coastal areas of southern Louisiana and Mississippi. *Journal of Geophysical Research: Solid Earth*, *116*(6), 1–25. https://doi.org/10.1029/2010JB008008

Ecology and Environment, I. (2011). Recommendations for a Statewide Ground Water Management Plan. *Baton Rouge, LA: Louisiana Department of Natural Resources.*

Eddards, M. L. R., Kister, L. R., & Scarcia, G. (1956). Water Resources of the New Orleans Area: Louisiana. *U.S. Geological Survey Circular 374, 41p.* Retrieved from https://books.google.nl/books?hl=nl&lr=&id=Fvez_1q-cIIC&oi=fnd&pg=PP6&dq=WATER+RESOURCES+OF+THE+NEW+ORLEANS+AREA+LOUISIANA++1956&ots=5-Ec5yz4tr&sig=X93NPGuhMBQLhRimZTHdBN0a_5A#v=onepage&q=WATER RESOURCES OF THE NEW ORLEANS AREA LOUISIANA 1956&f=false

Elshall, A. S., Tsai, F. T. C., & Hanor, J. S. (2013). Indicator geostatistics for reconstructing Baton Rouge aquifer-fault hydrostratigraphy, Louisiana, USA. *Hydrogeology Journal*, *21*(8), 1731–1747. https://doi.org/10.1007/s10040-013-1037-5

Faneca Sanchez, M., Bashar, K., Janssen, G. M. C. M., Vogels, M., Snel, J., Zhou, Y., … Oude Essink, G. H. P. (2015). *SWIBANGLA : Managing salt water intrusion impacts in coastal groundwater systems of Bangladesh*.

Fitts, C. R. (2013). *Groundwater Science* (2nd ed.). Oxford, UK: Academic Press (Elsevier).

Ghijben, W. B. (1888). Nota in verband met de voorgenomen putboring nabij Amsterdam. *Tijdschrift van Het Koninklijk Instituut Voor Ingenieurs*, 8–22.

Giambastiani, B. M. S., Antonellini, M., Oude Essink, G. H. P., & Stuurman, R. J. (2007). Saltwater intrusion in the unconfined coastal aquifer of Ravenna (Italy): A numerical model. *Journal of Hydrology*, *340*(1–2), 91–104. https://doi.org/10.1016/j.jhydrol.2007.04.001

Gingerich, S. B., Voss, C. I., & Johnson, A. G. (2017). Seawater-flooding events and impact on freshwater lenses of low-lying islands: Controlling factors, basic management and mitigation. *Journal of Hydrology*, *551*, 676–688. https://doi.org/10.1016/j.jhydrol.2017.03.001

Gossel, W., Sefelnasr, A., & Wycisk, P. (2010). Modelling of paleo-saltwater intrusion in the northern part of the Nubian Aquifer System, Northeast Africa. *Hydrogeology Journal*, *18*, 1447–1463. https://doi.org/10.1007/s10040-010-0597-x

Griffith, J. M. (2003). Hydrogeologic Framework of Southeastern Louisiana. *Water Resources Technical Report 72, Louisiana*

Department of Transportation and Development, Baton Rouge, LA.

Griffith, J. M. (2017). Water Resources of St. Tammany Parish, Louisiana. *U.S. Geological Survey & U.S. Department of the Interior, Fact Sheet 2009-3064. Version 1.3, January 2017*.

Griffith, J. M., & Fendick, R. B. (2011). Water Resources of Ascension Parish. *U.S. Geological Survey & U.S. Department of the Interior, Fact Sheet 2009–3063, Revised September 2011*.

Grubb, H. F. (1984). Planning report for the Gulf Coast Regional Aquifer-System Analysis in the Gulf of Mexico Coastal Plain, United States. *U.S. Geological Survey, Water-Resources Investigations Report 84-4219*.

Guo, W., & Langevin, C. D. (2002). *User's Guide to SEAWAT: A computer program for simulation of three-dimensional variable-density ground-water flow*. *USGS Techniques of Water Resources Investigations*. Tallahassee, Florida: U.S. Geological Survey. https://doi.org/10.1007/s00125-006-0486-y

Hanor, J. S. (1993). Effective Hydraulic Conductivity of Fractured Clay Beds at a Hazardous Waste Landfill, Louisiana Gulf Coast. *Water Resources Research*, *29*(11), 3691–3698. https://doi.org/0043-1397/93/93 WR-01913

Harbaugh, A. W., Banta, E. R., Hill, M. C., & Mcdonald, M. G. (2000). MODFLOW-2000, the U.S. Geological Survey Modular Ground-Water Model—User guide to modularization concepts and the ground-water flow process. *U.S. Geological Survey Open-File Report 00-92*, 121.

Hassanizadeh, S. M. (2017). *Summary Lecture Notes - Hydrogeological Transport Phenomena*. Utrecht University, Utrecht.

Hayashi, M. (2004). WATER FOR ENVIRONMENTAL MONITORING AND GEOPHYSICAL DATA INVERSION, 119–128.

Henry, H. R. (1964). Effects of Dispersion on Salt Encroachment in Coastal Aquifers. *Sea Water in Coastal Aquifers: Geological Survey Water-Supply Paper 1613-C*.

Herzberg, A. (1901). Die Wasserversorgung einiger Nordseebaden. *Zeitung f Ur Gasbeleuchtung Und Wasserversorgung*, *44*(6), 815–819.

Hill, M. C. (1990). Preconditioned conjugate-gradient 2 (PCG2), a computer program for solving ground-water flow equations. *U.S. Geological Survey Water-Resources Investigations Report 90–4048*, 43.

Hussain, M. S., Javadi, A. A., Ahangar-Asr, A., & Farmani, R. (2015). A surrogate model for simulation-optimization of aquifer systems subjected to seawater intrusion. *JOURNAL OF HYDROLOGY*, *523*, 542–554. https://doi.org/10.1016/j.jhydrol.2015.01.079

Hussain, M. S., Javadi, A. A., & Sherif, M. M. (2015). Three dimensional simulation of seawater intrusion in a regional coastal aquifer in UAE. *Procedia Engineering*, *119*, 1153–1160. https://doi.org/10.1016/j.proeng.2015.08.965

Huyakorn, P. S., Anders, P. F., Mercer, J. W., & White, H. O. (1987). Saltwater intrusion in aquifers: Development and testing of a three-dimensional finite element model. *Water Resources Research*, *23*(2), 293–312.

Illangasekare, T., Tyler, S. W., Clement, T. P., Villholth, K. G., Perera, A. P. G. R. L., Obeysekera, J., … Jensen, K. (2006). Impacts of the 2004 tsunami on groundwater resources in Sri Lanka. *Water Resources Research*, *42*(5), 1–9. https://doi.org/10.1029/2006WR004876

IPCC. (2013). Summary for Policymakers. In T. F. Stocker, D. Qin, G.-K. Plattner, M. Tignor, S. K. Allen, J. Boschung, … P. M. Midgley (Eds.), *Climate Change 2013: The Physical Science Basis. Contribution of Working Group I to the Fifth Assessment Report of the Intergovernmental Panel on Climate Change* (pp. 1–32). Cambridge University Press, Cambridge, United Kingdom and New York, NY, USA. https://doi.org/10.1016/j.renene.2009.11.012

Javadi, A. A., Hussain, M. S., Sherif, M. M., & Farmani, R. (2015). Multi-objective Optimization of Different Management Scenarios to Control Seawater Intrusion in Coastal Aquifers. *Water Resources Management*, *29*, 1843–1857. https://doi.org/10.1007/s11269-015-0914-1

Jones, C. E., An, K., Blom, R. G., Kent, J. D., Ivins, E. R., & Bekaert, D. (2014). Anthropogenic and geologic influences on subsidence in the vicinity of New Orleans, Louisiana. *Journal of Geophysical Research: Solid Earth*, *121*(5), 3867–3887. https://doi.org/10.1002/2013JB010933.Received

Kacimov, A. R., Sherif, M. M., Perret, J. S., & Al-Mushikhi, A. (2009). Control of sea-water intrusion by salt-water pumping: Coast of Oman. *Hydrogeology Journal*, *17*, 541–558. https://doi.org/10.1007/s10040-008-0425-8

Kates, R. W., Colten, C. E., Laska, S., & Leatherman, S. P. (2006). Reconstruction of New Orleans after Hurricane Katrina: A research perspective. *PNAS*, *103*(40), 14653–14660.

Ketabchi, H., Mahmoodzadeh, D., Ataie-Ashtiani, B., & Simmons, C. T. (2016). Sea-level rise impacts on seawater intrusion in coastal aquifers: Review and integration. *Journal of Hydrology*, *535*, 235–255. https://doi.org/10.1016/j.jhydrol.2016.01.083

Khublaryan, M. G., Frolov, A. P., & Yushmanov, I. O. (2008). Seawater Intrusion into Coastal Aquifers. *Water Resources*,

35(3), 274–286. https://doi.org/10.1134/S0097807808030032

Kolb, C. R., & Van Lopik, J. R. (1966). Depositional Environments of the Mississippi River Deltaic Plain - Southeastern Louisiana. *Deltas in Their Geologic Framework, Houston Geological Society*, 17–61.

Kopsiaftis, G., Mantoglou, A., & Giannoulopoulos, P. (2009). Variable density coastal aquifer models with application to an aquifer on Thira Island. *Desalinisation*, *237*, 65–80. https://doi.org/10.1016/j.desal.2007.12.023

Kottek, M., Grieser, J., Beck, C., Rudolf, B., & Rubel, F. (2006). World Map of the Köppen-Geiger climate classification updated. *Meteorologische Zeitschrif*, *15*(3), 259–263. https://doi.org/10.1127/0941-2948/2006/0130

Lang, J. W. (1972). Geohydrologic Summary of the Pearl River Basin , Mississippi and Louisiana. *Geological Survey Water-Supply Paper 1899-M*, 1899–M.

Langevin, C. D., Thorne, D. T., Dausman, A. M., Sukop, M. C., & Guo, W. (2008). *{SEAWAT} version 4: A computer program for simulation of Multi-Species Solute and Heat Transport. Techniques and Methods Book 6, Chapter A22. {US} Department of the Interior*. U.S. Geological Survey. Reston, Virginia.

Lehner, B., Verdin, K., & Jarvis, A. (2008). New global hydrography derived from spaceborne elevation data. *Eos, Transactions American Geophysical Union*, *89*(10), 93–94. https://doi.org/10.1029/2008EO100001

Liu, Y., & Huang, H.-J. (2013). Characterization and mechanism of regional land subsidence in the Yellow River Delta, China. *Natural Hazards*, *68*(2), 687–709. https://doi.org/10.1007/s11069-013-0648-4

Lovelace, J. K. (2007). Chloride Concentrations in Ground Water in East and West Baton Rouge Parishes, Louisiana, 2004–05. *U.S. Geological Survey Scientific Investigations Report 2007–5069*, 27.

Lu, C., Shi, W., Xin, P., Wu, J., & Werner, A. D. (2017). Replenishing an unconfined coastal aquifer to control seawater intrusion: Injection or infiltration? *Water Resources Research*, *53*, 4775–4786. https://doi.org/10.1002/2016WR019625.Received

Lu, C., Werner, A. D., Simmons, C. T., Robinson, N. I., & Luo, J. (2013). Maximizing Net Extraction Using an Injection-Extraction Well Pair in a Coastal Aquifer. *Groundwater*, *51*(2), 219–228. https://doi.org/10.1111/j.1745-6584.2012.00973.x

Lu, C., Xin, P., Li, L., & Luo, J. (2015). Seawater intrusion in response to sea-level rise in a coastal aquifer with a general-head inland boundary. *Journal of Hydrology*, *522*, 135–140. https://doi.org/10.1016/j.jhydrol.2014.12.053

Luyun Jr., R., Momii, K., & Nakagawa, K. (2011). Effects of Recharge Wells and Flow Barriers on Seawater Intrusion. *Ground Water*, *49*(2), 239–249. https://doi.org/10.1111/j.1745-6584.2010.00719.x

Mantoglou, A. (2003). Pumping management of coastal aquifers using analytical models of saltwater intrusion. *Water Resources Research*, *39*(12). https://doi.org/10.1029/2002WR001891

Martin Jr., A., & Whiteman Jr., C. D. (1999). Hydrology of the Coastal Lowlands Aquifer System in parts of Alabama, Florida, Louisiana, and Mississippi. *U.S. Geological Survey Professional Paper*, *1416–H*, 51.

Mazi, K., Koussis, A. D., & Destouni, G. (2013). Tipping points for seawater intrusion in coastal aquifers under rising sea level. *Environmental Research Letters*, *8*. https://doi.org/10.1088/1748-9326/8/1/014001

McFarlan, E., & LeRoy, D. O. (1988). Subsurface geology of the Late Tertiary and Quaternary deposits, coastal Louisiana and the adjacent continental shelf. *Gulf Coast Association of Geological Societies Transactions*, *38*(1965), 421–433.

Meckel, T. A., ten Brink, U. S., & Williams, S. J. (2006). Current subsidence rates due to compaction of Holocene sediments in southern Louisiana. *Geophysical Research Letters*, *33*(11), 1–5. https://doi.org/10.1029/2006GL026300

Muskat, M. (1937). The flow of homogeneous fluids through porous media. *McGraw-Hill Book Company, Inc. New York*, 763.

Naik, P. C. (2018). Seawater Intrusion in the Coastal Alluvial Aquifers of the Mahanadi Delta. *Springer Briefs in Water Science and Technology*, *123*.

NASA. (2019). Shuttle Radar Topographic Mission: The Mission to Map the World. Retrieved from https://www2.jpl.nasa.gov/srtm/

NHMRC, & NRMMC. (2011). *Australian Drinking Water Guidelines Paper 6 National Water Quality Management Strategy*. *National Health and Medical Research Council, National Resource Management Ministerial Council, Commonwealth of Australia,*. National Health and Medical Research Council, National Resource Management Ministerial Council, Commonwealth of Australia, Canberra. https://doi.org/1864965118

Nienhuis, J. H., Törnqvist, T. E., Jankowski, K. L., Fernandes, A. M., & Keogh, M. E. (2017). A New Subsidence Map for Coastal Louisiana. *GSA Today*, *27*(9), 58–59. https://doi.org/10.1130/GSATG337GW.1

NOAA. (2018). *Costliest U.S. tropical cyclones tables updated*.

Nunn, J. A. (1985). State of stress in the northern Gulf Coast. *Geology*, *13*(6), 429–432. https://doi.org/10.1130/0091-7613(1985)13<429:SOSITN>2.0.CO;2

Nyman, D. J., & Fayard, L. D. (1978). Ground-water resources of Tangipahoa and St. Tammany Parishes, southeastern Louisiana. *Louisiana Department of Transportation and Development, Office of Public Works Water Resources Technical Report No. 15, 76 P.*

Oude Essink, G. H. P. (2001a). Improving fresh groundwater supply -- problems and solutions. *Ocean & Coastal Management*, *44*, 429–449.

Oude Essink, G. H. P. (2001b). Saltwater intrusion in 3D large-scale aquifers: A Dutch case. *Physics and Chemistry of the Earth, Part B: Hydrology, Oceans and Atmosphere*, *26*(4), 337–344. https://doi.org/10.1016/S1464-1909(01)00016-8

Oude Essink, G. H. P., Van Baaren, E. S., & De Louw, P. G. B. (2010). Effects of climate change on coastal groundwater systems: A modeling study in the Netherlands. *Water Resources Research*, *46*(10), 1–16. https://doi.org/10.1029/2009WR008719

Paniconi, C., Khlaifi, I., Lecca, G., Giacomelli, A., & Tarhouni, J. (2001). Modeling and Analysis of Seawater Intrusion in the Coastal Aquifer of Eastern Cap-Bon, Tunisia. *Transport in Porous Media*, *43*, 3–28.

Paz, A. R. da, Collischonn, W., Risso, A., & Mendes, C. A. B. (2008). Errors in river lengths derived from raster digital elevation models. *Computers and Geosciences*, *34*(11), 1584–1596. https://doi.org/10.1016/j.cageo.2007.10.009

Pham, H. V., & Tsai, F. T. C. (2017). Modeling complex aquifer systems: a case study in Baton Rouge, Louisiana (USA). *Hydrogeology Journal*, *25*(3), 601–615. https://doi.org/10.1007/s10040-016-1532-6

Pickens, J. F., & Grisak, G. E. (1981). Scale-dependent dispersion in a stratified granular aquifer. *Water Resources Research*, *17*(4), 1191–1211. https://doi.org/10.1029/WR017i004p01191

Pickwell, A. G. G. (2012). *Development of a Novel Invertebrate Indexing Tool for the Determination of Salinity in Aquatic Inland Drainage Channels*. University of Lincoln.

Pool, M., & Carrera, J. (2010). Dynamics of negative hydraulic barriers to prevent seawater intrusion. *Hydrogeology Journal*, *18*, 95–105. https://doi.org/10.1007/s10040-009-0516-1

Post, V. E. A. (2005). Fresh and saline groundwater interaction in coastal aquifers: Is our technology ready for the problems ahead? *Hydrogeology Journal*, *13*, 120–123. https://doi.org/10.1007/s10040-004-0417-2

Post, V. E. A., Kooi, H., & Simmons, C. T. (2007). Using hydraulic head measurements in variable-density ground water flow analyses. *Ground Water*, *45*(6), 664–671. https://doi.org/10.1111/j.1745-6584.2007.00339.x

Prakken, L. B. (2009). *Groundwater Resources in the New Orleans Area, 2008*. *Water Resources Technical Report No.80*. Retrieved from https://la.water.usgs.gov/publications/pdfs/TR80.pdf

Prakken, L. B. (2013a). Water Resources of Plaquemines Parish, Louisiana. *U.S. Geological Survey & U.S. Department of the Interior, Fact Sheet 2013-3031, June 2013*.

Prakken, L. B. (2013b). Water Resources of St . Bernard Parish, Louisiana. *U.S. Geological Survey & U.S. Department of the Interior, Fact Sheet 2013-3030, May 2013*.

Prakken, L. B., & Lovelace, J. K. (2013a). Water Resources of Assumption Parish, Louisiana. *U.S. Geological Survey & U.S. Department of the Interior, Fact Sheet 2013-3061, September 2013*.

Prakken, L. B., & Lovelace, J. K. (2013b). Water Resources of Lafourche Parish, Louisiana. *U.S. Geological Survey & U.S. Department of the Interior, Fact Sheet 2013-3075, November 2013*.

Prakken, L. B., & Lovelace, J. K. (2014). Water Resources of Jefferson Parish , Louisiana. *U.S. Geological Survey & U.S. Department of the Interior, Fact Sheet 2013-3073, March 2014.*

Prakken, L. B., Lovelace, J. K., & White, V. E. (2014a). Water Resources of Orleans Parish, Louisiana. *U.S. Geological Survey & U.S. Department of the Interior, Fact Sheet, 2014–3017 May 2014*.

Prakken, L. B., Lovelace, J. K., & White, V. E. (2014b). Water Resources of Terrebonne Parish, Louisiana. *U.S. Geological Survey & U.S. Department of the Interior, Fact Sheet 2014-3016, May 2014*.

Prakken, L. B., & White, V. E. (2015). Water Resources of St. Charles Parish, Louisiana. *U.S. Geological Survey & U.S. Department of the Interior, Fact Sheet 2014–3118, February 2015*. Retrieved from https://pubs.usgs.gov/fs/2013/3102/pdf/fs2013-3102.pdf

Rahmawati, N., Vuillaume, J.-F., & Purnama, I. L. S. (2013). Salt intrusion in Coastal and Lowland areas of Semarang City. *Journal of Hydrology*, *494*, 146–159. https://doi.org/10.1016/j.jhydrol.2013.04.031

Ranjan, P., Kazama, S., & Sawamoto, M. (2006). Effects of Climate Change on Coastal Fresh Groundwater Resources. *Global Environmental Change*, *16*(4), 388–399.

Rhoades, J. D., Kandiah, A., & Mashali, A. M. (1992). The use of saline waters for crop production. *FAO Irrigation and Drainage Paper*, *48*, 145.

Rollo, J. R. (1966). Ground-water resources of the greater New Orleans area, Louisiana. *Department of Conservation, Louisiana Geological Survey, and Louisiana Department of Public Works Water Resources Bulletin No. 9, 69 P.*

Rollo, J. R. (1969). Salt-water encroachment in aquifers of the Baton Rouge area, Louisiana. *Department of Conservation, Louisiana Geological Survey, and Louisiana Department of Public Works.*

Sargent, B. P. (2011). Water use in Louisiana, 2010. *Special Report No. 17 (Revised), Louisiana Department of Transportation and Development Water Resources, Baton Rouge, LA, 135 Pp*, *17*(17), 0–2. Retrieved from http://la.water.usgs.gov/publications/pdfs/WaterUse2010.pdf

Schemel, L. E. (2001). Simplified conversions between specific conductance and salinity units for use with data from monitoring stations. *Interagency Ecological Program Newsletter*, *14*(1), 17–18.

Schulze-Makuch, D. (2005). Longitudinal dispersivity data and implications for scaling behavior. *Ground Water*, *43*(3), 443–456. https://doi.org/10.1111/j.1745-6584.2005.0051.x

Shen, Z., Törnqvist, T. E., Autin, W. J., Mateo, Z. R. P., Straub, K. M., & Mauz, B. (2012). Rapid and widespread response of the Lower Mississippi River to eustatic forcing during the last glacial-interglacial cycle. *Geological Society of America Bulletin; May/June 2012*, *124*(5/6), 690–704. https://doi.org/10.1130/B30449.1

Sherif, M. M., & Hamza, K. I. (2001). Mitigation of Seawater Intrusion by Pumping Brackish Water. *Transport in Porous Media*, *43*, 29–44.

Sherif, M. M., & Singh, V. P. (1999). Eff€ect of climate change on sea water intrusion in coastal aquifers. *Hydrological Processes*, *13*, 1277–1287.

Sherif, M. M., Singh, V. P., & Amer, M. (1990). A Note on Saltwater Intrusion in Coastal Aquifers. *Water Resources Management*, *4*, 123–134.

Shi, L., & Jiao, J. J. (2014). Seawater intrusion and coastal aquifer management in China : a review. *Environmental Earth Sciences*, *72*, 2811–2819. https://doi.org/10.1007/s12665-014-3186-9

Shinkle, K. D., & Dokka, R. K. (2004). Rates of Vertical Displacement at Benchmarks in the Lower Mississippi Valley and the Northern Gulf Coast. *NOAA Technical Report NOS/NGS*, *50*, 135.

Siarkos, I., Latinopoulos, D., Mallios, Z., & Latinopoulos, P. (2017). A methodological framework to assess the environmental and economic effects of injection barriers against seawater intrusion. *Journal of Environmental Management*, *193*, 532–540. https://doi.org/10.1016/j.jenvman.2017.02.051

Simmons, C. T. (2005). Variable density groundwater flow: From current challenges to future possibilities. *Hydrogeology Journal*, *13*, 116–119. https://doi.org/10.1007/s10040-004-0408-3

Simpson, M. J., & Clement, T. P. (2004). Improving the worthiness of the Henry problem as a benchmark for density-dependent groundwater flow models. *Water Resources Research*, *40*. https://doi.org/10.1029/2003WR002199

Smith, C. G., & Hanor, J. S. (1975). Underground storage of treated water: A field test. *Ground Water*, *15*(5), 410–417.

Stem, J. E. (1990). *State Plane Coordinate System of 1983*. *NOAA Manual NOS NGS 5, US Department of Commerce, Rockville, MD*. Retrieved from papers3://publication/uuid/548DF830-3EB1-4C34-BB86-56E4C1734EB1

Stewart, M. T. (1999). Geophysical Investigations. In J. Bear, A. H. D. Cheng, S. Sorek, D. Ouazar, & I. Herrera (Eds.), *Seawater Intrusion in Coastal Aquifers – Concepts, Methods and Practices* (pp. 9–50). Dordrecht: Kluwer Academic Publishers.

Stuart, C. G., Knochenmus, D., & McGee, B. D. (1994). *Guide to Louisiana's ground-water resources*. Retrieved from https://pubs.usgs.gov/wri/1994/4085/report.pdf

Theis, C. V. (1935). The relation between the lowering of the Piezometric surface and the rate and duration of discharge of a well using ground-water storage. *Eos, Transactions American Geophysical Union*, *16*(2), 519–524. https://doi.org/10.1029/TR016i002p00519

Timár, G. (2003). Controls on channel sinuosity changes: A case study of the Tisza River, the Great Hungarian Plain. *Quaternary Science Reviews*, *22*(20), 2199–2207. https://doi.org/10.1016/S0277-3791(03)00145-8

Tomaszewski, D. J. (1996). Distribution and Movement of Saltwater Aquifers in the Baton Rouge Area, Louisiana, 1990-92. *Louisiana Department of Transportation and Development Water Resources Technical Report No. 59.*

Tomaszewski, D. J. (2003). *Ground-water Resources along the Lower Mississippi River, Southeastern Louisiana*. *Water Resources Technical Report No.69*. Retrieved from https://la.water.usgs.gov/publications/pdfs/TR76.pdf

Tsai, F. T.-C., & Li, X. (2008). Saltwater Intrusion and Hydraulic Conductivity Estimation in East Baton Rouge Parish, Louisiana. *20th Salt Water Intrusion Meeting*, 274–277.

US Climate Data. (2019). Climate data for New Orleans, LA - 70112 - 1981-2010 normals - weather. Retrieved from https://www.usclimatedata.com/climate/new-orleans/louisiana/united-states/usla0788

USEPA. (2017). National Secondary Drinking Water Standards: Guidance for Nuisance Chemicals. Retrieved March 7, 2019, from https://www.epa.gov/dwstandardsregulations/secondary-drinking-water-standards-guidance-nuisance-chemicals

USGS. (2018). U.S. Geological Survey Water Resources Cooperative Program: Louisiana Water Use Program. Retrieved December 23, 2018, from https://la.water.usgs.gov/WaterUse/default.asp

USGS. (2019a). USGS Surface-Water Data for the Nation. Retrieved March 14, 2019, from https://waterdata.usgs.gov/nwis/sw

USGS. (2019b). Water Quality Samples for Louisiana: Sample Data. Retrieved February 12, 2019, from https://nwis.waterdata.usgs.gov/la/nwis/qwdata

USGS. (2019c). Water Quality Samples for Mississippi: Sample Data. Retrieved February 12, 2019, from https://nwis.waterdata.usgs.gov/ms/nwis/qwdata

Van Baaren, E. S., Oude Essink, G. H. P., Janssen, G. M. G. M., de Louw, P. G. B., Heerdink, R., & Goes, B. (2016). *Verzoeting en verzilting freatisch grondwater in de Provincie Zeeland: Regionaal 3D model voor zoet-zout grondwater, Deltares rapport*.

van Dam, J. C. (2013). Exploitation, Restoration and Management. In J. Bear, A. H. D. Cheng, S. Sorek, D. Ouazar, & I. Herrera (Eds.), *Seawater Intrusion in Coastal Aquifers – Concepts, Methods and Practices* (pp. 73–125). Dordrecht: Kluwer Academic Publishers. https://doi.org/10.1007/978-94-017-2969-7_4

Verkaik, J., & Janssen, G. M. C. M. (2015). iMOD-SEAWAT, User Manual. *Version 0.1, 15 July 2015, Deltares, Delft, The Netherlands*.

Vermeulen, P. T. M., Burgering, L. M. T., Roelofsen, F. J., Minnema, B., & Verkaik, J. (2017). iMOD user manual. *Version 4.2, December 21, 2017. Deltares, The Netherlands. (Http://Oss.Deltares.Nl/Web/IMOD)*.

Wada, Y., Van Beek, L. P. H., Van Kempen, C. M., Reckman, J. W. T. M., Vasak, S., & Bierkens, M. F. P. (2010). Global depletion of groundwater resources. *Geophysical Research Letters*, *37*(20), 1–5. https://doi.org/10.1029/2010GL044571

Weatherall, P., Marks, K. M., Jakobsson, M., Schmitt, T., Tani, S., Arndt, J. E., … Wigley, R. (2015). A new digital bathymetric model of the world's oceans. *Earth and Space Science*, *2*, 416–430. https://doi.org/10.1002/ 2015EA000107

Wendeborn, F. C., & Hanor, J. S. (2013). Use of Spatial Variations in Groundwater Salinity to Assess Pathways of Saline Contamination through the Baton Rouge Fault, Southeastern Louisiana. *Gulf Coast Association of Geological Societies Transactions*, *63*, 461–472.

Werner, A. D. (2010). A review of seawater intrusion and its management in Australia. *Hydrogeology Journal*, *18*, 281–285. https://doi.org/10.1007/s10040-009-0465-8

Werner, A. D., Bakker, M., Post, V. E. A., Vandenbohede, A., Lu, C., Ataie-Ashtiani, B., … Barry, D. A. (2013). Seawater intrusion processes, investigation and management: Recent advances and future challenges. *Advances in Water Resources*, *51*, 3–26. https://doi.org/10.1016/j.advwatres.2012.03.004

Werner, A. D., & Simmons, C. T. (2009). Impact of sea-level rise on sea water intrusion in coastal aquifers. *Ground Water*, *47*(2), 197–204. https://doi.org/10.1111/j.1745-6584.2008.00535.x

Werner, A. D., Ward, J. D., Morgan, L. K., Simmons, C. T., Robinson, N. I., & Teubner, M. D. (2012). Vulnerability indicators of sea water intrusion. *Ground Water*, *50*(1), 48–58. https://doi.org/10.1111/j.1745-6584.2011.00817.x

White, V. E. (2017). Water Resources of the Southern Hills Regional Aquifer System , Southeastern Louisiana. *U.S. Geological Survey & U.S. Department of the Interior, Fact Sheet 2017-3010, March 2017*.

White, V. E., & Prakken, L. B. (2015a). Water resources of East Baton Rouge Parish, Louisiana. *U.S. Geological Survey & U.S. Department of the Interior, Fact Sheet 2015–300, May 2015*. https://doi.org/10.3133/fs20153001

White, V. E., & Prakken, L. B. (2015b). Water Resources of St. James Parish, Louisiana. *U.S. Geological Survey & U.S. Department of the Interior, Fact Sheet 2015–3038, June 2015*.

White, V. E., & Prakken, L. B. (2016a). Water Resources of Livingston Parish, Louisiana. *U.S. Geological Survey & U.S.*

Department of the Interior, Fact Sheet 2016–3048, July 2016.

White, V. E., & Prakken, L. B. (2016b). Water Resources of St. Helena Parish, Louisiana. *U.S. Geological Survey & U.S. Department of the Interior, Fact Sheet 2016–3047, July 2016.*

White, V. E., & Prakken, L. B. (2016c). Water resources of Tangipahoa Parish, Louisiana. *U.S. Geological Survey & U.S. Department of the Interior, Fact Sheet 2016–3049, July 2016.* https://doi.org/10.3133/fs20163049

White, V. E., & Prakken, L. B. (2016d). Water Resources of Washington Parish, Louisiana. *U.S. Geological Survey & U.S. Department of the Interior, Fact Sheet 2015–3083, June 2016.*

White, V. E., & Prakken, L. B. (2016e). Water resources of West Baton Rouge Parish, Louisiana. *U.S. Geological Survey & U.S. Department of the Interior, Fact Sheet 2016-3068, November 2016*, 6. https://doi.org/10.3133/fs20153001

White, V. E., & Prakken, L. B. (2017). Water resources of East Feliciana Rouge Parish, Louisiana. *U.S. Geological Survey & U.S. Department of the Interior, Fact Sheet 2016-3069, January 2017*, 6. https://doi.org/10.3133/fs20153001

White, V. E., Prakken, L. B., & Fendick, R. B. (2015). Water Resources of St. John the Baptist Parish, Louisiana. *U.S. Geological Survey & U.S. Department of the Interior, Fact Sheet 2014–3102, February 2015*.

Wolstencroft, M., Shen, Z., Törnqvist, T. E., Milne, G. A., & Kulp, M. (2014). Understanding subsidence in the Mississippi Delta region due to sediment, ice, and ocean loading: Insights from geophysical modeling. *Journal of Geophysical Research: Solid Earth*, *119*(4), 3838–3856. https://doi.org/10.1002/2013JB010928.Received

Yuill, B., Lavoie, D., & Reed, D. J. (2009). Understanding Subsidence Processes in Coastal Louisiana. *Journal of Coastal Research*, *SI*(54), 23–36. https://doi.org/10.2112/si54-012.1

Zech, A., Attinger, S., Cvetkovic, V., Dagan, G., Dietrich, P., Fiori, A., … Teutsch, G. (2015). Is unique scaling of aquifer macrodispersivity supported by field data? *Water Resources Research*, *5*, 7662–7679. https://doi.org/10.1002/2015WR017220.

Zheng, C. (2010). *MT3DMS v5.3: Supplemental User's Guide*. *Technical Report*. Tuscaloosa, Alabama.

Zheng, C., & Wang, P. P. (1999). *MT3DMS: A modular three-dimensional multispeces transport model for simulation of advection, dispersion, and chemical reactions of contaminants in groundwater systems: Documentation and User's Guide*. *A modular three-dimensional multi-species …*. Washington, DC. Retrieved from http://www.geo.tu-freiberg.de/hydro/vorl_portal/gw-modellierung/MT3DMS Ref Manual.pdf

Zimmermann, K. A. (2015). Hurricane Katrina: Facts, Damage & Aftermath. Retrieved from https://journals.sagepub.com/doi/pdf/10.1177/0893318916646454

Appendix A – Figure 3 of Griffith (2003)

System	Series	Ma[1]	Stratigraphic unit	Aquifer system or confining unit	Hydrogeologic units — Aquifer or confining unit				
					Baton Rouge area — North	Baton Rouge area — South	Eastern Florida Parishes — North	Eastern Florida Parishes — South	New Orleans area
Quaternary	Holocene	? 0.01	Mississippi River and other alluvial deposits	Near-surface aquifers or surficial confining unit ?	Mississippi River alluvial aquifer		No regionally extensive hydrogeologic units		Shallow aquifers
									Mississippi River alluvial aquifer
	Pleistocene		Unnamed Pleistocene deposits	Chicot equivalent aquifer system or surficial confining unit	No regionally extensive hydrogeologic units				Gramercy aquifer
									Norco aquifer
					Shallow sands				Gonzales-New Orleans aquifer
		2			Upland terrace aquifer	"400-foot" sand	Upland terrace aquifer	Upper Ponchatoula aquifer	"1,200-foot" sand
						"600-foot" sand			
Tertiary	Pliocene		Blounts Creek Member	Evangeline equivalent aquifer system or surficial confining unit	"800-foot" sand		Lower Ponchatoula aquifer		Generally, no fresh ground water occurs in deeper units
					"1,000-foot" sand				
		? 5			"1,200-foot" sand		Big Branch aquifer		
					"1,500-foot" sand		Kentwood aquifer	Abita aquifer	
					"1,700-foot" sand			Covington aquifer	
							Slidell aquifer		
			Castor Creek Member	Unnamed confining unit	Unnamed confining unit				
	Miocene		Williamson Creek Member	Jasper equivalent aquifer system	"2,000-foot" sand		Tchefuncte aquifer		
			Dough Hills Member		"2,400-foot" sand		Hammond aquifer		
			Carnahan Bayou Member				Amite aquifer		
					"2,800-foot" sand		Ramsay aquifer		
			Lena Member	Unnamed confining unit	Unnamed confining unit				
	Oligocene	? 24	Catahoula Formation	Catahoula equivalent aquifer system	Catahoula aquifer		Franklinton aquifer		

(Southern Hills regional aquifer system[2]; New Orleans aquifer system[3]; Fleming Formation spans Blounts Creek through Lena Members)

Figure 3. Correlation of hydrogeologic units in southeastern Louisiana

85

Appendix B – Table of Extraction Wells

Parish	Location source	Extraction rate per aquifer (m³/d)														
		Gramercy	Norco	Gonzales-New Orleans	1200-foot	Upper Ponchatoula	Lower Ponchatoula	Big Branch	Abita	Covington	Slidell	Tchefuncte	Hammond	Amite	Ramsay	Franklinton
Michoud	Prakken, Lovelace, & White (2014)	76	0	41261	0	0	0	0	0	0	0	0	0	0	0	0
Orleans 2		0	0	8475	0	0	0	0	0	0	0	0	0	0	0	0
Jefferson 1	Prakken & Lovelace (2014)	76	151	18363	0	0	0	0	0	0	0	0	0	0	0	0
Jefferson 2		0	0	7117	0	0	0	0	0	0	0	0	0	0	0	0
Plaquemines	Prakken (2013)	151	0	0	0	0	0	0	0	0	0	0	0	0	0	0
St. Tammany	Griffith (2017)	0	0	0	0	21955	8706	1552	10221	1552	24605	7192	7949	1514	0	0
Washington	White & Prakken (2016d)	0	0	0	0	22788	136	182	182	182	0	16588	16588	16588	16588	16588
Tangipahoa	White & Prakken (2016c)	0	0	6120	0	12239	1870	2493	2493	2493	0	11915	11915	11915	11915	0
St. Helena	White & Prakken (2016b)	0	0	0	0	2650	0	0	0	0	0	221	442	442	221	0
Livingston	White & Prakken (2016a)	0	0	1173	2347	4694	7450	3725	3725	1862	1862	4076	8151	8151	4076	0
East Feliciana	White & Prakken (2017)	0	0	0	0	1287	439	220	220	110	110	0	0	0	0	2877
East Baton Rouge	White & Prakken (2015)	0	0	0	31116	31116	92425	46212	46212	23106	23106	45633	91266	91266	45633	0
West Baton Rouge	White & Prakken (2016e)	0	0	0	189	189	11053	5527	5527	2763	2763	95	189	95	0	0
Ascension	Griffith & Fendick (2011)	0	11356	17413	0	0	0	0	0	0	0	0	0	0	0	0
St. John the Baptist	White, Prakken, & Fendick (2015)	16769	19306	151	0	0	0	0	0	0	0	0	0	0	0	0
		0	0	0	0	0	0	0	0	4959	4959	4959	0	0	0	0
St. James	White & Prakken (2015b)	10751	0	0	0	0	0	0	0	0	0	0	0	0	0	0
St. Charles	Prakken & White (2015)	76	1817	14157	0	0	0	0	0	0	0	0	0	0	0	0
Assumption	Prakken & Lovelace (2013)	0	8404	0	0	0	0	0	0	0	0	0	0	0	0	0

Appendix C – Run-File used for FS2

```
################################################################################################################
# MISSISSIPPI DELTA   iMOD runfile for SEAWAT v4
# Valid tokens to use with _T (species), _P (stress period),
# _S (sub-system), _L (model layer), _R (row), _C (column) are: $, ? and &
################################################################################################################


[GEN] # GENeral settings
   MODELNAME = FS_MISSISSIPPI                                      # Model name
   WRITEHELP = TRUE                                               # If true, write run-file help to a csv-file
   RESULT_DIR = .\Results\                                        # Results directory
   PACKAGES  = DIS, BAS6, OC, LPF, DRN, GHB, RCH, RIV, WEL, PCG, GCG, BTN, SSM, ADV, DSP, GCG, VDF   # Set active packages
   COORD_XLL = 996000.000                                        # lower left X-coordinate
   COORD_YLL = 42000.000                                         # lower left Y-coordinate
   START_YEAR = 2019                                             # starting year of the simulation
   RUNTYPE = SEAWAT


################################################################################################################


[DIS] # MODFLOW DIScretization Package
   NLAY   = 34                                                   # number of layers
   NROW   = 237                                                  # number of rows
   NCOL   = 203                                                  # number of columns
   NPER   = 11                                                   # number of stress periods
   DELC_R? = 1000.                                               # cell width along columns (or y-axis)
   DELR_C? = 1000.                                               # cell width along rows (or x-axis)
   TOP = .\DEM\GEBCO_CROP.idf                                    # Top of model
   BOTM_L? = .\BOT\BOTTOM_L?.idf                                 # bottom of model layers
   LAYCBD_L? = 0                                                 # Flag indicating whether of not a layer has a Quasi-3D confining bed below
   PERLEN_P1 = 0.0001                                            # Length stress period 1
   PERLEN_P2:11 = 3652.4                                         # Length stress period 2-11
   NSTP_P1 = 1                                                   # Number of flow time-steps stress period 1
   NSTP_P2:11 = 15                                               # Number of flow time-steps stress period 2-11
   TSMULT_P? = 2.0                                               # Time-step multiplier
   SSTR_P1 = SS                                                  # Transient/steady-state flag stress period 1
   SSTR_P2:11 = SS                                               # Transient/steady-state flag stress period 2-11

[BAS6] # MODFLOW BASic Package
   IBOUND_L? = .\BND\IBOUND.IDF                                  # Boundary indicator array
   HNOFLO   = -9999.000                                          # Value of head to be assigned to all no-flow cells
   STRT_L? = .\BND\Pointwaterhead_L?.idf                         # Initial (starting) head
```

[OC] # MODFLOW Output Control options
  SAVEHEAD_P?_L? = TRUE   # save head at the end of the stress period
  SAVECONCLAYER_L? = TRUE   # save concentrations for specific layers
  SAVEBUDGET_P?_L? = TRUE   # save budget at the end of the stress period
  SAVEHEADTEC_P?_L? = TRUE   # Save head at the end of the stress period (Tecplot)
  SAVECONCTEC_P?_L? = TRUE   # Save concentration at the end of the stress period (Tecplot)
  SAVEVXTEC_P?_L? = TRUE   # Save vx at the end of the stress period (Tecplot)
  SAVEVYTEC_P?_L? = TRUE   # Save vy at the end of the stress period (Tecplot)
  SAVEVZTEC_P?_L? = TRUE   # Save vz at the end of the stress period (Tecplot)

[LPF] # MODFLOW Layer-Property Package
  HDRY = 1E+30   # Head that is assigned to cells that are converted to dry during a simulation
  LAYTYP_L? = 0   # Flag for each layer that specifies the layer type (confined = 0; else convertible)
  LAYAVG_L? = 0   # Flag for each layer that defines the method of calculating interblock transmissivity
  CHANI_L? = 1.0   # Horizontal anisotropy factor for each layer
  HK_L? = .\LPF\Knew_L?.IDF   # Hydraulic conductivity along rows
  VKA_L? = .\LPF\Kv_L?.IDF   # Vertical hydraulic conductivity

[GHB] # MODFLOW General Head Boundary Package
  MXACTB = 250000   # Maximum number of general-head boundary in use during any stress period
  IGHBCB = 0   # Flag and a unit number for saving
  MGHBSYS = 2   # Maximum number of general-head boundary systems
  BHEAD_L? = .\GHB\POINTWATERGHB_L?.IDF   # The head on the boundary for layer 1
  COND_L1 = .\GHB\GHBCOND_L1.IDF   # The hydraulic conductance of the interface between the aquifer cell and the boundary (model layer 1)
  COND_L2:34 = .\GHB\GHBCOND_LX.IDF   # The hydraulic conductance of the interface between the aquifer cell and the boundary (model layer 2-34)
  GHBSSMDENS_L? = .\GHB\GHBDENS_L?.IDF   # Boundary general-head water density for each layer

[RIV] # MODFLOW RIVer package.
  MXACTR = 2500000   # Maximum number of river reaches
  IRIVCB = 0   # Flag and unit number for saving
  MRIVSYS = 3   # Maximum number of river systems
  STAGE_S1_L1 = .\RIV\MISHEAD.IDF   # Head in the river system 1
  COND_S1_L1 = .\RIV\MISCOND.IDF   # Riverbeds hydraulic conductance in river system 1
  RBOT_S1_L1 = .\RIV\MISBOT.IDF   # Riverbed bottom elevation in river system 1
  STAGE_S2_L1 = .\RIV\RIVHEAD.IDF   # Head in the river system 2
  COND_S2_L1 = .\RIV\RIVCOND.IDF   # Riverbeds hydraulic conductance in river system 2
  RBOT_S2_L1 = .\RIV\RIVBOT.IDF   # Riverbed bottom elevation in river system 2
  STAGE_S3_L1 = .\RIV\DITCHHEAD.IDF   # Head in the river system 3
  COND_S3_L1 = .\RIV\DITCHCOND.IDF   # Riverbeds hydraulic conductance in river system 3
  RBOT_S3_L1 = .\RIV\DITCHBOT.IDF   # Riverbed bottom elevation in river system 3
  RIVSSMDENS_S?_L1 = .\RIV\DENS_RIV?.IDF   # Boundary river density

```
[DRN] #Drain
  MXACTD = 25000000                                                          # Maximum number of drains in use during any stress period
  IDRNCB = 0                                                                 # Flag and a unit number for saving
  MDRNSYS = 1                                                                # Maximum number of drain systems
  ELEVATION_L1 - 0.5 = .\DEM\GEBCO_CROP.idf                                  # The elevation of the drain
  COND_L1 = .\DRN\DRNCOND.IDF                                                # The hydraulic conductance of the interface between the aquifer and the drain


[RCH] #Recharge
  NRCHOP = 3                                                                 # Recharge option code (3: recharge is applied to the highest active cell)
  IRCHCB = 0                                                                 # Flag and unit number for saving
  RECH_P? = .\RCH\RCH.IDF                                                    # Recharge flux

[WEL] #Wells
  MWELSYS = 1                                                                # Maximum number of wells in use during any stress period
  WEL_L5 = .\WEL\wells_L5.ipf                                                # Well point-file L5
  WEL_L7 = .\WEL\wells_L7.ipf                                                # Well point-file L7
  WEL_L9 = .\WEL\wells_L9.ipf                                                # Well point-file L9
  WEL_L11 = .\WEL\wells_L11.ipf                                              # Well point-file L11
  WEL_L13 = .\WEL\wells_L13.ipf                                              # Well point-file L13
  WEL_L15 = .\WEL\wells_L15.ipf                                              # Well point-file L15
  WEL_L17 = .\WEL\wells_L17.ipf                                              # Well point-file L17
  WEL_L19 = .\WEL\wells_L19.ipf                                              # Well point-file L19
  WEL_L21 = .\WEL\wells_L21.ipf                                              # Well point-file L21
  WEL_L23 = .\WEL\wells_L23.ipf                                              # Well point-file L23
  WEL_L25 = .\WEL\wells_L25.ipf                                              # Well point-file L25
  WEL_L27 = .\WEL\wells_L27.ipf                                              # Well point-file L27
  WEL_L29 = .\WEL\wells_L29.ipf                                              # Well point-file L29
  WEL_L31 = .\WEL\wells_L31.ipf                                              # Well point-file L31
  WEL_L33 = .\WEL\wells_L33.ipf                                              # Well point-file L33


[PCG] # MODFLOW Preconditioned Conjugate-Gradient Package
  MXITER = 1000                                                             # Maximum number of outer iterations
  ITER1  = 30                                                               # Maximum number of inner iterations
  HCLOSE = 0.005                                                            # Head change criterion for convergence
  RCLOSE = 10000.                                                          # Residual criterion for convergence
  RELAX  = 0.98                                                            # Relaxation parameter used with NPCOND = 1
  NBPOL  = 0                                                                # Flag for eigenvalue estimation if NPCOND = 2
  IPRPCG = 1                                                                # Printout interval for PCG
  MUTPCG = 1                                                                # Flag that controls printing of convergence information for the solver

#####################################################################################################################################################
```

[BTN] # MT3DMS Basic Transport Package
  DZ_L?   = .\BOT\DZ_L?.IDF   # Cell thickness
  PRSITY_L? = .3   # Porosity
  ICBUND_L1:33 = .\BND\ICBUND_LX.IDF   # Concentration boundary indicator array shared by all species (L1-33)
  ICBUND_L34 = .\BND\ICBUND_L34.IDF   # Concentration boundary indicator array shared by all species (L34)
  SCONC_T1_L? = .\BTN\CONC_L?.IDF   # Starting concentration
  CINACT   = -9999   # Value indication inactive cells
  NPRS   = 0   # Interval for printing or saving simulation results
  IFMTCN   = 0   # Output control option
  CHKMAS   = True   # Flag for saving mass budget summary file
  NPRMAS   = 1   # Output frequency. Esther: 1
  NPROBS   = 1   # Observation point output frequency
  DT0_P?   = 0.   # Transport time size
  MXSTRN_P? = 10000   # Maximum transport time step
  TTSMULT_P? = 1.   # Transport step multiplier (only for fully implicit finite-difference method)

[SSM] # MT3DMS Sink Source Mixing Package
  MXSS = 20000000   # Maximum number of all point sinks and sources included in the flow model
  CRCH_P? = .\RCH\RCH_CONC.IDF   # Concentration of recharge flux
  CRIV_S1_L1 = .\RIV\CONC_RIV1.IDF   # Concentration of river system 1
  CRIV_S2_L1 = .\RIV\CONC_RIV2.IDF   # Concentration of river system 2
  CRIV_S3_L1 = .\RIV\CONC_RIV3.IDF   # Concentration of river system 3
  CGHB_L? = .\GHB\GHBCONC_L?.IDF   # Concentration of general-head-dependent boundary cells
  CDRN_L1 = .\BTN\CONC_L1.IDF   # Concentration of draining

[ADV] # MT3DMS ADVection package
  MIXELM = -1   # Advection solution option (= 0: Finite-Difference; = 1: MOC; = 2: MMOC; = 3: HMOC; = -1: TVD)
  PERCEL = 0.75   # Number of cells that advection is allowed to move in one transport step (Courant number)
  MXPART = 100000000.   # Maximum number of moving particles allowed
  ITRACK = 1   # Particle tracking option (= 1: first-orderEuler; = 2: fouth-order Runge-Kutta; = 3: hybrid)
  WD = 0.5   # Concentration weighting factor

[DSP] # MT3DMS DiSPersion package
  AL_L?   = 1.0   # Longitudinal dispersivity 0.01
  TRPT_L? = 0.1   # Ratio of horizontal transverse dispersivity to longitudinal dispersivity
  TRPV_L? = 0.1   # Ratio of vertical transverse dispersivity to longitudinal dispersivity
  DMCOEF_L? = 0.0000864   # Effective molecular diffusion coefficient

[GCG] # MT3DMS Generalized Conjugate Gradient Solver Package
  MXITER = 10   # Maximum number of outer iterations
  ITER1 = 500   # Maximum number of inner iterations
  ISOLVE = 2   # Type of preconditioner used with Lanczos/ORTHOMIN acceleration (= 1: Jacobi; = 2: SSOR; = 3: MIC)

```
[VDF]
  MTDNCONC = 1            # Number of species
  MFNADVFD = 2            # Flag determining internodal density value calculation (2= central in space)
  NSWTCPL = 1             # Maximum number of nonlinear coupling iterations for the flow and transport solutions
  IWTABLE = 0             # Flag used to activate the variable-density water-table corrections
  DENSEMIN = 1000.        # Minimum fluid density
  DENSEMAX = 1025.        # Maximum fluid density
  DENSEREF = 1000.        # Reference fluid density
  DENSESLP = 0.7143       # The slope d(rho)/d(C) of the linear equation of state that relates solute concentration for fluid density
```